Synoptic-scale rainfall patterns over southern Africa: Scale-interactions with large-scale modes of variability

Neil C. G. Hart

UNIVERSITY OF CAPE TOWN

Thesis submitted for the degree Doctor of Philosophy

Department of Oceanography
University of Cape Town
South Africa

March 2012

For from him and through him and to him are all things;
To him be the glory forever!

Abstract

This dissertation attempts to describe atmospheric dynamics and processes operating over southern Africa at timescales from days to years. The choice is made to focus on a dominant synoptic rainfall system in the region, the tropical temperate trough (TTT). The first investigation details the dynamics of three extreme rainfall-producing systems over southern Africa. The Angola Low, an upper-level trough, and large-scale planetary wave structures are identified as important synoptic controls of such systems. This work highlights the loss of detail associated with the cluster analysis and principal component methods of identifying TTTs.

In order to retain these details, a novel cloud band "metbot" is developed to automatically identify individual events and provide a detailed description of their meteorology, including upper- and lower-level circulation and rainfall. The methodology is applied to observed outgoing longwave radiation, reanalysis circulation fields and daily station rainfall, capturing 821 events during 1979-2011. The metbot avoids the need for prescribing seasonal bounds, thus the first seasonal cycle of systems in the region is constructed. Systems start forming in October, peak in November at 3-4 events and then decline until April when events are rare. The detail retained by the method produces a more nuanced climatology of cloud band activity in the Southwest Indian Ocean than previous work. Two preferential locations for cloud band development exist, one over the continent and another over Madagascar.

This TTT-event data base is used to accurately assess the importance of these systems to summer rainfall and their ability to drive intraseasonal to interannual variability. Contributions to seasonal total rainfall vary between 30-60% depending on location, with peak contributions in November. The results suggest firstly, that the Madden-Julian Oscillation may be able to modulate event rainfall intensities and secondly, that individual extreme TTT events can modify seasonal totals by over 20%.

Having built an appropriate tool to link synoptic-scale weather to interannual variability, the final question addressed is, how does ENSO project into cloud bands over southern Africa? Even with this regional focus, novel insight is gained into the variability of the South Indian Convergence Zone. Most El-Niño years show substantial reduction in system numbers, but little change in rainfall characteristics. However, during La-Niña, the number of events remains near the climatological value, but with more persistent and intense TTT rainfall. The results are mixed regarding an eastward shift of cloud band activity during El-Niño, however years with a strong response seems to result in region-wide suppression of cloud band formation. This finding challenges the conclusions of previous studies. Investigation of the sensitivity of the region to the flavour of El-Niño using an idealised model experiment suggested that there is a stronger regional influence during central Pacific warm events, however this is confined to the Madagascan location for cloud bands. The implications are that there is difficulty in the ENSO signal reaching southern Africa through a direct atmospheric bridge, either tropical or extratropical. This aspect has been noted in other modelling studies. However, the limitations of this experiment setup and analysis suggest cautious interpretation is required.

Supervisors

Prof. Chris Reason
Department of Oceanography, University of Cape Town, South Africa

Dr. Nicolas Fauchereau
National Institute of Water and Atmospheric Research, Auckland, New Zealand
Formerly at Department of Oceanography, University of Cape Town, South Africa

Funding

I am grateful for funding from the South African National Antarctic Programme of the National Research Foundation.

A University of Cape Town PhD Fellowship from the David and Elaine Potter Foundation has greatly assisted with the completion of this dissertation, and I extend sincere thanks to Dr David and Elaine Potter for their support.

Declaration

I declare that this thesis is my own unaided work, both in concept and execution, and that apart from the normal guidance from my supervisor, I have received no assistance except as acknowledged. I declare that neither the substance nor any part of the above thesis has been submitted in the past, or is being, or is to be submitted for a degree at this University or at any other university.

Part I of this manuscript has been published in Monthly Weather Review. I confirm that this above declaration holds true for this publication too, and authorship of my two supervisors represents their assistance with improving style and grammar and advice in managing the paper through the peer-review process.

Acknowledgements

My supervisors, Prof. Chris Reason and Dr. Nic Fauchereau are thanked for their support, guidance and patience. Most of all, I thank them both for the freedom of inquiry they afforded to me during these past 5 years. Chances to pursue one's own curiosity seem ever rarer, and I have immensely enjoyed and appreciated this opportunity. I especially thank Chris for the time and effort he has spent on helping improve my scientific writing; the speed with which he has returned valuable reviews of my writing is greatly appreciated.

Early in my post-graduate career I had the opportunity to spend a semester at the Geofisken Institute, University of Bergen. The course work I completed during that stay has greatly improved much of this thesis, especially Part 1. The Norwegian Agency for Development is thanked for funding this exchange.

I am grateful to Mathieu Rouault for numerous discussions which have helped shaped the direction of inquiry, especially with regards to ENSO teleconnections to the region. Benjamin Pohl and Nico Viguad are thanked for helpful conversations which have helped sharpen the scientific questions addressed in this dissertation. Researchers in UCT's Climate System Analysis Group have had substantial influence in what I ended up recognising as important research questions. Bruce Hewitson, Babatunde Abiodun, Chris Lennard, Lisa Coop and Peter Johnston are thanked for many long conversations on the state of climate science. Mark Tadross is thanked especially, for taking the time to help me get HadAM3P running my experiments. Chris Jack: your technical advice and help, long coffees and availability as a sounding board for some crazy ideas has been invaluable.

Björn Backeberg, Christo Whittle and Jen Veitch provided much encouragement and support; thanks for putting up with all my interruptions, however geek they were. Nats, for being a similarly-minded nerd for all things GFD. Seb and Ross were great office colleagues and made for an brilliant work environment that I always looked forward to entering. I have benefited hugely from a passion for meteorology shared by Ross.Thanks to Marlan for help with the more tricky mathematics. Rachie, for all your enthusiasm, excellent administration and amazing carrot cakes with which you blessed our department. Prof Frank Shillington and Prof John Field offered wise words from the other end of the research career road. UCT interlibrary loans was superb in getting hold of long lost theses from around South Africa.

Marlan, Ross, Linz, Debbie, Ashleigh, and my Mom and Dad, Chris and Robin are thanked for their time in proofreading the different parts of the final manuscript.

To all my friends, but especially Dunc, Melch, Wes, for cheering me on and providing opportunities to forget about all things thesis related and regain some social skills.

I thank my family especially Nigel, Debbie and Ashleigh and my aunts and uncles for their enthusiasm and support to finish this work.

My parents' support has been unwavering and I am deeply thankful for their encouragement of the pursuit of my passions and curiosity. My grandparents have set such remarkable example of maintaining inquiring minds late into life. I thank my brother Geoff for many words of encouragement along the way. Much of this work , often late into the night, was carried out on a laptop Grandpa Brian and Gran Sue bought for me at the outset of my postgrad studies, thank you for this.

To my wife, Linz: thank you for your encouragement, patience, support and for sharing in the ups and downs of my pursuing a PhD, long after the many expected completion dates. I love you babe!

Contents

List of Figures

List of Tables

Introduction

Fluids facilitate transfer of energy between time and space scales. The essence of this was captured by L. F. Richardson's 1922 rhyme; "big whirls have little whirls that feed on their velocity, and little whirls have lesser whirls and so on to viscosity" (Richardson, 1922). It is said that he formulated this while watching cumulus clouds build and dissipate. This pithy statement is the starting point to understanding small-scale turbulence, however it captures a fundamental feature of the ocean-atmosphere climate system too: a spatio-temporal continuum of processes. Meehl et al. (2001) elucidated this and proposed a conceptual framework with which to approach these scale-interactions. This dissertation attempts to understand aspects of these multi-scale processes over southern Africa. Thus, central thesis is this:

> **The application of the multiscale interaction conceptual framework to southern African rainfall variability will yield novel insights into the mechanisms driving climate variability over the sub-continent, as well as adding new knowledge to the understanding of scale-interactions in the global ocean-atmosphere system.**

Applying this framework is not trivial as it requires quantification of the coherent atmospheric processes that operate on this continuum of scales. To achieve this, robust methodologies are required to identify these processes. Sometimes, principal component analysis (PCA) is sufficient to describe processes, especially at intraseasonal to longer time scales. For example, the Madden-Julian Oscillation activity is well quantified by a pair of empirical orthogonal functions (EOFs) obtained from the multivariate data of tropical upper- and lower-level zonal winds and outgoing longwave radiation (Wheeler and Hendon, 2004). Despite wide usage, the physical reality of PC modes, especially in variability studies, can be dubious (Dommenget and Latif, 2002; Monahan et al., 2009). Further difficulties are encountered when variability modes vary on timescales from weeks to decades (eg. the Southern Annular Mode; Thompson and Wallace, 2000) however, quantifying these modes in terms of their synoptic regime frequencies presents an interesting alternative (Pohl and Fauchereau, 2012). The key point is that quantifying physical processes at different timescales is important for scale-interaction studies, however, it is difficult to achieve.

As indicated by the title, this dissertation is concerned with synoptic-scale weather. Approaches to describing weather in this temporal range (1-3 days) are varied, however they fall broadly into two categories: weather regimes (see review; Demuzere et al., 2011) and feature identification and tracking (eg. Murray and Simmonds, 1991b; Hodges, 1999). In general, weather regime methodologies favour recurrent patterns and ultimately provide a summary of the dominant meteorology of the region of interest. Feature identification retains more detail, hence provides a better description of individual events. Therefore, this dissertation will adopt a feature-based approach to quantifying the synoptic-scale processes in the region. This choice resulted in the formulation of a methodological thesis too:

> **Recent advances in computer vision technology can be adapted to develop an automatic feature identification tool, which can reliably identify and describe individual synoptic weather systems.**

This brief discussion provides the conceptual overview to the work that is presented in this manuscript. An overview of the current understanding of the southern African climate follows.

Southern African summer rainfall variability

Highly variable annual rainfall over southern Africa is widely acknowledged (Mason and Jury, 1997). As such, rainfall variability studies for the region, as elsewhere, have huge societal relevance. Reliable information about the upcoming season or years can inform decisions in many sectors of society to mitigate damages from, or take advantage of, the likely weather for that season. Southern Africa has large-scale rain dependent agriculture with both commercial and subsistence sectors (Hansen et al., 2011). Within South Africa in particular, water demand from heavy industry has long been an issue (Mason and Joubert, 1995). More recently acid mine water is becoming a growing concern; heavy summer rains fill up old mine shafts increasing the risk of highly acidic mine water contaminating surface river systems (eg. Cobbing, 2008). With such a heavy mining industry presence in the region, water resources are often under substantial pressure. These societal needs have largely been the driving force behind a well established and ongoing research effort to better understand and predict regional climate variability (Mason and Jury, 1997; Reason et al., 2006; Landman and Beraki, 2012).

With the exception of the extreme southwest of the continent, the main wet season is during the austral summer. The focus of this study is the subtropics so, while the atmosphere knows no political boundaries, the country of South Africa fills a large part of subtropical southern Africa and as such findings in this study have most relevance to South African rainfall variability.

During the warm season, the region is affected by weather systems of both tropical and extratropical origin and interactions between the two. Extreme events such as cut-off lows or tropical cyclones that make landfall can drastically modify seasonal totals (eg. Singleton and Reason, 2007; Reason and Keibel, 2004). Mesoscale convective systems can have a similar impact at a more local scale (eg. Blamey and Reason, 2009). However, most of the rainfall is due to more frequent convective activity which persists throughout the wet season provided sufficient moisture is available (Tyson and Preston-Whyte, 2000). While not always necessary, large-scale forcing often provides the impetus to trigger convection. This synoptic forcing is often provided by anticyclones ridging eastward along the coast promoting upslope flow, low-level convergence encouraged by strong land-based heat lows, and upper-level divergence provided by upper-tropospheric westerly waves propagating into the subtropics (Taljaard, 1996). However, based on work presented in Harrison (1984), it has been widely accepted that tropical-extratropical cloud bands are the primary rainfall producing system. In short, these represent an interaction between a continental low-level depression supporting moisture convergence and the leading edge of an upper-level trough, promoting uplift (Harrison, 1986). The systems have become regionally known as tropical temperate troughs (TTTs), however for much of this manuscript both the term tropical-extratropical cloud band and TTT will be used.

Most of the research into rainfall variability has been performed by relating monthly and seasonal mean circulation anomalies to accumulated rainfall totals. This research has revealed that rainfall variations are strongly linked to variability in oceanic moisture sources in the tropical and subtropical Indian Ocean (Walker, 1990; D'Abreton and Lindesay, 1993; Reason and Mulenga, 1999; Hansingo and Reason, 2006) and the southeast Atlantic Ocean (Rouault et al., 2003; Hermes and Reason, 2009). These relationships are complicated by large-scale interannual variability in tropical and extratropical mean circulation. El-Niño events generally seem to shift the rising branch of the Walker circulation from southern Africa eastward into the central Indian Ocean and suppress convection over subtropical southern Africa (Harrison, 1986; Lindesay, 1988). Generally, this is accompanied by an eastward migration and weakening of the South Indian High, which reduces the easterly moisture fluxes towards the African coast. Changes in the positioning and amplitude of standing waves in the extratropical Southern Hemisphere are common and have been shown to influence the high pressure cells in all three ocean basins (eg. Fauchereau et al., 2003). For this reason and because of the importance of upper-level westerly waves in summer rainfall, its has been

suggested that extratropical variability may have an influence on summer season variability over southern Africa (Mason and Jury, 1997). However, there has not yet been a definitive study establishing a relationship.

A number of studies have investigated seasonal circulation anomalies associated with warm and cool ENSO events (Van Heerden et al., 1988; Landman and Mason, 1999; Reason et al., 2000; Richard et al., 2000, 2001). An often cited consequence of the general offshore shift of tropical convection, is a concomitant eastward shift in TTT location. A few studies in the last decade have started to investigate non-linearities of the ENSO response, especially since the largest El-Niño/La-Niño event of the 20th century (1997) failed to produce the expected region-wide drought (eg. Reason and Jagadheesha, 2005; Lyon and Mason, 2007).

Most of the rainfall variability studies that have elaborated on the above mechanisms have a common conclusion, implication or suggestion: the effect on rainfall is produced through a modification of the location, frequency or intensity of TTTs during the anomalously wet or dry seasons. However, these suggestions are based on Harrison (1984), which was limited to 10 years of satellite data, daily rainfall stations in central South Africa and PCA of monthly rainfall district totals. PC analysis on a satellite-derived daily precipitation product confirmed that TTTs are responsible for the most coherent large-scale pattern of rainfall in the region (Todd and Washington, 1998, 1999; Washington and Todd, 1999; Todd et al., 2004), however this did not explicitly quantify importance for continental rainfall.

Scale-interactions in the regional climate system

Mechanistic understanding of scale-interaction processes can be aided by quantifying three aspects of the meteorology of rainfall: frequency of occurrence, intensity of precipitation, and persistence. There are already some indications of how these unfold over southern Africa. To summarise at this point, substantial mid-latitude influence is present year round in the region, however in summer this is mostly confined to the upper-tropospheric westerly flow, with an eddy-driven sub-tropical jet often situated across the continent. Wave activity in this upper-level flow modulates the frequency of convection, inhibiting or promoting conditions associated with upper-level convergence or divergence. Moisture supply from the tropics and the adjacent oceans is often facilitated by quasi-stationary features such as the Angola Low or South Indian High; this supply is vital to precipitable water availability, hence is a controlling factor in intensity of precipitation. Finally, persistence of synoptic rainfall systems will likely be due to interactions between the moisture supply, the upper-level flow, and nonlinear feedbacks between the two.

In the last decade a number of studies have been published, which link the subseasonal variability to interannual variability. Indications are that wet summer seasons are characterised by more persistent and intense wet spells, but not an increased frequency (Cook et al., 2004). Dry spell frequency however, is well correlated to El-Niño Southern Oscillation (ENSO) with increased frequency during El-Niño events (Usman and Reason, 2004; Reason et al., 2005). Rainy season onset dates also exhibit links to ENSO-related changes in circulation (Tadross et al., 2005; Hachigonta et al., 2008). Again, these studies invoke changes to TTT climatology as the likely mechanism behind changes observed in the rainfall characteristics.

Recently, a suite of studies focused on scale-interactions in the region has uncovered nuances of the effect of the MJO (Pohl et al., 2007), ENSO and local SSTs (Fauchereau et al., 2009) on regional rainfall (Crétat et al., 2010). Pohl et al. (2009) demonstrated that while the MJO modulates convection unrelated to TTTs, it has little effect on TTT occurrence. They also showed that El-Niño is generally associated with suppressed convection over the continent at subseasonal time scales. Further work indicated difficulty in separating the effect of the tropical variability modes

from the extratropical southern annular mode (also referred to as the Antarctic Oscillation; AAO) in understanding a mid-latitude influence on southern African rainfall variability (Pohl et al., 2010). A conclusion in both Pohl et al. (2009, 2010) suggests that the MJO may modulate a part of rainfall variability unrelated to TTTs. These papers made use of a weather regimes approach by discretising daily outgoing longwave radiation with either k-means cluster analysis or daily PC scores. These methodologies have produced a robust description of the recurrent daily configuration of the summertime convection over the subcontinent and adjacent ocean, however for reasons elaborated further in this dissertation, these may not be sufficiently precise descriptions.

In summary, the synoptic climatology of the subtropical southern Africa is relatively well understood. This dissertation contends, however, that the role of TTTs in particular, is poorly quantified and since these systems are often invoked in explanations of regional rainfall variability, this presents a substantial gap in knowledge. Indeed, as will be shown in Part I, even detailed understanding of the meteorology of these systems is weak. However, this situation is not only for lack of work on these systems (eg. D'Abreton, 1993) but also due to the paucity of data available to many early researchers.

This dissertation will seek to build on earlier work and address these deficiencies by making use of the abundance of data now available and will tackle the problem of quantifying TTTs, at the synoptic-scale, with a novel approach. The detail created by the methodology will be used to describe the seasonal cycle of tropical-extratropical cloud bands over southern African and the Southwest Indian Ocean and the importance of this to summer rainfall. The novel quantification of TTT activity and associated rainfall presents a promising approach with which to explore regional scale-interactions. Therefore, the influence of the MJO and ENSO on TTT frequency, intensity and persistence at intraseasonal and interannual time scales is investigated with a detail that has been unavailable to previous studies.

A dissertation in parts

I have chosen to structure this manuscript in four parts. Each part follows a format similar to a journal article, indeed Part I is already published. The introduction of each article contains the pertinent literature, hence the lack of detail provided in the brief introduction above. Since this is a coherent manuscript, I have tried to ensure that when results in previous or subsequent articles are referred to, this will be denoted as "Part x".

Even though each part is written as an individual study, there is a overarching theme that binds them, that of linking the synoptic-scale to large-scale interannual variability. Each study builds on the work of the previous, with each addressing a specific question:

1. **What are the dynamics of the primary synoptic rainfall system over southern Africa?**
2. **How can the dynamics of these synoptic rainfall systems (TTTs) be quantified in a way that provides links to intraseasonal and interannual variability?**
3. **What is the signature of the mean annual cycle of TTTs in synoptic climatology and rainfall?**
4. **How does ENSO project onto this annual cycle and into weather timescales?**

To help carry the thread through, each part starts by re-stating its overarching question and identifying four more detailed questions it will address.

Part I

Case studies of tropical-extratropical interactions over southern Africa

What are the dynamics of the primary summer synoptic rainfall system over southern Africa?

Specific Questions:

- What are the dynamics of heavy precipitation-producing tropical temperate troughs?
- Can a generalised description for these systems be developed?
- Do tropical temperate troughs fit within the general theoretical framework for tropical plumes?
- What meteorological features may be open to influence by large-scale climate modes?

"Details create the big picture" - Sanford I. Weill

Tropical-Extratropical Interactions over Southern Africa: Three Cases of Heavy Summer Season Rainfall

Abstract

The synoptic evolution of three tropical-extratropical (TE) interactions, each responsible for extreme rainfall events over southern Africa, is discussed in detail. Along with consideration of previously studied events, common features of these heavy rainfall producing tropical temperate troughs (TTTs) over southern Africa are discussed. It is found that 2 days prior to an event, northeasterly moisture transports across Botswana, set up by the Angola Low, are diverted further south into the semi-arid region of subtropical southern Africa. The TTTs reach full maturity as a TE cloud band, rooted in the central subcontinent, is triggered by upper-level divergence along the leading edge of an upper-tropospheric westerly wave trough. Convection and rainfall within the cloud band is supported by poleward moisture transports with subtropical air rising as it leaves the continent and joins the mid-latitude westerly flow. It is shown that these systems fit within a theoretical framework describing similar TE interactions found globally.

Uplift forcing for the extreme rainfall of each event is investigated. Unsurprisingly, quasigeostrophic uplift is found to dominate in the mid-latitudes with convective processes strongest in the subtropics. Rainfall in the semi-arid interior of South Africa appears to be a result of quasigeostrophically triggered convection.

Investigation of TTT formation in the context of planetary waves shows that early development is sometimes associated with previous anticyclonic wave breaking south of the subcontinent, with full maturity of TTTs occurring as a potential vorticity trough approaches the continent from the west. Sensitivity to upstream wave perturbations and effects on anticyclonic wave breaking in the South Indian Ocean are also observed.

A paper based on this part was published in the July 2010 issue of
Monthly Weather Review (vol. 138), pages: 2608-2623:
"Tropical-Extratropical Interactions over Southern Africa: Three Cases of Heavy Summer Season Rainfall"
N.C.G Hart, C. J. C Reason and N. Fauchereau

1 Introduction

Cloud bands resulting from tropical-extratropical (TE) interactions are common features in many regions, typically presenting as an elongated region of cloudiness rooted in the tropics and extending poleward and eastward into the mid-latitudes (eg. Kuhnel, 1989; Iskenderian, 1995). These events typically involve the export of moisture and heat from the tropics to the mid-latitudes which may replace deep Hadley Cell overturning during periods of weakened ITCZ activity (McGuirk et al., 1987).

On seasonal timescales, subtropical moisture convergence zones (CZ's) can support persistent TE cloud band features and thus are often excluded from synoptic studies (eg. McGuirk et al., 1987). The South Atlantic Convergence Zone (SACZ) and South Indian Ocean Convergence Zone (SICZ) however, exhibit high synoptic variability (eg. Lyons, 1991; Liebmann et al., 1999; Pohl et al., 2009). Work by Cook (2000) on the SICZ, which forms in austral summer over southern Africa and the southwest Indian Ocean, produced a conceptual model applicable to land-based convergence zones and their formation but did not address synoptic variability.

Over the southern African region of interest here, cloud bands are the major synoptic rainfall producing weather system (Harrison, 1984) during the summer yet their dynamics and variability remains to be well understood. Regionally, these cloud bands are known as tropical temperate troughs (TTTs) and will be referred to as such for the rest of this study.

Globally, a wealth of studies of similar TE interactions exist. These regions include Australia, South America, North Pacific, North Atlantic and North Africa, with many recent dynamical studies focusing on the latter two regions (Knippertz, 2003; Knippertz et al., 2003; Knippertz, 2005; Knippertz and Martin, 2005). A full summary of this literature is not provided here but for an extensive overview of previous TE interaction case studies the reader is referred to Ziv (2001) and Knippertz et al. (2003).

Knippertz (2007, KP07 hereafter) synthesized the current body of knowledge regarding these interactions and developed a theoretical framework for their formation and evolution. The key feature of these phenomena is the presence of a low-latitude upper-tropospheric trough which facilitates the TE interaction and resulting cloud band. Despite very similar events occurring over southern Africa, TTTs recieve little mention in general TE cloud band studies. The present study seeks to address this gap in the literature, further motivated by the considerable importance of TTTs for rainfall in the semi-arid central southern Africa.

The primary goal of this paper is to consider the dynamics common to the development, maturation and decay of TTTs over southern Africa. Additionally, the study examines whether TTTs fit within the theoretical framework set out in KP07. To help acheive these goals upper- and lower-tropospheric circulation and associated moisture transports are presented for three extreme, warm season, rainfall events caused by TTTs over southern Africa.

Forcing factors for uplift that produces heavy rainfall are presented to gain insight into the dynamics driving the high precipitation rates associated with TE interactions. Three primary mechanisms have been identified as drivers of uplift: positive vorticity advection, adiabatic uplift and diabatic processes (see section 5 and 6, KP07). Following Knippertz and Martin (2005), quasigeostrophic (QG) omega is calculated to include the contributions of upper-level positive vorticity advection and low-level adiabatic uplift to the heavy rainfall of the events presented here.

Finally, a brief investigation of upper-tropospheric potential vorticity (PV) evolution for each event is presented to get a perspective on the association of TTTs to planetary wave activity over the South Atlantic and South Indian Oceans, an aspect of TE interactions over southern Africa which has not been previously explored.

Three TTT events that resulted in heavy rainfall over large parts of South Africa on 1 January 1998, 5 - 6 January 1998 and 16 December 2007 are examined. The data and methods are described in section 2. The synoptic evolution of these three events is presented in section 3 while section 4 addresses the forcing for uplift on extreme precipitation days. The large-scale context of TTT-development is discussed in section 5 with common synoptic features and aspects addressing TTTs in light of the KP07 theoretical framework mentioned in section 6. Climatological implications are considered in section 7 and conclusions are summarised section 8.

2 Data and Methods

Three extreme rainfall events were chosen through two selection procedures outlined below: Case I: 1 January 1998; Case II: 5 - 6 January 1998 and Case III: 16 December 2007.

The South African Water Research Commission (WRC) daily rainfall data set (Lynch, 2003) comprising 7665 stations within South Africa (Fig.1), only available for the period 1979 to 1998, was used for Case I and II with Tropical Rainfall Monitoring Mission (TRMM) satellite daily accumulated rainfall covering the period 1998-present at 0.5^o x 0.5^o resolution used for Case III. The November to February (NDJF) period, representative of the core wet summer season was extracted to calculate extreme rainfall days in both data sets.

Extreme rainfall criteria to be met were: 1) Daily rainfall be above the 90th percentile rainfall value for all rain days at that location (grid point or station); 2) This criterion is valid for at least 10% of locations to ensure that the extreme rainfall had a large areal extent.

In Fauchereau et al. (2009), it was shown that the daily outgoing longwave radiation (OLR) variability over southern Africa is well defined by seven statistically distinct clusters, one of which represented TTT-events producing continental rainfall. As a final filter for events of interest, only extreme rain days that matched days assigned to this cluster were used. Thus, a candidate pool of TTT-events associated with heavy precipitation was created from which these three events were chosen.

The synoptic evolution of the three cases are investigated using the 2.5^ox 2.5^o NCEP-DOE Reanalysis II (NCEP2) Data set (Kanamitsu et al., 2002) with 17 pressure levels. These data are 6-hourly and were averaged to daily means to match the time resolution of the rainfall data. Daily OLR values from the data set described in Liebman and Smith (1996) were used as a proxy for deep convection.

Both upper-troposphere PV and low-level moisture transports are plotted on isentropic surfaces. Interpolation of the NCEP data to isentropic levels was performed in a two step process. Firstly, pressure was interpolated to 19 isentropic surfaces assuming a constant lapse rate between the pressure surfaces. This assumption used by Shen et al. (1986) was shown in Ziv and Alpert (1994) to be the method of choice when performing such interpolation, especially when applied to obtain PV on an isentropic surface. Pressure on the isentropic surfaces was then used to interpolate all other atmospheric variables using polynomial interpolation, assuming $variable \propto (\ln p)^2$ (for details see Shen et al., 1986).

The assumption that the potential temperature (θ) is conserved during motion of the air parcels implies that flow on isentropic surfaces is a truer representation of atmospheric motion than flow on pressure surfaces (Ziv, 2001, see section 4.3). This allows some inferences regarding air parcel trajectories to be made, especially when synoptic situations exhibit some stationarity for a few days.

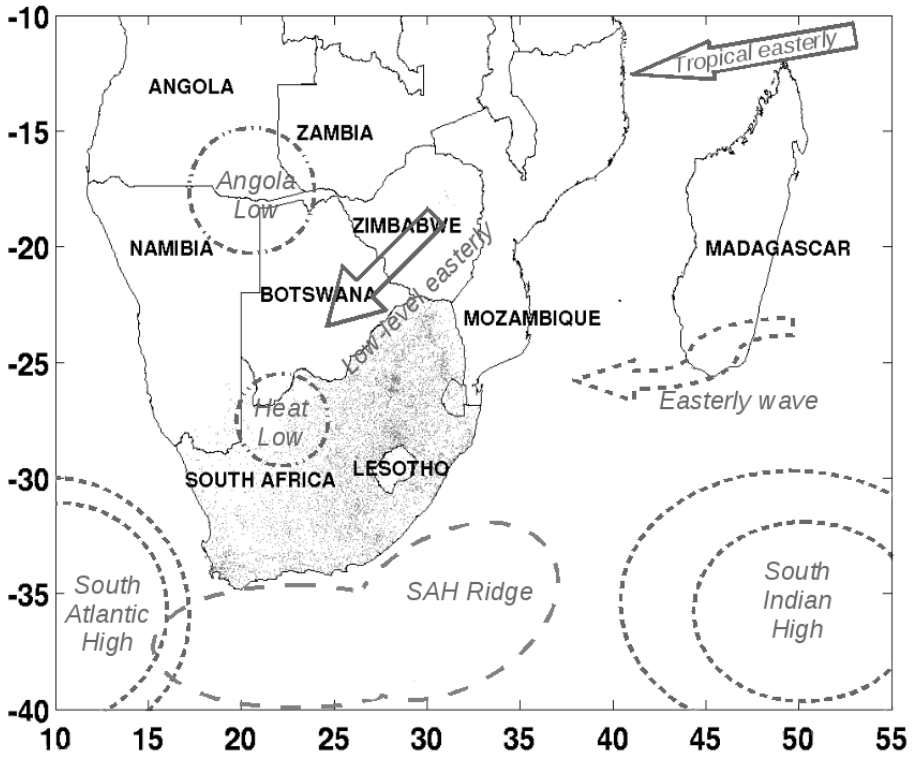

Figure 1: Southern African political boundaries, WRC rainfall stations (dots) and key summer season synoptic features.

3 Synoptics of TTT Development

For ease of reference, key circulation features of the southern African summer pertinent to TE cloud bands are highlighted by Fig. 1. The Angola Low is a semi-permanent feature of tropical southern African circulation during summer (Reason et al., 2006), dominating the lower- to mid-troposphere circulation. Often a weak surface high over southern Mozambique and the neighbouring ocean helps enhance the pressure gradient across Botswana and Zimbabwe. This pressure gradient then sets up strong low-level northeasterly flow across the central subcontinent which then promotes the flow of tropical easterlies north of Madagascar deep into the subcontinent. Continental heat lows (Racz and Smith, 1999) often form over the central Kalahari Desert helping to induce a weak cyclonic circulation which can then divert the low-level northeasterlies further south. Eastward ridging of the South Atlantic High (SAH) often induces onshore flow and coastal showers along the south coast and sometimes up the east coast. Northwestward extension of the South Indian High (SIH), coupled with a surface depression in the Mozambique channel can then produce an easterly wave flow into Mozambique and eastern South Africa.

In this scenario, TTTs may then occur across southern Africa and extend from the Angola Low, southeast to a location of the South Indian Ocean that is typically just east of the ridging SAH pressure system and associated with a mid-latitude westerly wave depression.

The term TTT is used to describe the full complement of synoptic features that relate to these TE interactions over southern Africa. These synoptic features however, will be referred to as TE features, eg. TE cloud band.

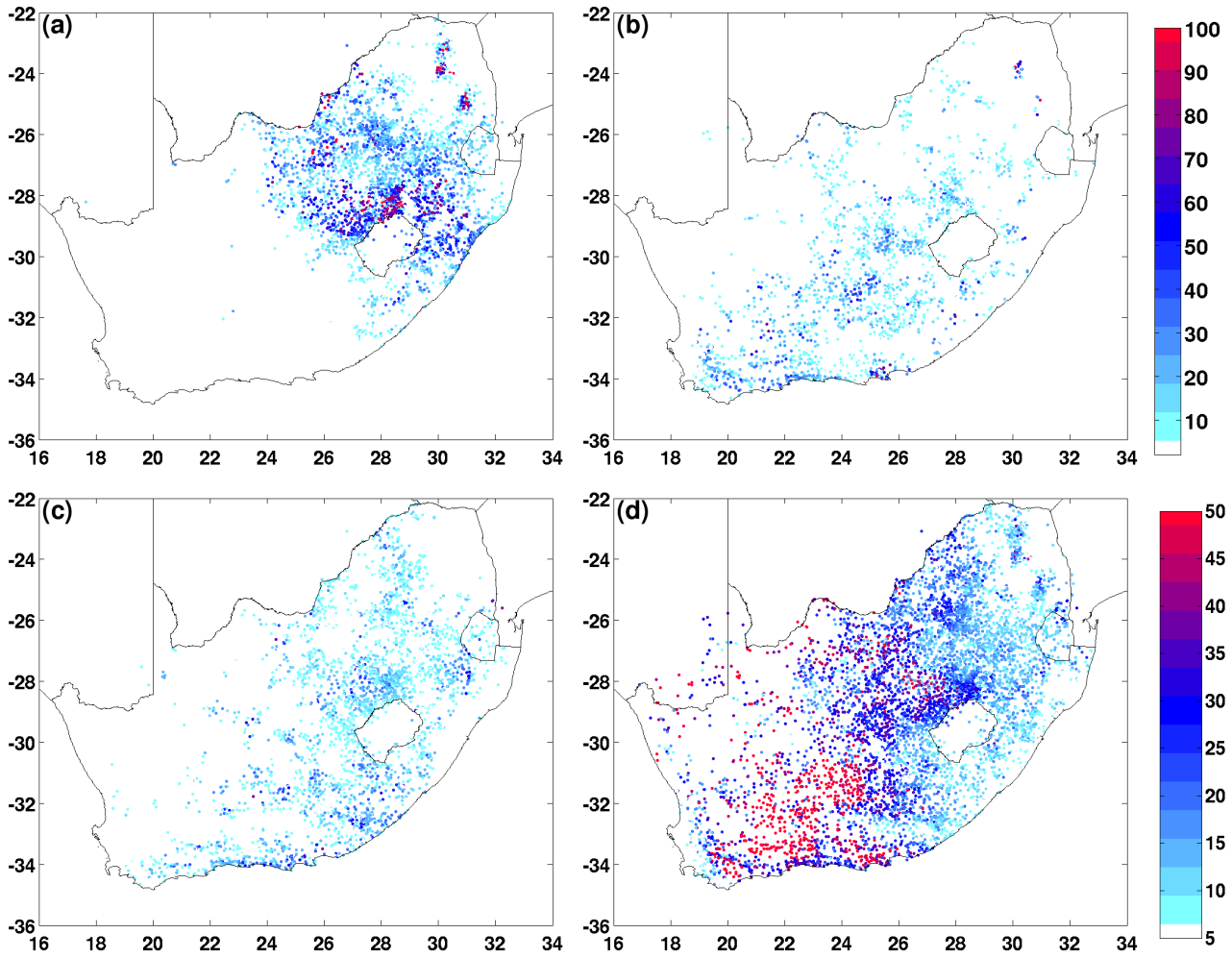

Figure 2: 24 hr accumulated rainfall at WRC stations on 1 January 1998 (a), 5 January 1998 (b) and 6 January 1998(c). (d) displays contribution to NDJF season rainfall for period 1-7 January 1998. Upper color scale denotes rainfall in mm for (a), (b) and (c), with the lower color scale denoting contribution % for (d).

3.1 Case I: 31 December 1997 - 2 January 1998

The 24hr accumulated rainfall for 1 January 1998 is presented in Fig.2 (a). Upper (right panels) and lower-level (left panels) synoptic evolution for case I is presented in Fig.3. Low-level moisture transports for this case appear in Fig.5 (a-c), represented on the 309K isentropic surface.

On 31 December 1997, key features of the developing TTT were well manifested. Low-level northeasterlies across Zimbabwe and Botswana were found on the southeastern flank of the well formed Angola Low, as evidenced by the 850hPa divergence field (Fig.3 a).

The low OLR signature over the central subcontinent indicates that convection had already begun in the semi-arid region, aided by upper-level divergence in the entrance zone of a moderate southwesterly jet region. This cause of this jet was likely to be deep convection over tropical Africa during previous days. This convection enhanced the upper-level anticyclone over the central subcontinent, leading to a stronger gradient wind over its southwestern flank, as suggested by the ageostrophic wind (Fig.3 b).

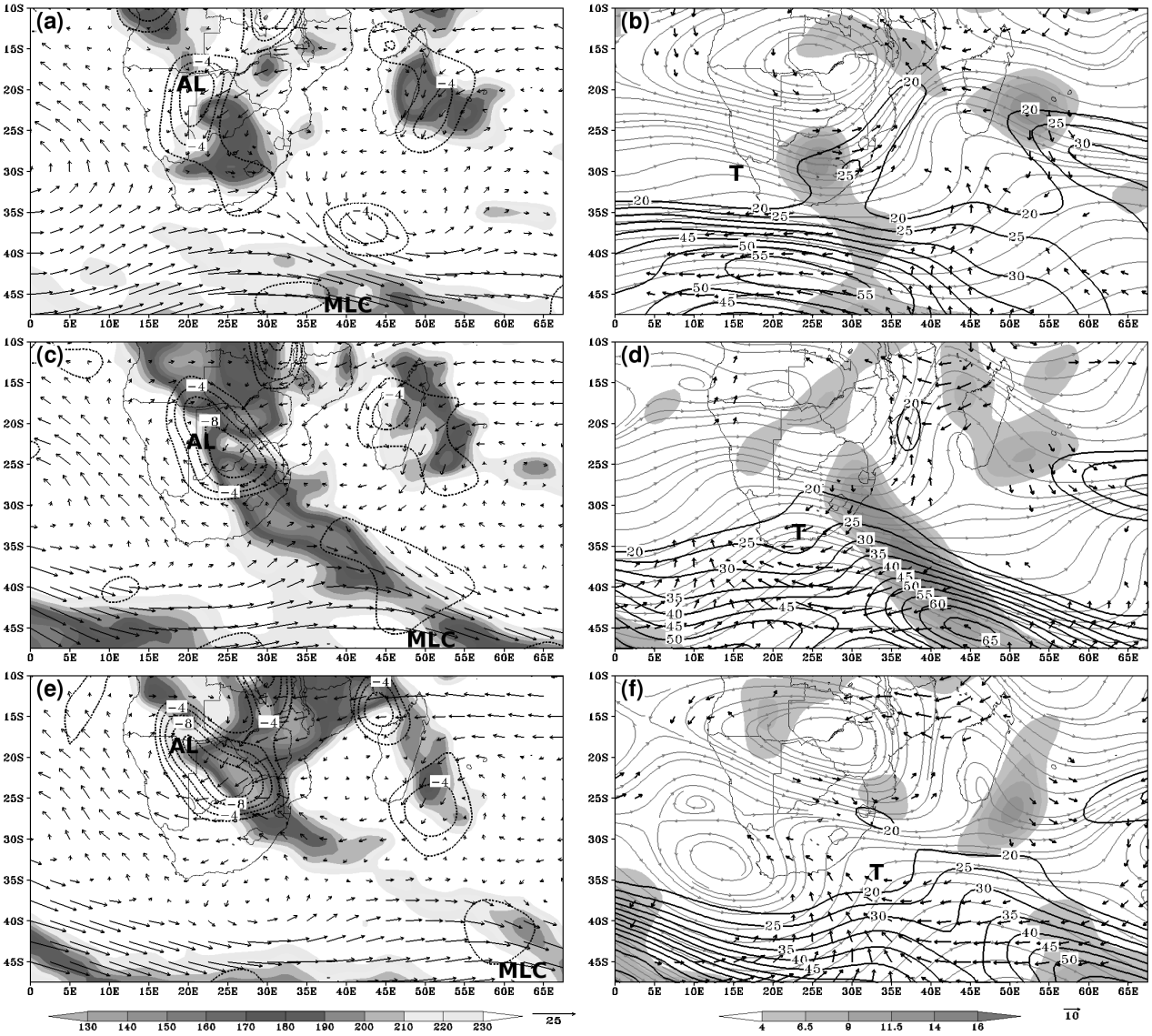

Figure 3: Left panels: Winds (vectors, m.s^{-1}) and convergence (contoured, 1*10^{-6} s^{-1}) at 850hPa and OLR (shaded, W.m^{-2}) on 31 December 1997 (a), 1 January 1998 (c) and 2 January 1998 (e). Right panels: Full winds at 250hPa (streamlines, m.s^{-1}), 250hPa ageostrophic winds (vectors, >4 m.s^{-1}) and 250hPa divergence (shaded, 1*10^{-6} s^{-1}) on 31 December 1997 (b), 1 January 1998 (d) and 2 January 1998 (f). Positions of the Angola Low (AL), low-level cyclonic disturbances (L), mid-latitude cyclones (MLC) and upper-level troughs (T) are indicated.

The low-level northeasterlies resulted in strong transports of tropical moisture converging in the semi-arid subtropics, supporting the convection (Fig.5 a). The first indication of a TE link about to form was the weak warm moist conveyor transporting moisture off the southeastern African coast ahead of the approaching mid-latitude wave.

By 1 January 1998, the TTT was fully developed with a band of low OLR values extending from tropical southern Africa into the southwest Indian Ocean (SWIO), terminating in a mid-latitude cyclone near 45°S (Fig.3 c). The Angola Low convergence maxima had intensified to the southeast, weakening the northeasterlies. Although not clear on the 850hPa surface, the isentropic flow field clearly indicated a warm conveyor feeding moisture from subtropical Africa into the mid-latitude depression over the SWIO (Fig.5 b).

The amplification of the westerly wave as warm subtropical air moved poleward and upward, increased the gradient

wind effect, promoting a band of upper-level divergence along the leading edge of the wave. This amplification was further encouraged by the divergent response to the deep convection in the TE cloud band (Fig.3 d). These factors promoted the intensification of the the jet core above the mid-latitude cyclone to 65 m.s^{-1} .

Substantial precipitation had begun on 31 December, but it was the amplifying upper-level wave, strong moisture supply and enhanced low-level convergence of 1 January 1998 that supported the heaviest rainfalls. Many stations throughout central northeastern South Africa recorded daily totals exceeding 50mm (Fig.2 a). The heaviest precipitation was found in the mountainous region near Lesotho (28°S, 28°E) with some stations recording up to 80mm.

On 2 January 1998 light rainfall (not shown) was still recorded for central South Africa. The TE cloud band (Fig.3 e)

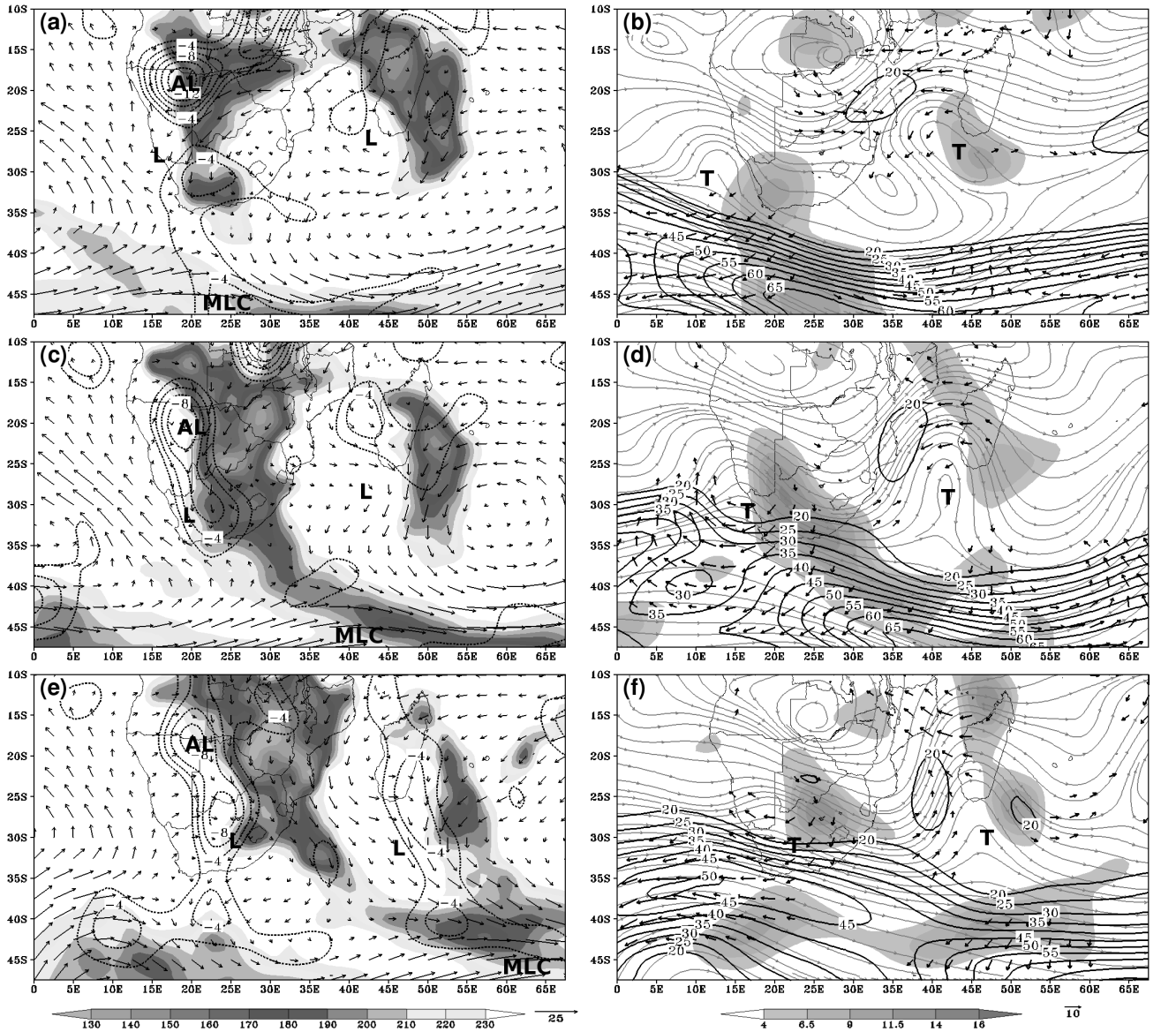

Figure 4: As in Fig. 3, but for 5 January 1998 (a and b), 6 January 1998 (c and d), and 7 January 1998 (e and f) (case II).

was still present, but contiguous flow from subtropical Africa into the mid-latitudes was shut off by the eastward ridging of the SAH under the trailing edge of the upper-level wave (Fig.3 f).

Intensification of the the Angola Low shown in this case was evident in both the coherent low-level cyclonic circulation and strong convergence as well as in the strengthened northeasterly moisture transports across much of central subtropical southern Africa (Fig.5 c). This pattern was important for the next event, which occurred a few days later as discussed below.

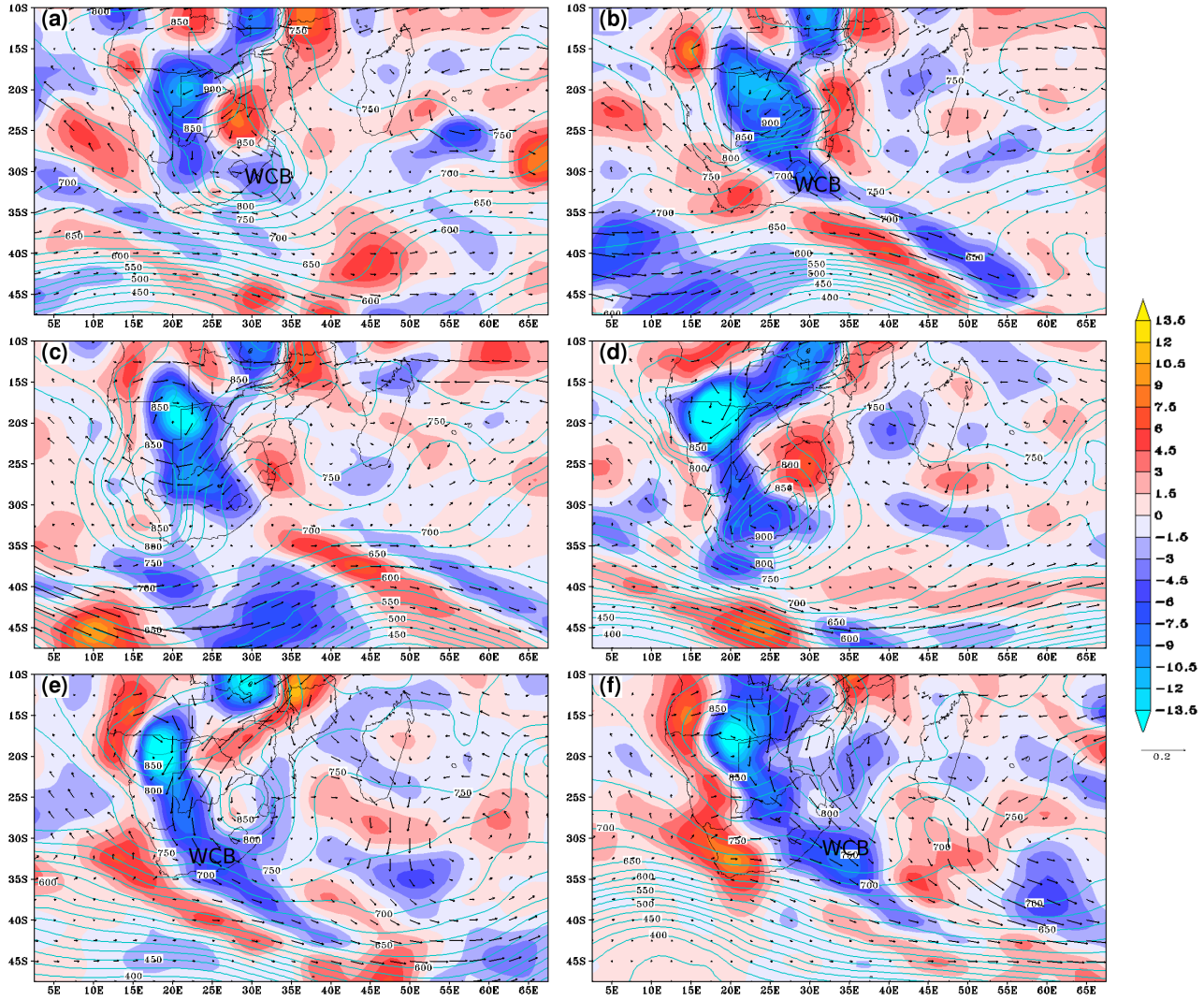

Figure 5: Moisture transports (vectors, $g.kg^{-1}.s^{-1}$), moisture convergence (shaded, $1*10^{-8}g.kg^{-1}.s^{-1}$) and pressure (contours, hPa) at 309K for 31 December 1997 (a), 1 January 1998 (b), 2 January 1998 (c) [case I] and 5 January 1998 (d), 6 January 1998 (e), and 7 January 1998 (f) [case II]. Regions of moisture export off Africa and into the mid-latitudes are noted as warm conveyor belts (WCB).

3.2 Case II: 5-7 January 1998

Rainfall on 5 and 6 January 1998 is shown in Fig.2 (b and c) with the synoptic evolution of the event presented Fig.4 (panels as in case I). Near-surface moisture transports are displayed in Fig.5, panels (d), (e) and (f).

The development of this second event was promoted by a strong Angola low facilitating transport of moisture into the semi-arid subtropical southern Africa during 2 - 4 January 1998. The stationarity of the synoptic situation during this period allows a tentative inference to be made from the isentropic plots that the moisture was primarily sourced from the tropical Indian Ocean and transported in a low-level easterly jet across the northern Madagascar (Fig.5 c). The tropical southeast Atlantic was a secondary source with moist onshore flow over Angola (Fig.5 c, d, e) during this build-up period.

On 5 January 1998, strong low-level northeasterlies were present on the southeastern flank of the intense Angola Low as indicated by strong 850hPa convergence (Fig.4 a). OLR indicated convection had already begun to occur in the extreme southeastern interior of South Africa (Fig.4 a). This convection was promoted by upper-level divergence ahead of an upper-tropospheric trough, approaching from the west (Fig.4 b).

Moisture transport deep into subtropical southern Africa was likely due to the formation of a low-level west coast trough as suggested by both 850hPa surface and 309K surface circulation. The favourable large-scale synoptic situation and continued moisture supply resulted in the dry central to western South Africa experiencing station rainfall totals of up to 50mm for 5 January 1998 (Fig.2 b).

By 6 January, a mature TTT had formed linking deep convection over much of southern Africa to the frontal cloud of a mid-latitude cyclone in the SWIO (Fig.4 c). Although not visible at 850hPa, substantial export of moisture into the mid-level extratropics was occurring along the axis of this cloud band (Fig.5 e).

Baroclinic wave growth, due to the warm, poleward flow in the lower troposphere rising into the temperate latitudes, had amplified the upper-level trough as it moved over southern Africa (Fig.4 d), increasing curvature in the upper-level flow. This wave growth intensified the upper-level divergence favouring convection and was further reinforced by the upper-level divergent response to convective activity already occurring in the cloud band. Heavy showers, supported by the intensified large-scale forcing, continued to fall over much of South Africa on 6 January, although generally further east than the previous day (Fig.2 c).

Substantial precipitation was recorded on 7 January 1998 over the eastern subcontinent with intensified convection indicated by very low OLR east of 25°E (Fig.4 e). The TE cloud band was not as prominent as the previous day due to rapid westward propagation of the mid-latitude frontal cloud, however strong TE flow at lower-levels continued to support significant export of moisture from the tropics (Fig.5 f). The upper-tropospheric flow over southern Africa had become more zonal with upper-level divergence now confined to the subtropical subcontinent and the mid-latitude cyclone in the SWIO.

Interestingly, a second OLR minimum (Fig.4 a, c, e, 25°S, 50°E), associated with a sharp upper-level trough over Madagascar, formed during 2-6 January 1998. This feature linked up to the mid-latitude cyclone on 7 January 1998 to form a secondary TE interaction site southwest of Madagascar.

During the following 2 days (8-9 January 1998), a second higher-amplitude mid-latitude trough approached from the west (not shown) reinvigorating the export of tropical moisture to the extratropics. As as result, heavy rainfall occurred over Mozambique and the SWIO. A particularly striking feature of this renewed TTT is that there was a well defined cloud band present over both South America and the central South Indian Ocean. The co-manifestation of South American and southern African cloud bands is addressed further in section 5.

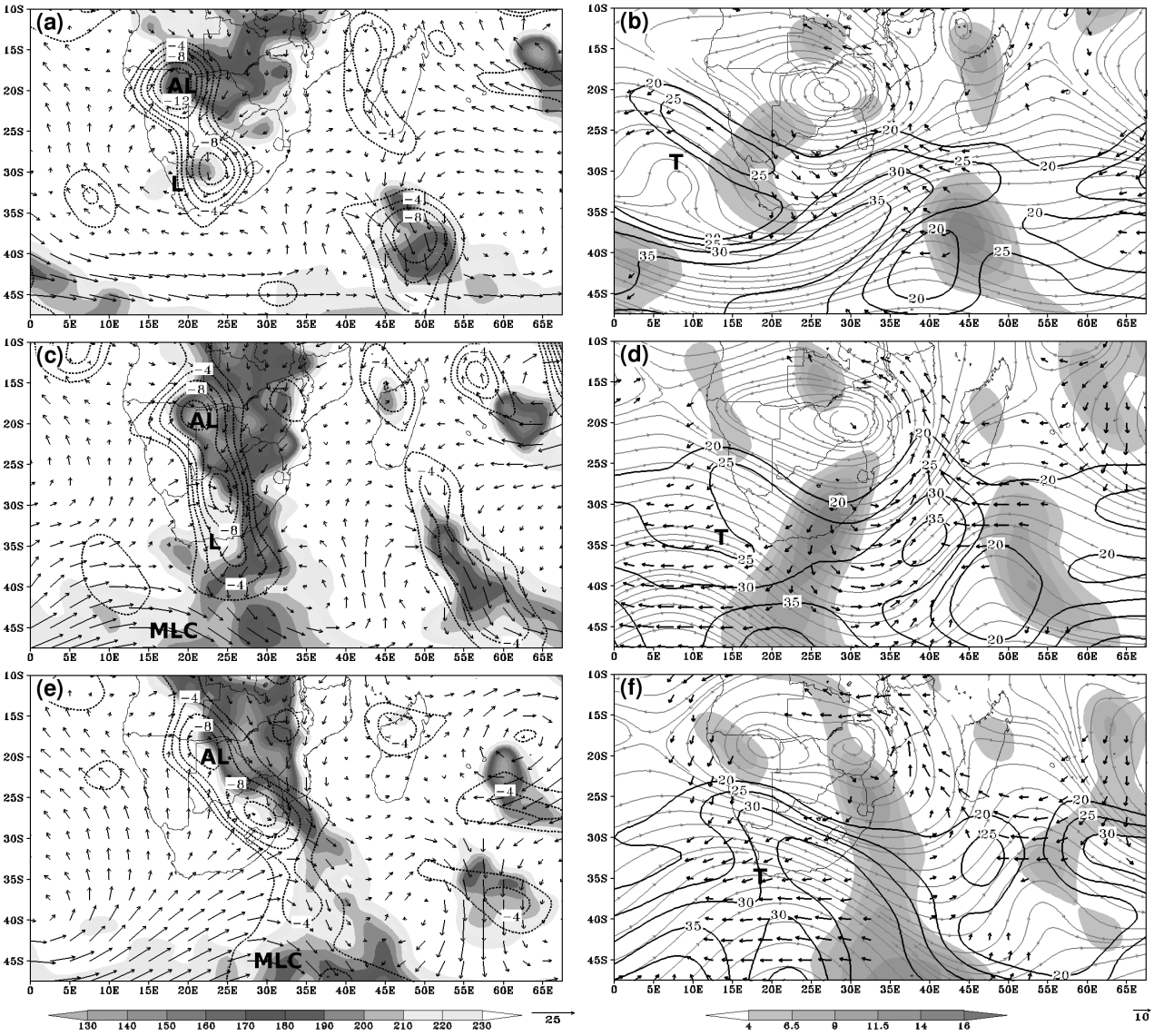

Figure 6: As in Fig. 3, but for 15 December 2007 (a and b), 16 December 2007 (c and d), and 17 December 2007 (e and f) (case III).

3.3 Case III: 15-17 December 2007

Upper and lower-level synoptic evolution is shown in Fig.6 for 15, 16 and 17 December 2007 with satellite rainfall estimates for 16 and 17 December 1998 displayed in Fig.8. Unfortunately, WRC station data are not available after 1999. Moisture transports on the 312K surface are presented in Fig.7 for the period 15-18 December 2007.

On 15 December 2007, cyclonic circulation around the well-expressed Angola Low resulted in the northwesterlies over Angola, converging with northeasterlies across Botswana. The latter extended into South Africa, where weak convective activity was beginning to occur (Fig.6 a). Divergence ahead of an approaching upper-level trough (Fig.6 b) appeared to have encouraged a cyclonic disturbance to form in the lower troposphere (30°S, 17°E) and promote onshore flow into the more southerly 850hPa convergence maximum.

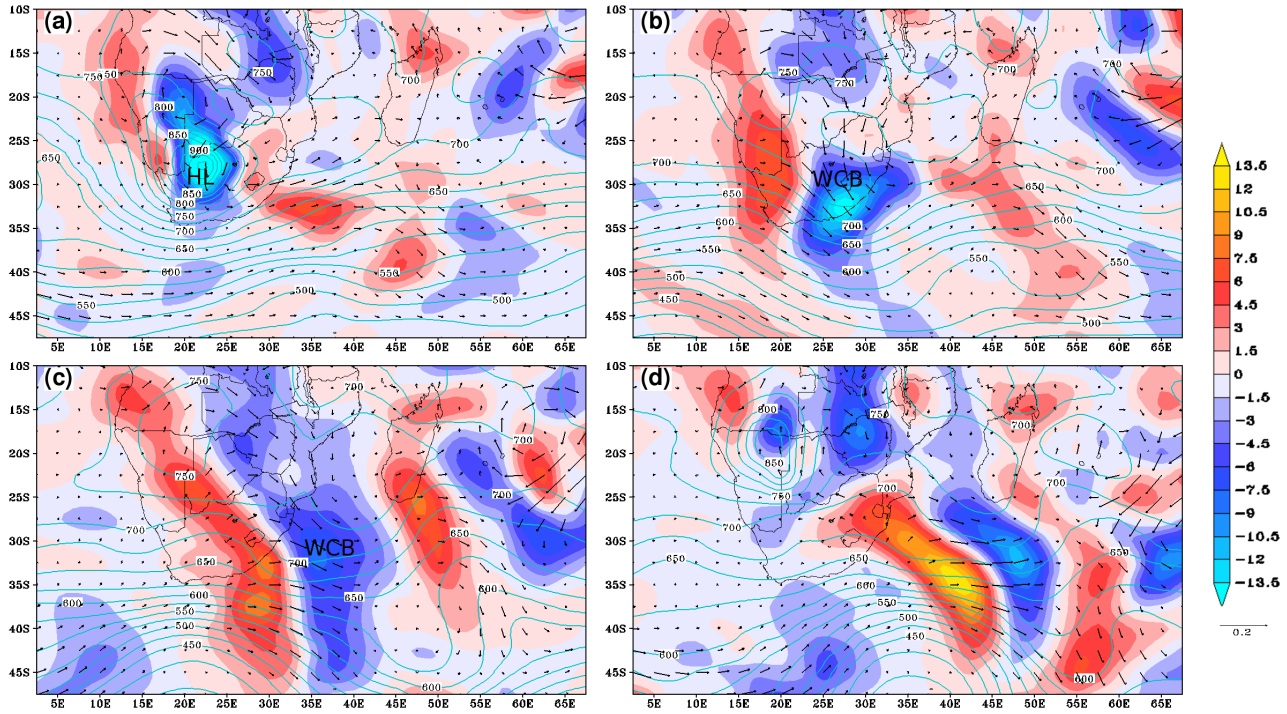

Figure 7: As in Fig. 4 but at 312K on 15 December 2007 (a), 16 December 2007 (b), 17 December 2007 (c) and 18 December 2007 (d) (case III).

Moisture transport into the subtropical subcontinent was facilitated by the Botswanan northeasterlies, with at least some moisture entering from the east, below the 312K level (not shown). A substantial contribution also seemed to come from central tropical Africa (Fig.7 a). A similar moisture transport field persisted into 16 December, allowing time for air parcels to follow trajectories implied by these daily mean moisture fields. Strong moisture convergence in the arid Kalahari Desert was co-located with a continental heat low, implied by a sharp drop in isentropes in a vertical cross section (not shown) of the feature.

By 16 December 2007, a band of cloud extended from tropical Africa through the subtropics into the frontal cloud of a mid-latitude depression (Fig. 6 c). Cyclonic flow around the Angola Low, was being diverted further south into the strengthened cyclonic disturbance over South Africa.

Baroclinic growth, due to poleward flow of warm continental air in lower-levels, deepened the upper-tropospheric trough and strengthened the upper-level divergence on its leading edge (Fig.6 d). Deep convection likely helped reinforce this divergence, further strengthening the near-surface depression.

Tropically sourced moisture was transported along the cloud band axis into a region of strong moisture convergence where flow was rising polewards, into mid-levels, as it left the continent (Fig.7 b). This substantial supply of moist air supported the widespread heavy rainfall over much of southern Africa (Fig.8 a). Interestingly, there was a split in regions of heavy precipitation over South Africa; namely, a north-eastern region with maximum rainfall in Mozambique, and a southern region maintained by strong vertical velocities below the upper-level divergence here.

By 17 December 2007, the cloud band gained the typical NW-SE orientation of Case I and II as the southerly cyclonic disturbance was incorporated into the eastward moving mid-latitude cyclone (Fig.6 e). The Angola Low retained its expression continuing to encourage flow of tropical air in the subtropics and supporting the deep convection over Zimbabwe.

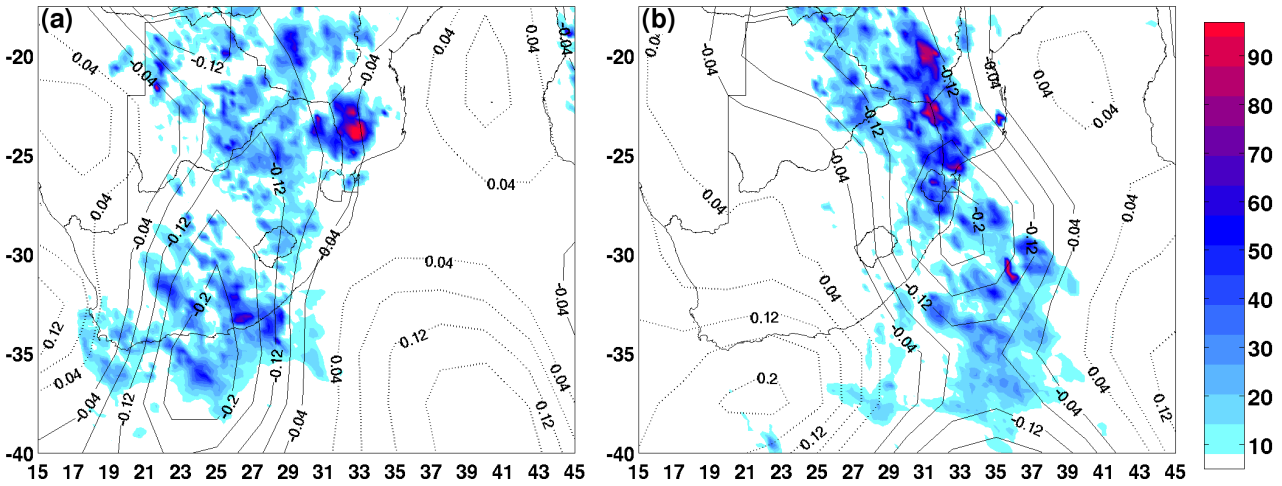

Figure 8: TRMM estimated accumulated 24hr rainfall (mm) and 700hPa full omega (contoured every 0.04 Pa.s^{-1}) on 16 December 2007 (a) and 17 December 2007 (b) (case III).

The upper-level trough became positively tilted, with subgeostrophic flow near its axis and convection in the cloud band promoting a TE band of upper-level divergence (Fig.6 f). This large-scale situation favoured continued heavy precipitation over Mozambique and the SWIO (Fig.8 b).

Tropical moisture supporting this rainfall pattern was still directed off the continent, rising into the mid-level troposphere above the SWIO, along a well-defined band of moisture convergence (Fig.7 c). By the following day, the moisture flow off the continent ceased as the mid-latitude wave continued eastward, breaking the band of moisture convergence (Fig.7 d). Despite this situation, a weak expression of the TE cloud band remained visible on 18 December 2007.

Similar to Case II, full maturation of this event during 17 to 18 December 2007 was also synchronous with weak TE cloud band development rooted in South America.

4 Forcing Factors for Precipitation

In this section, processes producing the uplift responsible for the heavy precipitation of these three events are explored. A simple calculation of topographic uplift using NCEP winds produced no useful result since the regional topography is poorly represented at such a coarse resolution. Similarly, lack of mesoscale data limited investigations into uplift due to convection. Thus, only large-scale synoptic forcing is assessed here.

In the QG framework, uplift can be produced by adiabatic temperature advection, which is generally stronger in the lower troposphere, and positive vorticity advection, which is primarily performed by upper-tropospheric troughs. QG omega was calculated using the traditional omega equation (Eq. 1) for a limited domain (7.5 to 45°S, 7.5 to 60°E) on the standard 17 pressure levels of the NCEP 2 reanalysis.

$$\left(\nabla_p^2 + \frac{f_0^2}{\sigma}\frac{\partial^2}{\partial p^2}\right)\omega = -\frac{f_0}{\sigma}\frac{\partial}{\partial p}\left(-\vec{v}_g \cdot \nabla_p \zeta_g\right) - \frac{R}{\sigma p}\nabla_p^2\left(-\vec{v}_g \cdot \nabla_p T\right) \quad (1)$$

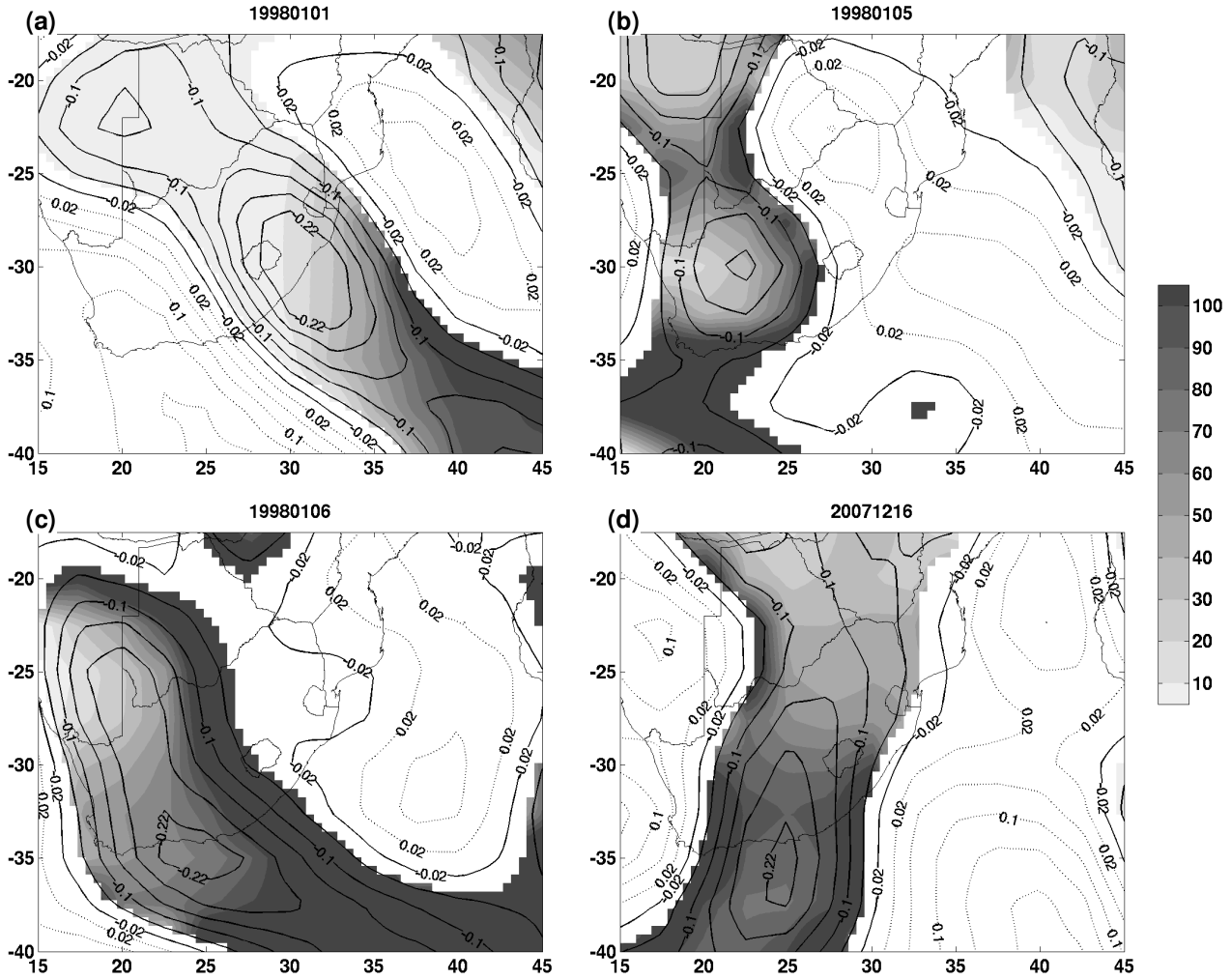

Figure 9: 500 hPa NCEP omega (contoured every 0.04 Pa.s^{-1}) and percentage of NCEP omega explained by QG uplift (shaded, %) on (a) 1 January 1998, (b) 5 January 1998, (c) 6 January 1998 and (d) 16 December 2007.

In solving Eq.1, QG omega (ω) was assumed to equal full NCEP2 omega (w) at the domain boundaries and f_o was calculated for 30°S. The equation was solved using the freely available Octave software's built-in linear equation solver, which relies on the LAPACK libraries.

The Rossby number was calculated at each grid point for each day with $R_0 < 0.15$ for the whole domain in days prior to and including the extreme rainfall days. Low R_0 indicated that the assumption of nearly-geostrophic flow was appropriate, which allows use of the QG framework and Eqn. 1. Values only exceeded 0.3 in days following the events as the baroclinic waves amplified and wind speeds increased. Good spatial coherence of QG omega field with the full uplift field was found, which together with the low Rossby numbers, gives confidence to the following analysis.

The percentage of total 500hPa upward motion attributable to QG forcing is displayed in Fig.9. The full omega field is overlaid for reference. Since this investigation focuses on uplift forcing only, this percentage was only calculated where w < -0.04 Pa.s^{-1}.

On 1 January 1998, 50% of uplift in the region of strongest vertical velocities (Fig.9 a, 30°S, 32.5°E) appeared to be due to QG forcing . QG forcing however, was clearly remote from the core precipitation region with convection

likely the dominant rain-producing process across the subcontinent. As expected from theory, QG forcing become more dominant in the mid-latitudes, towards the poleward end of the cloud band.

The 5 January 1998 case (Fig.9 b) showed half the total uplift explained by ω in the main precipitation zone over the southwestern interior of South Africa. This result suggests that QG forcing may have acted as a trigger for convection in a region which had been primed with tropically sourced moisture (see subsection 3 b).

On 6 January 1998 (Fig.9 c) much of the uplift was explained by QG processes, especially along the east of the core uplift region and extending polewards. Indeed much of the widespread precipitation on this day was to the east of this core uplift region, co-located with the dominant QG forcing.

On 16 December 2007, TRMM rainfall estimates had strong spatial coherence with the core uplift region (Fig.8 a). Results in Fig.9 (d) for the south coast zone of rainfall (25°E, Fig.8) suggest the QG forcing was the primary precipitation driver, which matches well with the strong upslope flow on the 312K surface in the region (Fig.7 b). This would be captured by the temperature advection term in Eq. 1 (2nd term, right-hand side). Rainfall in the north of the domain appeared to be more convectively driven with QG percentages less than 40%, implying a weakening role of QG forcing towards the tropics.

5 Planetary Waves

The large-scale planetary wave aspects of TTT formation are discussed with the aid of PV maps, an analysis which to the authors' knowledge, has never been performed for southern African TE interaction events. Diabatic destruction of PV is calculated following the method described in Posselt and Martin (2004) based on latent heating rates calculated after Emanuel et al. (1987) and applied to the PV context by Cammas et al. (1987). Positive values imply PV reduction by latent heating and, together with PV advection, provide a useful information regarding the evolution of the PV field. To avoid confusion due to Southern Hemisphere PV being negative, strongly negative values of this property will still be referred to as high PV and weakly negative values as low PV, consistent with this property increasing polewards, as in the Northern Hemisphere. Similarly, positive values of diabatic PV tendency and advection are regarded as reducing potential vorticity.

5.1 Case I

PV evolution for 31 December 1997 and 1, 2, 4 January 1998 is presented in Fig.10 (a-d).

On 31 December 1997, a PV trough passing south of Madagascar left a low-latitude streamer of marginally higher PV air (1 PVU) across subtropical southern Africa (Fig.10a). This streamer likely encouraged a surface depression, initiating moisture transport deeper into the subtropics. A weak PV trough had begun to form near 20°E, amplifying into 1 January 1998. It was on the the leading edge of this PV trough that the TE cloud band of case I occurred. The strongest (> 2 PVU.day^{-1}) diabatic PV destruction (Fig. 10 b, 75°E) of any of the cases presented here took place downstream of this trough in a PV ridge that rapidly amplified into the extratropics the following day (Fig. 10 c).

Meanwhile, upstream of the trough, moderate diabatic PV destruction near 10°E (Fig.10 b) and southeastward advection of low PV air initiated an anti-cyclonic wave breaking event on 2 January 1998 (Fig. 10 c) that ultimately

resulted in the PV field observed on 4 January 1998 (Fig. 10 d). The presence of the high PV air over the subcontinent in Fig.10 d would have favoured a surface depression facilitating advection of tropical moisture into the subtropics.

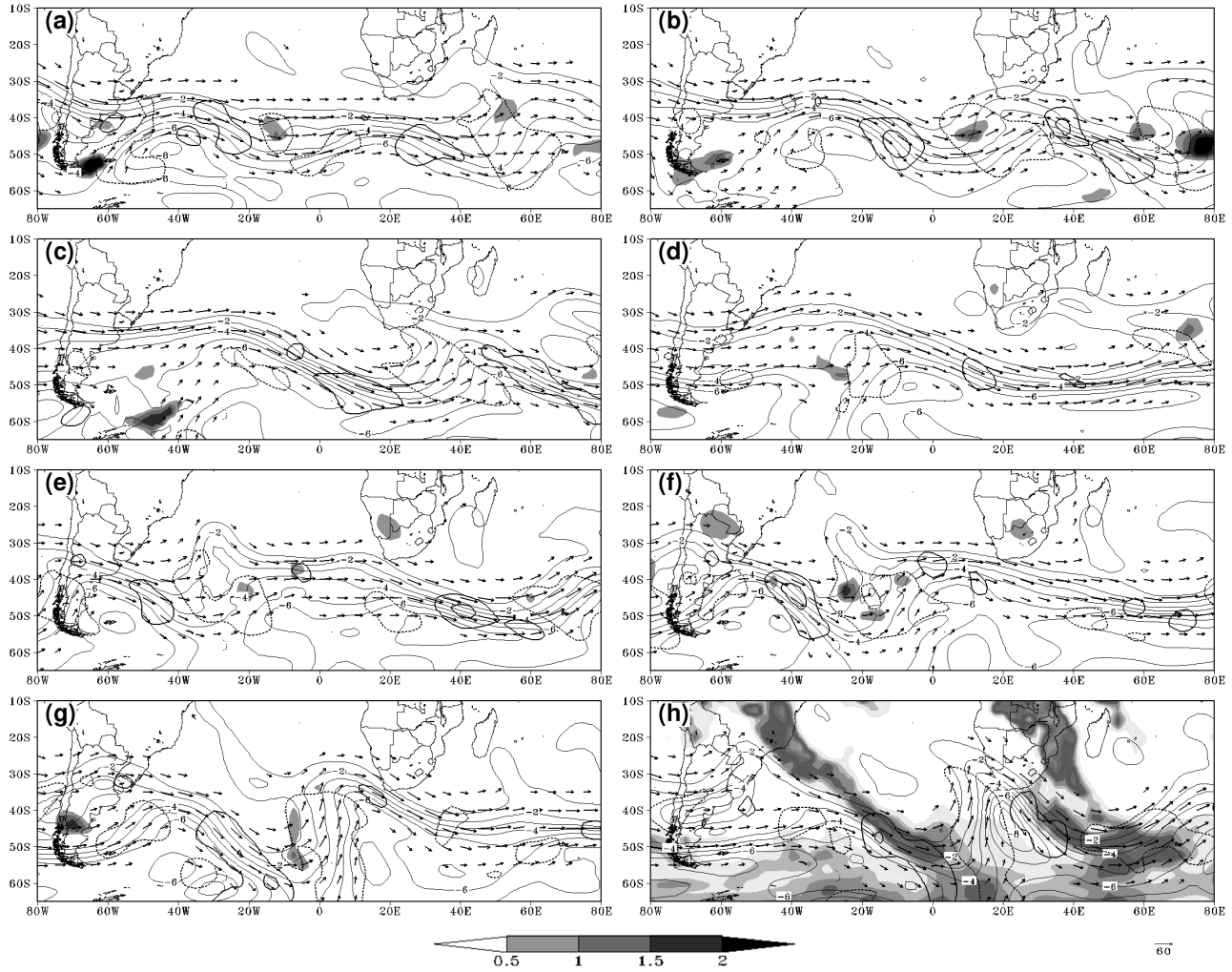

Figure 10: 345K potential vorticity (thin contours, PVU), PV advection (thick contours starting at +(-)3 PVU.day^{-1} with positive advection dotted, negative advection solid) and 345K diabatic PV tendency (shaded, PVU.day^{-1}) on 31 December 1997 (a) and 1 January 1998 (b), 2 January 1998 (c) [case I] then 4 January 1998 (d), 6 January 1998 (e), 7 January 1998 (f), 8 January 1998 (g), 9 January 1998 (h) [case II]. Vectors represent 345K winds >20 m.s^{-1}. Note: shading for (h) depicts OLR (W.m^{-2}, color scale as in Fig. 3)

5.2 Case II

PV maps for 6 - 9 January 1998 are shown in Fig. 10 (e-h). The PV situation on 5 January 1998 was very similar to 4 January 1998 and is therefore not plotted.

A broad, longwave PV trough to the east of southern Africa on 4 January 1998 (Fig. 10 d) finally neared southern Africa on 6 January 1998 (Fig.10 e). The case II TTT event thus did have some association with the leading edge of a weak trough.

Upstream, in the southeast Atlantic, substantial PV advection (>3 PVU.day^{-1}) had begun to deform a lower latitude PV trough (axis at 30°W), downstream of a confluence of a subtropical jet and polar jet over South America. This structure intensified into 7 January 1998 (Fig.10 f) with the PV gradients in the jet confluence (50°W) tightening and downstream diabatic PV destruction contributing to rapid ridging of low PV air into high latitudes as seen 8 January 1998 (Fig.10 g). The continued ridging contributed to strong equatorward advection of high PV air into a PV trough.

By 9 January 1998, the trough had reached southern Africa and the strong poleward flow on its leading edge reinvigorated the decaying TTT in the region (Fig.10 h). Downstream of Africa it appeared that the trough encouraged an anticyclonic wave breaking event over the South Indian Ocean in the following days (not shown).

Over South America, the subtropical jet had been displaced equatorward, leading to a TE cloud band linking tropical Brazil to the subtropical-polar jet confluence deep in the high-latitude South Atlantic.

5.3 Case III

PV evolution for the period 14 - 19 December 2007 is displayed in Fig.11. A low amplitude anticyclonic wave breaking event occurred near southern Africa at about 40°S on 15 December 2007 (Fig.11 b) as the PV streamer present on 14 December 2007 (Fig.11 a) was separated from the high PV reservoir. The cut-off appeared to become incorporated into a PV trough on 16 December 2007 (Fig.11 c), the arrival of which signified the start of heavy rainfall over southern Africa.

This trough appeared to be the remnant of a trough involved in minor anticyclonic wave breaking near 20°W (Fig.11 a) on 14 December 2007 which propagated quickly east and began to re-amplify as baroclinic growth occurred due to warm advection off the subcontinent.

By 17 December 2007 (Fig.11 d), the PV trough had gained a positive tilt as advection continued to deform the PV field south of Africa. The continued growth of the PV trough encouraged strong poleward flow of the TTT now positioned over the SWIO. Tilting of the trough continued into 18 December as anti-cyclonic wave breaking clearly began to occur (Fig.11 e). A clear TE cloud band on the trough's leading edge was now concomitant with a similar structure emanating from South America.

On 19 December 2007 (Fig.11 f) the wave breaking event left a PV streamer extending from the south coast of southern Africa into the SWIO, potentially prolonging showers in the wake of the TTT.

6 Discussion

In this section, common features of the three case studies are discussed and compared to previous TTT studies and TE interaction globally.

The Angola Low, a well-documented feature of southern African summer circulation (Reason et al., 2006), was well-formed during the early stages of all of the events and appeared to weaken somewhat during their evolution. Its primary role in these cases was to facilitate moisture transport into subtropical southern Africa. A relatively small contribution of moisture from the eastern tropical South Atlantic Ocean, a source noted in (D'Abreton and

Lindesay, 1993; D'Abreton and Tyson, 1995; Cook et al., 2004), was brought onshore by westerlies to the north of the Angola Low in case I and III. However, the primary moisture supply occurred in the low-level northeasterly flow on the southwest flank of the low. This flow conveyed moisture from the tropical Indian Ocean, a primary moisture source for southern African rainfall (Walker and Lindesay, 1989; D'Abreton and Tyson, 1995; Todd et al., 2004).

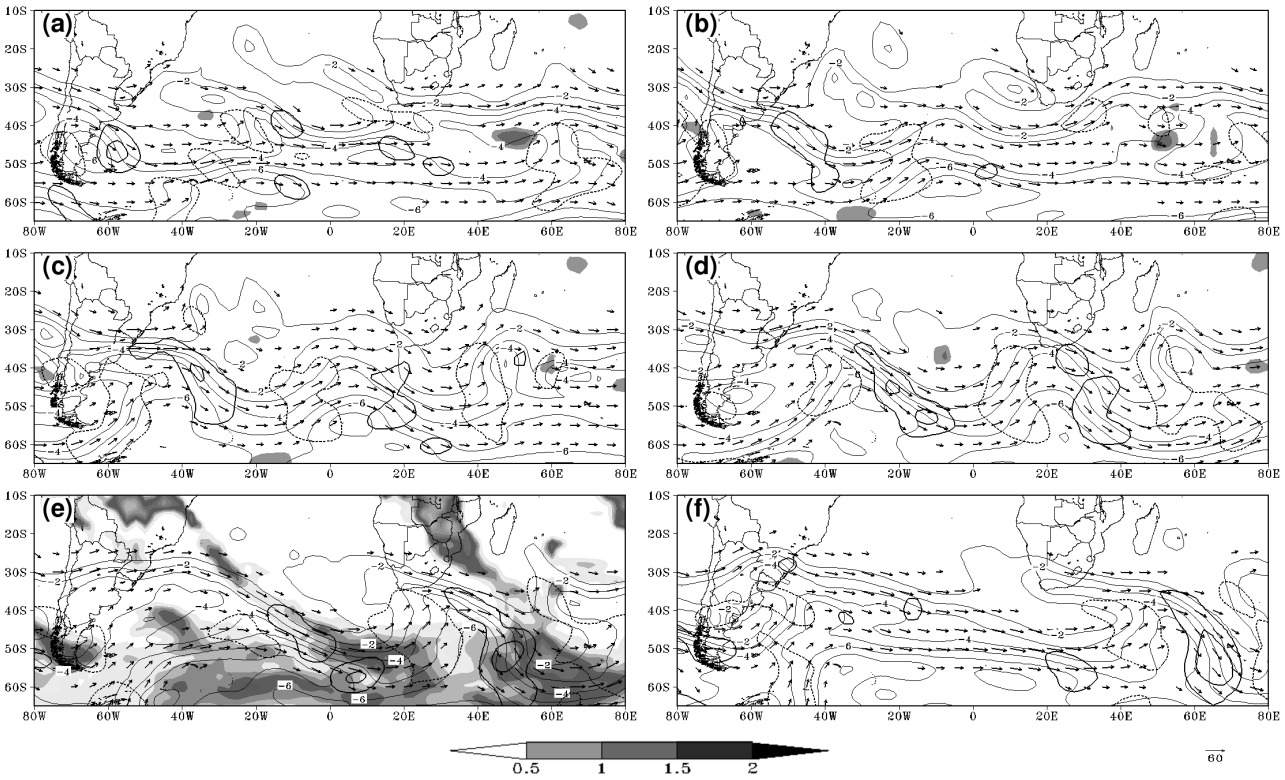

Figure 11: As in Fig. 10 but for 14 December 2007 (a), 15 December 2007 (b), 16 December 2007 (c), 17 December 2007 (d), 18 December 2007 (e), 19 December 2007 (f) [case III]. Note: shading in (e) depicts OLR, as in Fig.10 (h).

A secondary , low-level low pressure feature was present near the Namibia-South Africa border 2 days before extreme rainfall days in case II and III, acting to divert moisture deeper into the subtropics. Upper-level divergence downstream of an upper tropospheric trough was likely responsible for the development of the low-level cyclonic disturbance. In case III, a similar process occurred further east. Isentropic surface depressions in early stages of all cases but especially case III indicated that continental heat lows were co-located with regions of intense moisture convergence in the semi-arid Kalahari Desert.

In all three cases, TE cloud band formation was finally triggered by the arrival of an upper-level trough over southern Africa associated with band of divergence east of its leading edge. These cases corroborate the conclusion of previous studies regarding the importance of upper-tropospheric troughs to TTT development (eg. Harrison, 1984; Lindesay and Jury, 1991; Lyons, 1991). The poleward extremity of all three TTT events was associated with a mid-latitude depression beneath the jet core, downstream of the trough.

Once the TTTs were fully developed, moisture was transported off the continent along the axis of a band of moisture convergence, rising from near 800 hPa over the landmass into mid-level flow (700-650 hPa) in the mid-latitudes. This transport is consistent with trajectory analysis of a TTT event on 22 January 1981 (Fig. 4 D'Abreton and Tyson, 1996) and work on TE interactions over North Africa by Knippertz and Martin (2005).

All three cases exhibit the key ingredients common to the well studied tropical-extratropical interactions found in other regions of both the Northern Hemisphere and Southern Hemisphere, broadly termed tropical plumes (summarised in Fig.11, KP07). We argue that TTTs generally fall within the theoretical framework put forward in KP07. A distinction that TTTs have from similar events in the North Pacific and North Atlantic is their formation over a landmass. Many oceanic "tropical plumes" discussed in KP07 only have mid- to upper-level cloud through the subtropics. In the southern African context however, continental heating can support deep convection and heavy rainfall along the full extent of the cloud band.

The results of the uplift forcing analysis compare well with the results of Knippertz and Martin (2005) that QG forcing plays a significant role in promoting the uplift observed in TE interactions. Nevertheless, the heaviest rainfall of these three events was recorded in case I, where QG forcing was weak, implying the role of convective overturning. Spatial inhomogeneities in the magnitude of the rainfall for all cases (eg. the extreme precipitation over Mozambique during case III) suggests phenomenon such as mesocale convective systems (eg. Blamey and Reason, 2009) may be embedded in TE cloud bands, at least over South Africa. Indeed, De Coning et al. (1998) found the tropical root of a TTT on 12 February 1996 to be a mesocale convective vortex centered near the Angola Low.

Attempts were made to investigate the role of inertial (and symmetric) instability in aiding development of the TTTs (Mecikalski and Tripoli, 1998; Knippertz and Martin, 2005); however, calculating these parameters from the 2.5°x 2.5° NCEP reanalysis produce no regions of instability, which is not unexpected, given the coarse resolution of the data and the mesoscale nature of instability regions.

A final aspect of these TE interactions over southern Africa is that they are clearly related to planetary wave structures which, although alluded to in Todd et al. (2004), have not been demonstrated before. Anti-cyclonic wave breaking a few days before each TTT event left a weak (1-2 PVU) PV streamer across the southern subcontinent, with this low PV air aloft, encouraging a surface low to initiated poleward moisture transport into subtropical southern Africa. Convection and cloud band formation were triggered when the leading edge of an amplifying PV trough neared the subcontinent's western margin, promoted both by baroclinic wave growth near southern Africa and upstream deformation as low PV air was advected polewards. The wave breaking events in the South Atlantic agree well with research by Postel and Hitchman (1999).

In case II and III, similar cloud band features evolved concurrently over South America, emphasising these systems are results of large-scale planetary wave growth and decay. Indeed the TE interactions presented here, appear sensitive to upstream perturbations in both the subtropical and the polar jet over South America. Downstream of southern Africa ridging of low PV air into the extratropics (case II) and anticyclonic wave breaking (case I and II) suggested TTTs contribute to significantly South Indian Ocean planetary wave activity.

7 Climatological Implications

The key role of the Angola Low in TTT development in these three case studies provides support to previous climatological studies linking the strength of the Angola Low to rainfall variability over southern Africa on the seasonal to interannual timescale (Rouault et al., 2003; Cook et al., 2004; Reason and Jagadheesha, 2005; Reason et al., 2006). The weak moisture transports from the South Atlantic associated with the Angola Low also corroborates recent work by Hermes and Reason (2009) and Vigaud et al. (2009).

An interesting feature of case II and III was their development over the central subcontinent, but full maturation over Mozambique and the southwest Indian Ocean. Composite studies (Todd and Washington, 1999) and climatology

(Cook, 2000) do not capture this behaviour and indicate only that the dominant position of the systems lies over the southwest Indian Ocean, understandable due to this being the region in which the systems manifest most strongly. The current study reveals the importance of resolving these systems on the synoptic scale to capture the development stages of TTTs over the continent.

The development of these three cases over the subcontinent and their eastward propagation agrees well with the results of Fauchereau et al. (2009). Their cluster no. 3 looks very similar to the early stages of the three cases presented here and, although only 15% of the days following it are assigned to a cluster describing TTTs, we hypothesize that this 15% corresponds specifically to extreme rainfall events over semi-arid central South Africa. Further investigations would be needed to confirm this hypothesis.

Although TTTs are recognised as the primary rain producing system in the South African summer season, little work has been done to link them directly to wet spells. The quick succession of Case I and II produced a 7-day wet spell during which more than 40% of the 1997/1998 NDJF season's rainfall was recorded over much of South Africa (Fig.2 d). This contribution is particularly notable since South Africa recieved near-average rainfall during this season, despite a strong El Nino event, which often causes drought.

The influence of large-scale modes that produce significant mean Rossby wave perturbations, such as the Pacific-South America pattern (Mo and Nogues-Paegle, 2001; Colberg et al., 2004) and the El Nino Southern Oscillation extra-tropical response over the southern African region remain poorly understood. The clear link between synoptic scale PV wave activity and TTTs demonstrated here is therefore an important point to consider in studies looking for teleconnections between subtropical southern Africa and the Pacific Ocean. It further highlights the need for scale-interactions studies linking synoptic scale rainfall to season total precipitation.

8 Conclusion

Investigation of the three heavy precipitation producing TTT events over southern Africa was performed using the NCEP 2 gridded data set (Kanamitsu et al., 2002), allowing a comprehensive study of the synoptic evolution of each system. Comparison of these three events revealed clear similarities with one another and with previous TTT case studies. We conclude that TTTs, despite some minor differences, are similar to TE interactions observed elsewhere and do fit the theoretical framework developed by KP07.

Uplift forcing analysis of the vertical velocities and associated heavy rainfall of the three events presented here indicates adiabatic temperature advection and positive vorticity advection play a significant role in producing uplift in TTTs. It is clear however that local land-based convection is as important, especially in the subtropical portion of the cloudband. A high-resolution mesocale model would be needed however, to more fully assess this contribution and capture the details of the precipitation field. The fact that heavy rainfall is produced along the full length of these TTT cases highlights a key difference between TE interactions occurring over landmasses or oceans.

The importance of planetary waves for TTT-development is demonstrated, motivating for the necessity of a more detailed investigation of this aspect of TTTs. The key finding of this study is that TTTs are embedded within planetary wave structures, are influenced by upstream perturbations, and in turn, influence wave activity in the South Indian Ocean. This result highlights the South Atlantic and South Indian Ocean as regions where vigorous planetary wave activity influences lower latitude cloudiness associated with TE interactions, similar to processes occurring in the North Atlantic context as discussed in Knippertz and Martin (2007).

In conclusion, this study has identified the key components necessary for TTT development, providing insight to further studies investigating regional rainfall variability related to TTT formation over southern Africa. Additionally, the study has discussed TTTs in context to TE interactions that occur globally.

Acknowledgements

Marlan Perumal is thanked for assistance in calculating quasigeostrophic omega. Ross Blamey is thanked for helpful comments. Peter Knippertz is thanked for the effort he put into his reviews: they improved this paper, substantially. Interpolated OLR and NCEP2 data was obtained from NOAA/OAR/ESRL PSD, Boulder, Colorado, USA through http://www.cdc.noaa.gov.

Part II

Building an automatic cloud band identification system

How can the dynamics of these synoptic rainfall systems (TTTs) be quantified in a way that provides links to intraseasonal and interannual variability?

Specific Questions:

- What is an appropriate methodology to characterise the meteorology of all cloud bands in gridded data sets?
- Do characteristics identified in Part I hold in general for tropical temperature trough events?
- What are the preferred locations for cloud band development?
- Is the Angola Low a key feature in TTT synoptic development?

Robot n. *A mechanical device that sometimes resembles a human and is capable of performing a variety of often complex human tasks on command or by being programmed in advance.* - American Heritage Dictionary

Building a tropical-extratropical cloud band metbot

Abstract

An automated cloud band identification procedure is developed that incorporates detailed meteorology of such events over southern Africa. The conceptual background to the "metbot" development is discussed. Connected component labelling is used to detect blobs in various atmospheric fields. Outgoing longwave radiation is used to flag candidate days by thresholding the data and requiring detected blobs to have sufficient latitudinal extent and exhibit positive tilt. The Laplacian operator is used on gridded reanalysis variables to highlight features of meteorological interest. The methodology provides an automated detailing of the meteorology of 821 tropical temperate troughs in the region for the period 1979-2011. Those events that produce rainfall in a weather station data set for South Africa are used to explain advantages and pitfalls of the methodology. A case study of an event that occurred during 1 to 8 January 1998 illustrates the ability of the metbot to capture significant meteorology and rainfall of these weather systems. An assessment of event to event similarity of meteorological features is provided, highlighting features previous studies have noted as key ingredients to tropical temperate trough development. Finally, a composite life-cycle of cloud band development for southern Africa is presented. Usefulness of this tool to study multiscale interactions is discussed, emphasising the metbot's strength: it retains details of extreme and infrequent events. Suggestions are provided of uses and implications of the methodology to convergence zone studies, atmospheric river descriptions, and feature tracking in general.

A manuscript based on this part is in press in Monthly Weather Review:
"Building a tropical-extratropical cloud band metbot",
N.C.G Hart, C. J. C Reason and N. Fauchereau

1 Introduction

For the meteorologists of the 1970s and 1980s, manual inspection of satellite imagery and synoptic maps for features of interest was common place. Hours of work analysing series of images by hand substantially advanced our knowledge of earth's meteorology (eg. Streten, 1973; McGuirk and Ulsh, 1990). With continued growth of volumes of observational data available and computing advancements, automated feature detection in meteorological data became necessary and possible.

Many object-based methodologies, as they are commonly referred to, have been developed to identify weather features. Most widely applied examples include tropical and extratropical cyclone tracking (eg. Murray and Simmonds, 1991b; Benestad and Chen, 2006), cloud tracking including mesoscale convective systems (Carvalho and Jones, 2001)and remotely-sensed precipitation systems (Skok et al., 2009).

Feature detection is the corner stone of all these methodologies; a challenge that the field of computer vision is continually addressing. One the primary goals of this field is to provide computers with human-like visual processing abilities, an aim of all weather feature tracking algorithms. Hodges (1994) was perhaps the first to explicitly point this out and bring computer vision advances to bear. Scharenbroich et al. (2010) is a recent example of applying the huge leaps in computer vision and machine learning techniques to improve tropical storm tracking.

These methodologies have enabled automated production of climatologies of the various meteorological features they have been built to detect (eg. Murray and Simmonds, 1991a; Hodges and Thorncroft, 1998; Blamey and Reason, 2012). Their use in model evaluation and inter-comparison has provided invaluable insight into model performance (eg. Hodges et al., 2011). Perhaps the most elegant example of an objective automated feature-tracking procedure is presented by Hewson and Titley (2010). Their methodology identifies frontal systems and follows their evolution from the earliest point in their life cycle by incorporating mathematical definitions of extratropical cyclones into a feature identification procedure. A primary application is in producing storm track diagnostics from ensemble weather forecasts to aid human forecasters

These object detection methodologies exploit key identifying features of the weather systems they are built to track; however, they rarely provide a full meteorological description of these systems. This deficiency limits their use in describing and quantifying the mechanisms that facilitate scale interactions between weather and climate. Therein lies the thesis of this paper; a tool which can describe the full meteorology of many synoptic systems will be useful for studies attempting to link weather to large-scale climate variations.

Over subtropical southern Africa, a substantial portion of wet season rainfall is attributed to tropical-extratropical (TE) cloud bands (Harrison, 1984), know regionally as tropical temperature troughs (TTTs, Fig. 1). Part I described three heavy rainfall producing TTTs and by comparison with previous studies, summarised their typical meteorology for the region. Here that study is extended further to investigate scale interactions between these synoptic systems and large scale climate modes. To this end, a methodology is developed and presented in this paper.

The goal is to automate the synthesis of the meteorology of each cloud band, as described in gridded data sets such as reanalyses and general circulation model outputs. Key criteria for the success of the method include:

1. Robust and simple approach to flag potential cloud band events
2. Flexible method to recognise regions of interest in multiple meteorological fields

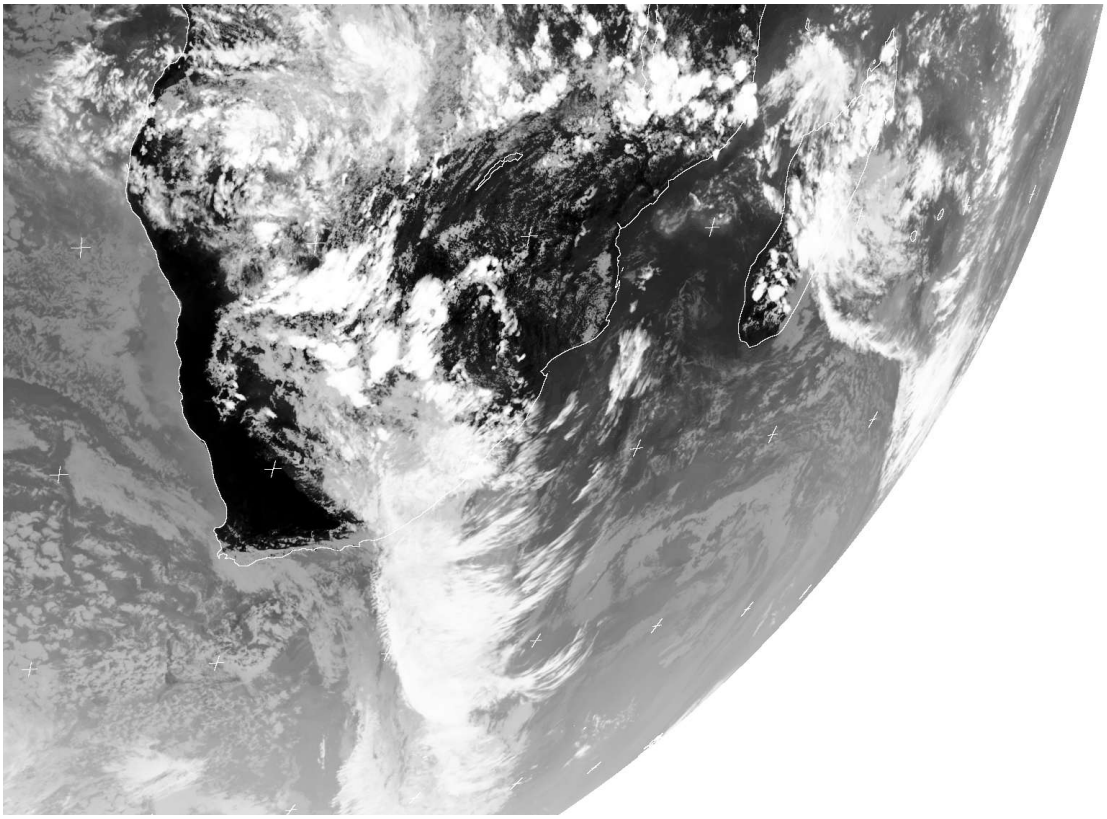

Figure 1: A TE cloud band over southern Africa at 12h00 on 19 January 2010 (Meteosat-9 ch. 9 - image courtesy of EUMETSAT)

3. Ability to synthesise regions of interest into a comprehensive description of the meteorology

In essence, this study seeks to develop a simple, computer-based approximation to the ability of a human meteorologist; a meteorology robot (metbot). This paper is intended as a short proof of the concept. To facilitate this, the approach is detailed in section 2, with three examples of the method's application presented in section 3. This manuscript demonstrates the ability of the methodology: to capture the meteorology of a previously well studied cloud band event, assess the likelihood of various features during cloud band formation over southern Africa, and use in creating composite evolutions based on the automated description of multiple events. The potential use of the methodology in scale interaction studies is discussed in the final section.

2 Methodology

2.1 Data

The Liebman and Smith (1996)optimally interpolated, outgoing longwave radiation (OLR) is used for the period 1979-2011 as the main observational data set. The daily mean OLR is the variable used to flag cloud band events. This is complemented by National Centre for Environmental Prediction/Department of Energy Reanalysis II (NCEP2) data for the same period, providing a description of thermodynamic and momentum variables (Kanamitsu et al., 2002). Example systems are confined to 1979-1999, a period covered by the Water Research Commission (WRC) daily station rainfall data set containing 7665 stations within South Africa (Lynch, 2003).

2.2 Building a metbot

Analysis of atmospheric data is primarily performed by humans visually analysing plotted data; this is what the approach tries to automate. Human experts can summarise images and identify notable features easily, for example, low pressure cells represented in sea level contour maps, or clusters of cold cloud. In short the problem can be stated: how do you enable a digital system to pick out meteorologically interesting features?

The analysis platform was Python: the Matplotlib with the Basemap toolkit provided plotting capabilities (Hunter, 2007; Whitaker, 2007), the NumPy module handled arrays (Oliphant, 2006), the PIL module was used for image manipulation, and the Python wrapper for OpenCV performed more advanced image manipulation (Bradski, 2000). Wrappers for CVblob C++ library (Liñán, 2008), built on OpenCV, identified blobs in images and obtained details of their location, size, and orientation. These open-source computer vision libraries are developed by the robotics research and applications community as part of the Robot Operating System (ROS) project.

The image analysis process is straightforward:

1. Stretch raw data, for example outgoing longwave radiation, onto the greyscale image range [0,255].
2. Translate a chosen threshold for raw variable into greyscale.
3. Plot image and fetch it from buffer to obtain a visual interpolation of data.
4. Apply threshold to this image array to produce binary image and perform connected component labelling to identify blobs.
5. Run appropriate filter through blobs to keep those of interest to your application, the "metblobs". In practise, filters were only used with rigour to flag cloud band blobs. They needed to have a certain latitudinal extent and be positively tilted (see below). With all other features a minimum area value filtered out the very small blobs.
6. Retain information describing blob contour, centroid position, orientation and area.
7. Repeat at each time step.

The implementation of the Chang et al. (2004) connected component labelling algorithm in Cvblob is the cornerstone of this methodology. It is a methodology for image segmentation. A short summary follows, however a detailed explanation of process in general can be found in Hodges (1994). Connected component labelling performs blob detection in a binary image by identifying adjacent pixels and labelling them as such. The process iterates until all pixels are labelled. Blobs thus emerge, and image moments are used to calculate their orientation, area and centroid (Fig. 2). This provides an intuitive summary of an image with massive reduction in dimensionality of data. For example, interpolated outgoing longwave radiation (OLR) at relatively coarse 2.5^oresolution may yield a 15 x 25 point lat-lon grid for a domain subset over southern Africa. These 375 data points may be reduced to 4 blobs of low OLR with position, area and orientation giving each blob 4 attributes; 16 meteorologically informative data points summarising 375.

Thresholding the images presents difficulty when the choice of an appropriate value is not clear. The frequency distribution of OLR values is bimodal (Fig. 3) describing a peak for cold cloud and one for clear skies so threshold choice is obvious. For geopotential height this is not the case however, the Laplacian ($\nabla^2_{x,y}$) of the field highlights

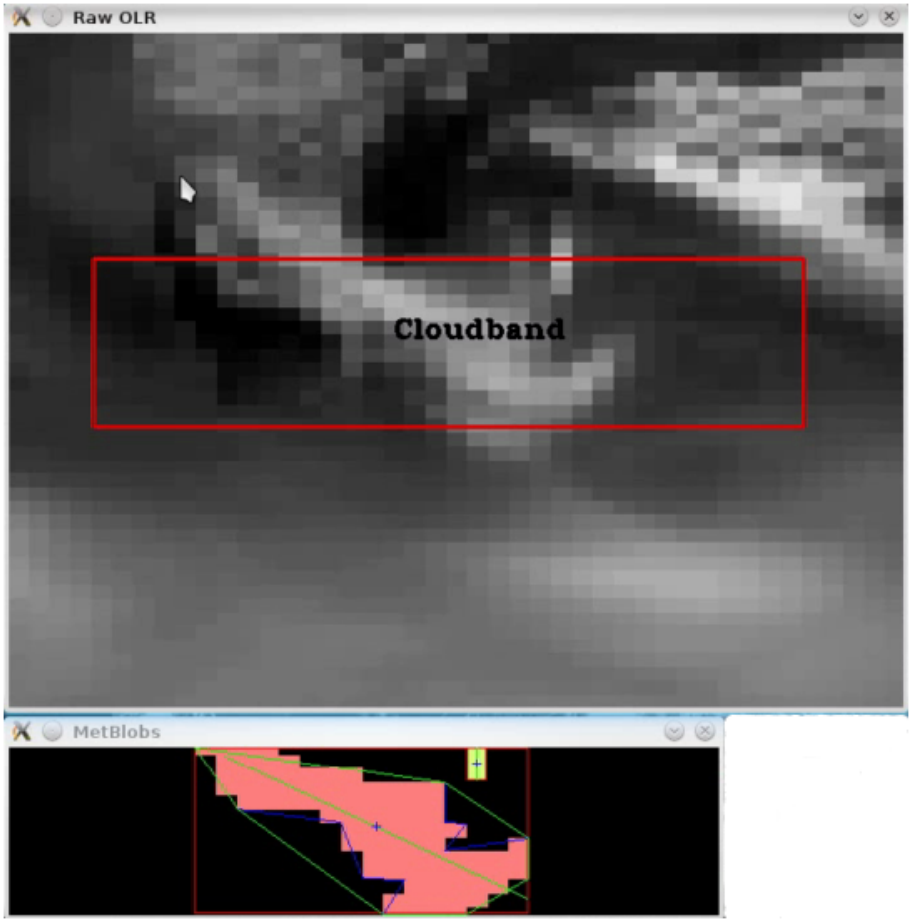

Figure 2: Raw OLR (top panel) and the results of connected component labelling (bottom panel) during the flagging process.

regions of lows or highs. $\nabla^2_{x,y}$ values are scaled by $1 - \frac{f}{f_0}$ ($f_0 = 2\Omega$) since intensities of depressions tend to be greater nearer the poles. This scaling by latitude meant both low and higher latitude depressions of interest can be displayed with the same colour scale. PyClimate is used to calculated Laplacians of the fields (Sáenz et al., 2002).

The frequency distribution of $\nabla^2_{x,y}$ values is well described by the Gaussian function (Fig. 3), so stretching and thresholding can be achieved simply: data is stretched onto interval $[-3\sigma, 3\sigma]$, thresholds can be specified as $\pm A\sigma$ where A is an arbitrary scaling term (σ = standard deviation of $\nabla^2_{x,y}$ values). Thresholding to select for meteorologically significant depressions is somewhat arbitrary, so in this study the parameter was chosen as $A = 1.3$, which seems to retain most interesting features. Using properties of the Gaussian distribution ensures comparability of analyses applied to different data sets as this is readily transferable.

The goal was to identify and describe tropical-extratropical cloud bands (Fig. 1). OLR was used to flag candidate events by ensuring blobs extended from 20^{o}S to 40^{o}S as a contiguous band and were positively tilted (the bearing from their continental root poleward was in the interval [95°,180°]). Fig. 2 illustrates this flagging process. An area criterion removes smaller features such as the yellow blob. The large blob meets both the required latitudinal extent and positive tilt requirement as indicated by the angle of the green line crossing through the blob centroid. The tilt criterion often failed due to contamination low OLR values along the ITCZ, producing blobs which extended eastward in the tropics. This produced negatively tilted angles. This problem was largely solved by only applying the positive tilt criterion, in a smaller domain (23-33°S) which only considers the subtropical portion of the band,

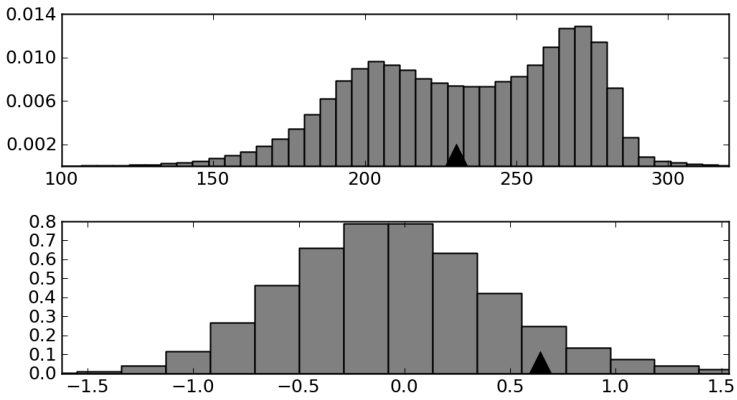

Figure 3: Probability distributions of grid-point values for OLR (top) and $\nabla^2\Phi_{850}$ (bottom). Triangles indicate threshold values (see section2.2)

while retaining the larger domain to ensure TE connection. Input NCEP2 data is reduced by only selecting for time periods 48 hours either side of these flagged OLR features.

The meteorology was described by calculating metblobs for geopotential height at 850, 500 and 250mb ($\nabla^2\Phi_{lev}$), uv-wind at 850 and 250mb, and moisture transports at 850, 700 and 500mb. Jet regions in both the wind and moisture flux fields were obtained by applying the Laplacian to the vector magnitude ($\nabla^2 |\langle u, v\rangle_{lev}|$). Again, somewhat arbitrarily, the amplitudes $A = 1.0$ and $A = 0.5$ were deemed appropriate to keep a useful level of detail in both the wind and moisture flux, respectively.

Meteorologists synthesise image features from different levels of different variables into coherent understandings of synoptic weather systems. Approximating this ability was the second key goal of building a metbot. It essentially involved further abstraction of the detected blobs on different levels. Tracks of blobs are built and then associated with tracks of the cloud band blobs. These associations are represented in events.

Blob feature synthesis:

1. Each set of metblobs is tracked by checking if there is any blob within a predefined radius in the subsequent image and matching to the closest if more than one exists.
2. Tracks of the reference blobs, OLR in this case, are checked for blobs that were flagged as cloud bands. If they do contain flags, they are kept as the basetrack, thus instantiating an event.
3. Each event is associated with tracks of other metblobs, which need to overlap in time within a predefined radius of the basetrack for a predefined period.
4. Finally, an array of each event describing its basetrack and associated tracks is formatted. Thus, each event describes the evolution of a suite of meteorological features associated with a flagged cloud band at some point in their shared lifespans.

Matching in step 1 is crudely yet effectively achieved by requiring matched blobs in subsequent images to have a centroid within the average radius of the blob of the previous image. This procedure works well for the 6-hourly NCEP2 data and the daily OLR data. Matching of other tracks to the base track in step 3 is achieved by ensuring that track points at concurrent time steps need to be within 3000km of each other. This has some theoretical

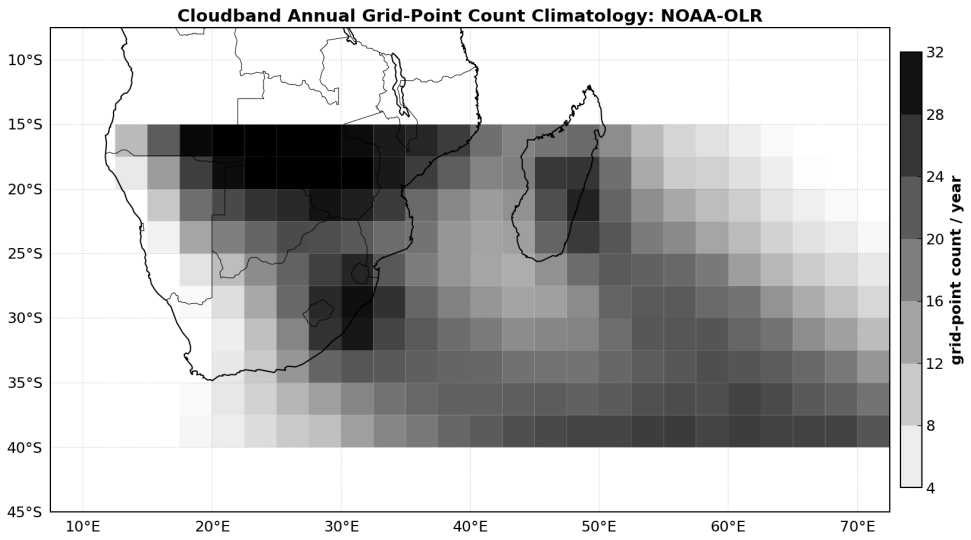

Figure 4: Seasonal grid-point frequency for cloud bands

underpinning since it constrains association of meteorological features to well within the theoretical short-wave cutoff for baroclinic instability (Holton, 2004). This simply ensures the metbot only describes a system associated with one ridge-trough-ridge structure, appropriate since the cloud bands are typically associated with the leading edge of the trough (see Part 1).

3 Results

For the data sets described above, the metbot identified 821 cloud band events over the period 1979-2011 in the domain 0°- 60°S, 0°- 80°E. Fig. 4 displays a climatology of cloud band positions produced by calculating the annual average for how many times a grid point falls within any flagged cloud band's contour. This figure displays the two preferred locations for tropical-extratropical interaction in the southwest Indian Ocean, a feature identifiable in principal component analysis of daily OLR (Todd and Washington, 1999), and indeed noted by early manual satellite imagery analysis (Harangozo and Harrison, 1983; Harrison, 1984).

The potential usefulness of this database however, lies in the meteorological detail it retains in of each of those events. Obtained results are documented here by projecting the database back into the raw data field from which it was built. This process is achieved simply by using the metblob contours to create arrays of data masks for the meteorological variables of each event.

Part I documented two heavy rainfall events that occurred in close succession over South Africa during 1-8 January 1998. This wet-spell is used as an example to illustrate the success and limitations of the metbot to highlight synoptic features. Fig. 5 presents selected times for this event. This figure also serves to illustrate how time is represented relative to event start dates.

The general format of the timeheader for each Fig. 5 panel, basetrack no. : timecode, is explained here. Since the time step for OLR, the reference variable used to flag cloud bands, is daily, each flagged time step is denoted "Dn_ hr" with n being the number of the flagged day for a given basetrack. The time stamp of the NCEP2 variables is contained in hr. Hence in Fig. 5, (c) and (d) respectively, show meteorology at 00h00 on the first day an event

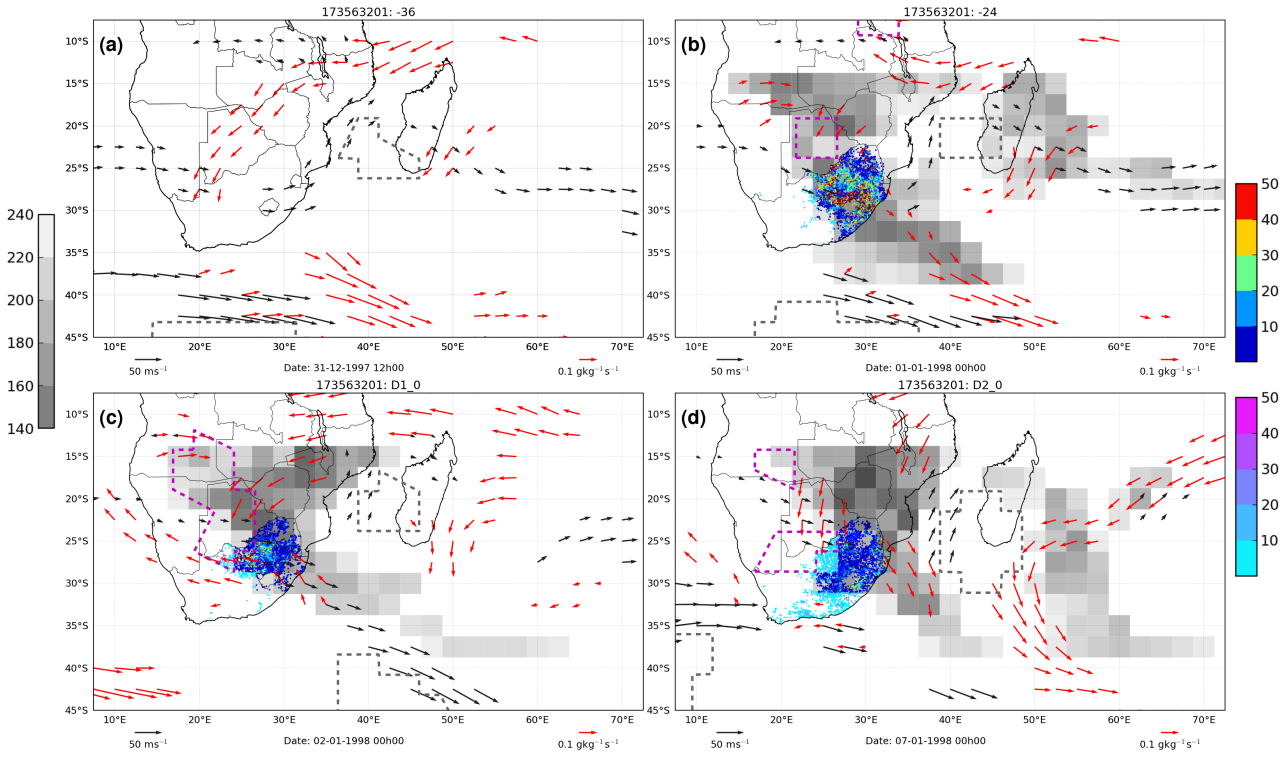

Figure 5: Synthesis of meteorology for cloud band event 01-08 January 1998: 250mb jets (black arrows), 850mb moisture jets (red arrows), 250mb troughs (gray dashed line), 850mb depressions (magenta dashed line), OLR (shaded grayscale) and WRC rainfall within (jet colormap dots) and outside (cool colormap dots) the OLR contour. (Dates displayed below each panel, see text for panel title explanation)

is flagged and the second day it is flagged, in this case 2 and 7 January 1998. Note the 4 day separation between flags; this can occur since one body of low OLR values was tracked through this time as indicated by the basetrack no.. Fig. 5(a) and (b) display NCEP2 variables 36hrs and 24hrs, respectively, before flagging of a cloud band in (c). Each panel describes the suite of meteorological features that the metbot related to the basetrack.

Although $\nabla^2 |\langle u, v \rangle_{250}|$ was used to detect jet regions in the 250mb wind field, the raw wind field is displayed in these panels (black arrows). The same follows the for 850mb moisture fluxes (red arrows). Blob contours of $\nabla^2 \Phi_{250}$ (light grey) and $\nabla^2 \Phi_{850}$ (magenta) are plotted to indicate locations of detected depressions. Raw OLR values within the metblobs contour are shaded. Station rainfall under the OLR footprint is displayed with the jet colormap (upper right colorbar), wet (>5mm) stations outside the OLR contour are shaded with the cool colormap (lower right colorbar).

Part I discussed the meteorology of this event in detail, so this discussion only highlights features that the metbot emphasised for this event. It should be noted that the system was not tuned to this event and thus some shortcomings are revealed that suggest important caveats.

Thirty-six hours (Fig. 5a) before the event was flagged, a northeast moisture conveyor was present across the central subcontinent. A weak upper tropospheric jet was positioned over Namibia. Enhanced upper-level winds extended up the east coast of Mozambique, upstream of an upper tropospheric trough situated near Madagascar. The signature low-level warm conveyor and upper tropospheric jet of a mid-latitude cyclone was present south of southern Africa. Twelve hours later (Fig. 5b), heavy rain was falling under a band of low OLR extending southeastwards off the continent, into the mid-latitude cyclone. Cyclonic low-level moisture movement was centred

around a depression over Botswana. The Namibian jet had gained a more poleward orientation and the Madagascan upper tropospheric trough had developed deep convection along its leading edge.

Fig. 5 (b) indicates the first problem encountered with the flagging process. This day should have been flagged as a cloud band, however it failed the positive tilt criterion within the tilt subdomain (23-33°C, see section 2.2). This occurred since it was broad (Fig. 5b) and the blob extended northeast towards Madagascar. These cases of failed tilt criterions were rare and since at some point in a system's life-cycle it should pass the criterion, this problem is not crucial.

The event was flagged as a cloud band on the 2 January 1998 (Fig. 5c) as the Madagascan cloud fell below the OLR threshold. Rainfall had eased over South Africa however intensification of the low-level depression, and associated moisture flow was evident by the expansion of the magenta blob contour and moisture flux vectors. This intensification continues through the day in time codes *D1_6* to *D1_18*. While not shown, this illustrates that the metbot retains information at the time resolution of the NCEP2 data. Sub-daily variability in meteorology is especially important for the tropical moisture fluxes.

Date	Mean	Max	Wet	Heavy	OutMean	OutMax	OutWet
01 Jan 1998	22.99	386.20	0.79	0.11	8.03	77.50	0.08
02 Jan 1998	**11.48**	**87.40**	**0.64**	**0.02**	**6.65**	**36.40**	**0.08**
03 Jan 1998	6.72	64.00	0.34	0.00	6.21	88.00	0.07
04 Jan 1998	5.16	13.30	0.47	0.00	8.28	180.00	0.27
05 Jan 1998	13.15	88.00	0.73	0.01	10.32	190.00	0.35
06 Jan 1998	11.80	77.50	0.75	0.01	6.67	78.40	0.32
07 Jan 1998	**9.48**	**128.00**	**0.75**	**0.01**	**6.35**	**103.50**	**0.42**

Table 1: Rainfall summary statistics for event 1-8 January 1998 (Mean/OutMean, Max/OutMax values are $mm.d^{-1}$, Wet/OutWet and Heavy values are frequencies)

By this stage, an upper tropospheric jet had developed along the axis of the cloud band, strengthening poleward ahead of an upper tropospheric trough associated with the extratropical cyclone. Deep convection continued over the southwest Indian Ocean with the metbot still noting an OLR blob which it then tracked "backwards" onto the continent to flag a second day in this event. The continental low-level depression was still present with poleward moisture fluxes contributing to a widespread daily rainfall total of ~10mm over much of South Africa. Upper tropospheric jet regions south of the continent were present, while the Madagascan upper tropospheric trough remained strong, with a jet zone still present on its western flank. An extended moisture conveyor was co-located with low OLR values downstream of this depression.

This second day that was flagged raises a concern about the integrity of the blob tracking algorithm which is, admittedly, crude. From prior knowledge of cloud band dynamics, there is an expectation that a second event should have been created, however due the the coarse temporal resolution of the data, and rapid deformation of patterns in the OLR field, the metbot tracked this blob back on to the continent. Applying a more rigorous tracking algorithm may address this issue; the method needs to be less sensitive to large variations in blob centroids that occur with drastic blob deformation as more cloud meets the OLR threshold. The MASCOTTE spatial correlation procedure could present a solution (Carvalho and Jones, 2001).

Attempting to better understand rainfall variability underpins why the methodology described here was developed. Fig. 5 indicates how rainfall can be precisely attributed to cloud band presence. While significant rain falls outside the deep convective footprint of low OLR (Fig. 5d) the core event rainfall does lie under this footprint. Delineating

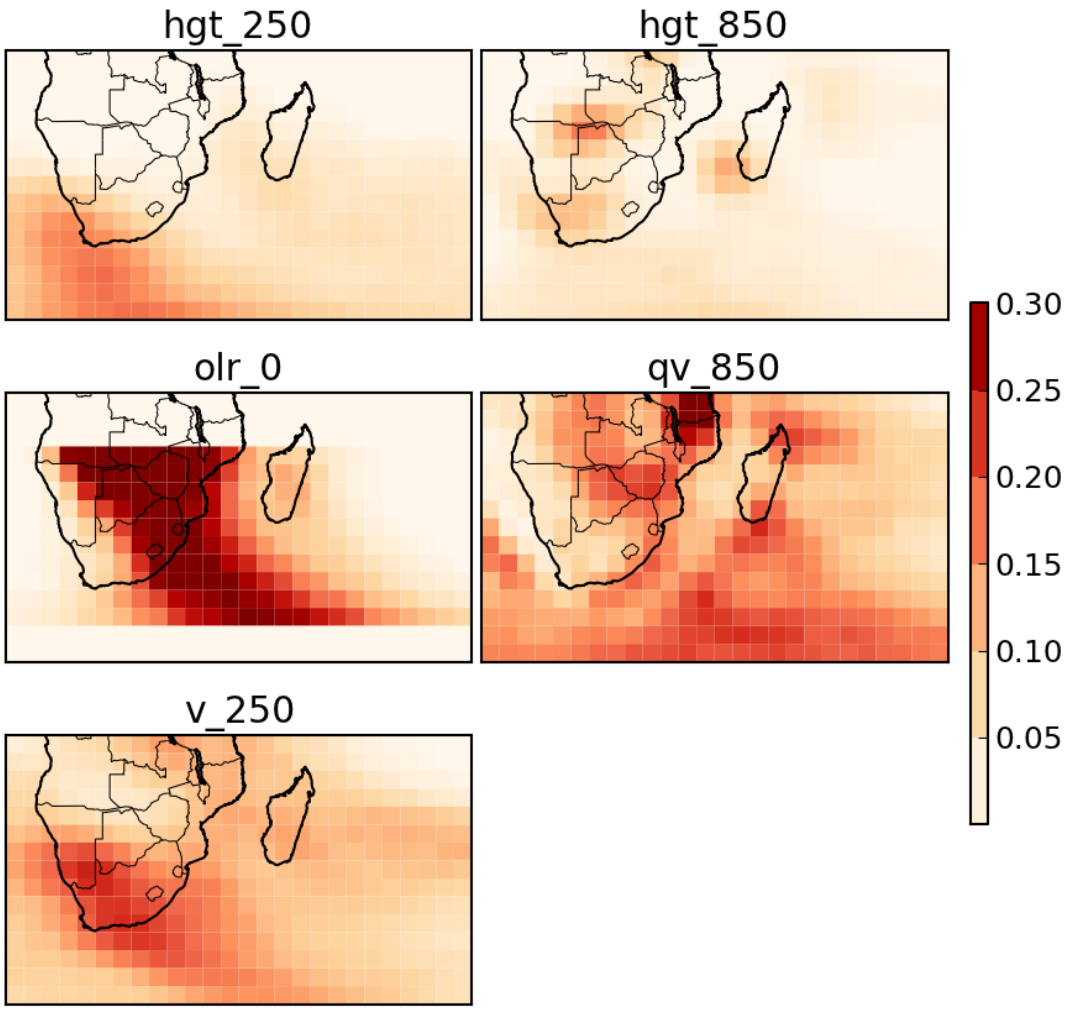

Figure 6: Frequency (n=268 events) that a grid point falls within a metblob's contour for features presented in Fig. 5.

stations through masks (as in Fig. 5) will prove to be useful in calculating rainfall metrics. However, for long-term variability studies, metrics summarising this information may be more appropriate. Table 1 presents summary statistics for each day of the cloud blob track. Flagged cloud band days are boldfaced. Within the OLR footprint the mean and maximum rainfall is calculated along with percentage wet stations (>1mm) and percentage heavy rainfall stations (>50mm). OutMean, OutMax and OutWet summarise the same values outside the footprint.

Wetness percentage outside the cloud contour is substantial towards the end of this event (table 1, 07 Jan 1998), as indicated in Fig. 5(b-d); however, during the first period of heavy rain, almost all of it is within the contour. 01 January 1998 clearly had the heaviest falls with a daily mean station rainfall of 23mm and maximum of 386mm. This table of rainfall information is built into each event object, allowing inter-comparison of system intensities across all events.

The question now arises: are any of these features in Fig. 5 common across events? The contours defining the edge of each metblob are exploited to calculate the frequency of each grid-point falling within the contour of a chosen meteorological feature. Fig. 6 presents these values for all events that produced rainfall in the WRC data set within the period [-24hr, +24hr] and had a centroid west of 45°E. This longitudinal delineation is appropriate since Fig.4

suggests two preferred locations of cloud band formation. All variables discussed in Fig. 5 are presented. The reader is reminded that the jet regions for 850mb moisture flux and 250mb winds, qv_850 and v_250 respectively, are calculated using the $\nabla^2 |\langle u, v \rangle_{lev}|$metblobs contours, hence, the same image applies for qu_850 and u_250 variables even though only the v-components are presented here.

By choice of OLR blobs for the basetrack, its grid-point frequencies (Fig. 6; olr_0) are the highest of all variables. This also illustrates the sharp east-west gradient in cloud band frequency across SA, closely resembling the annual rainfall gradient (not shown).

Upper tropospheric depressions (hgt_250) are detected over the southwestern coast in up to 20% of days accounted for by the methodology. A upper tropospheric jet (v_250) frequency maxima of 0.25 occurs equatorward of this region as expected. The slightly higher jet frequency may suggest the threshold for depression detection needs to be relaxed slightly as upper tropospheric troughs and jets should be closely linked. Nevertheless, occurrence of upper tropospheric troughs upstream of cloud band development is widely noted and expected.

The association of the central subcontinent low-level depression with cloud band development is supported by the frequency field for hgt_850, agreeing with previous studies (eg. Cook, 2000), indicating a quasi-stationary low pressure system, the Angola Low. The presence of a depression on the southwestern tip of Madagascar during up to 15% of event days suggests a synoptic feature which has received little attention.

The moisture jets frequency field (Fig. 6; qv_850) exhibits a number of features, despite the coarse resolution of the data. Firstly, moisture jets over the East African coast are common. Secondly, a broad region of strong moisture flux exists across Botswana and Zimbabwe, a feature present in the case studies of Hart et al. (2010). Thirdly, moisture jets over the Agulhas Current do occur in association with cloud bands. Finally, mid-latitude cyclones and their strong moisture fluxes frequently occur at the poleward end of cloud band systems.

Using frequency thresholds as a filter to retain the most common features, Fig. 7 presents a composite event for continental rainfall-producing cloud band systems. Positions of the cloud band centroids (blue dots) for all events used in the composite illustrate the zonal distribution of these systems. Plotting the composite in coordinates relative to these centroids has been tested. This process did sharpen the band of OLR and tighten up the vector fields; beyond this however, there was little qualitative difference to the panels presented here.

The accepted generalisation for the TTTs is apparent from Fig. 7 (c). An upper tropospheric trough lies off the west coast, with enhanced upper-level flow on its leading edge over southern Africa. Southwestward moisture fluxes across the western subcontinent help sustain deep convection in a band of cloud that terminates in a mid-latitude cyclone southeast of the continent. The continental low-level northeasterlies appear, in part at least, due to the presence of the Angola Low. This emphasises a key role the Angola Low may play in supplying moisture to TTTs (Cook et al., 2004). Its relation to summer rainfall variability (Rouault et al., 2003; Reason et al., 2006) and potential importance in modulating the regional response to ENSO (Reason and Jagadheesha, 2005) has already been explored.

Lack of coherent structures in Fig. 7 (a) and (d) indicate that large event to event differences exist in the early and decaying stages of TTTs lifecycles. Post-TTT intensification of tropical convection is indicated by the lower OLR values across Zimbabwe and Zambia in Fig. 7 (d).

Without more appropriate diagnostics, it is unwise to say too much about baroclinic wave growth in the region from this figure. Nevertheless, it is clear that wave growth does occur as suggested by the equatorward extension of upper tropospheric trough from -24hr to 0hr. This growth is expected by theory due to both poleward advection of warm moist air ahead of the trough and strong convective heating that is likely, within the band of cloud.

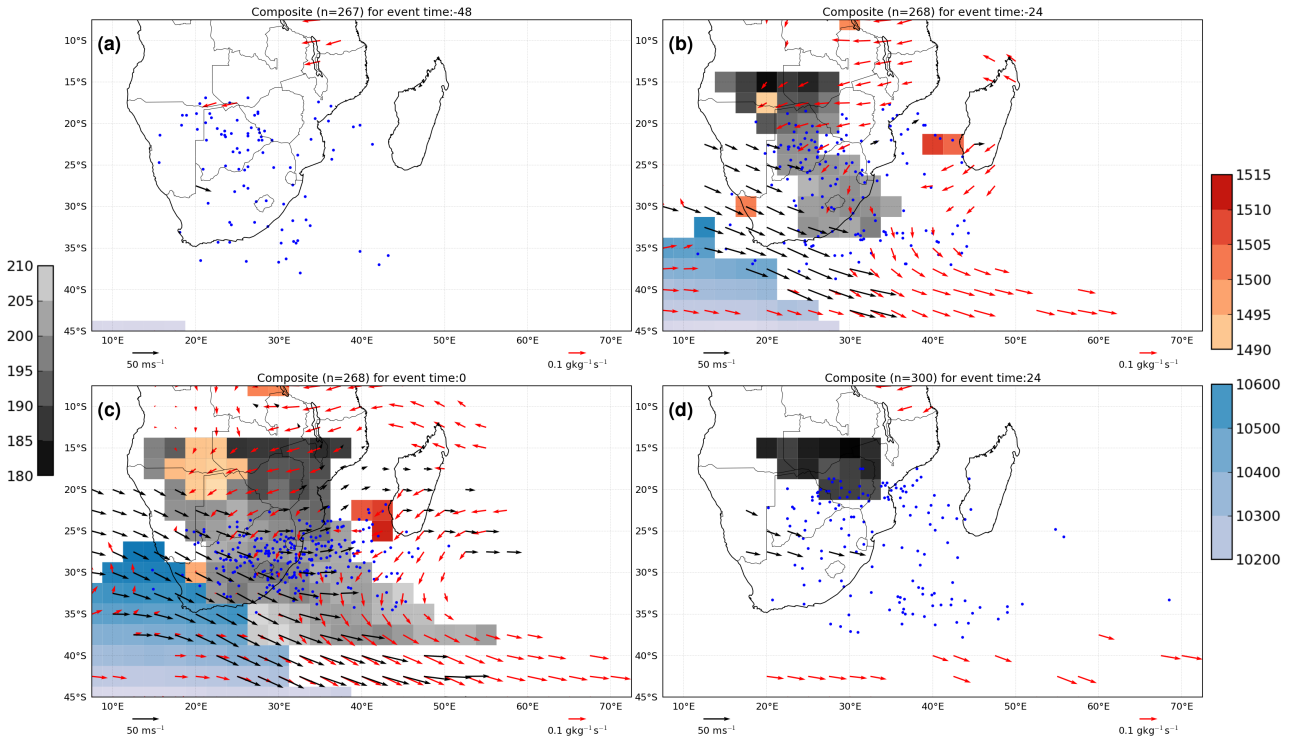

Figure 7: Composite event evolution for all events that produce continental rainfall in WRC station data set: 250mb troughs (shaded blue), 850mb depressions (shaded orange), OLR (gray shading) with 250mb jets (black arrows) and 850mb moisture jets (red arrows) and OLR blob centroid position (blob)

4 Discussion and Conclusions

In this section, the metbot is put into context in three research domains: South African rainfall variability, sub-tropical convergence zones and object-based methods for atmospheric science.

These results present an alternative method to the generalisation of TTTs. Previous TTT composites have been based on daily precipitation principal component (PC) extremes (Todd and Washington, 1999) or partitioning of days by cluster analysis (Fauchereau et al., 2009; Crétat et al., 2010). These composites were presented as circulation anomalies, whereas the the raw circulation field is presented here. The findings support earlier generalisations and give weight to the common synoptic features highlighted in Part I, based on analysis of available case studies. As expected however, there is substantial noise in the meteorology of individual event as shown by the low frequencies in Fig. 6. Conducting the analysis with a subset of events that caused extreme rainfall may reduce this noise and reveal higher frequencies of some of these features, if they manifest more clearly during intense events.

These authors, however, argue that explicitly retaining these event to event differences is the strength of this methodology over the previous methods. The literature has long noted the infrequency of continental TTTs (eg. Washington and Todd, 1999). Thus, individual events could substantially modify season total rainfall, especially if they exhibited unusual persistence or occurred farther west than expected in climatology. For example, note the few number of cloud band centroids over the semi-arid western South Africa in Fig. 7 (c). These represent rare events in a water scare region. The lack of dependence of the metbot on PC or cluster analysis, which favour recurrence, is its strength. It allows exploration of the interannual variability in extremes which it explicitly can identify. The ability to associate rainfall summary statistics with individual events further expands its use in this regard. The timecode value n (Dn_hr, as explained in section 3) also provides a simple measure of persistence of cloud band

conditions, an important property when considering intraseasonal wet spell variability and/or contribution to total season precipitation.

By nature of its geometry, the cloud band flagging process has potential use for two well documented atmospheric features: subtropical convergence zones and tropical plumes. Detailed description of the synoptic variability of the South Indian Convergence Zone is beyond the scope of this study, however this methodology could be well suited to such investigation. Its application to other convergence zones may help reveal nuances that PC analysis smooths away; it could be interesting, for example, to repeat a study such as Matthews (2012) with this approach. The metbot provides an avenue to explicitly capture the synoptic pulses fundamental to the South Pacific Convergence Zone dynamics (Matthews, 2012). Statistics of these pulses could be built up to offer a more detailed description of these dynamics than is feasible from PC analysis; in particular, the role different meteorological components play could be quantified with more rigour. This could be complementary to studies such as Widlanksy et al. (2011).

Applying this methodology to tropical plumes in general may require a different choice for the flagging variable. Plumes over the North Atlantic and North Pacific often have only mid- to high-level cloud in the tropics with deep cloud and heavy rainfall found near their termination points over land (Knippertz, 2007). Part I suggested that TTTs fit the theoretical framework for tropical plumes but highlighted this key difference. The lack of deep cloud along much of the axis would modify the necessary OLR thresholds, indeed preliminary work (not shown) attempting to apply this metbot in the North Pacific and Atlantic revealed this problem. Jiang and Deng (2011) applied an adaptive zonal and meridional thresholding technique to integrated water vapour to identify atmospheric river features in the NASA MERRA data set. Thus, robust methods to flag atmospheric rivers exist. However, they are unable to provide the level of meteorological detail that case studies inherently do (eg. Ralph et al., 2011). A proposal is that a similar metbot, based on the Jiang and Deng (2011) methodology to flag systems, could go some way to bridge the gap to case studies and provide a powerful tool to evaluate atmospheric river dynamics in a multiscale framework and across many data sets.

Herein lies a key point; while the case for (semi-) objective identification methods is made regularly, it is very difficult to achieve the level of detail of a case study since that is not their goal. However, these details are important when attempting to develop a mechanistic understanding of multiscale interactions.

The metbot methodology, while much cruder than many of the feature tracking methodologies referenced here, has potential as the tool to do this for the subtropics over southern Africa. The adaptability of the metbot is demonstrated in Part II, where mid-tropospheric cut-off low tracks produced by Favre et al. (2011) are associated with cloud band events. Coding a relation building tool such as this metbot, around the many, well-established, feature tracking methods, is likely to help bridge this object-case study gap in other regions that are dominated by different weather systems.

To conclude; the three criteria for a successful metbot, as outlined in the introduction, have been met. Blob detection provided an effective region of interest locator and applying two simple criteria to blob properties enabled cloud band flagging. A simple set of blob association rules were used to track blobs and build a data object which contained a detailed meteorology of each cloud band event. Some examples of the use of this set of event objects have been demonstrated and the authors conclude that the methodology captures essential features of the evolution and rainfall of TTTs over southern Africa.

Acknowledgements

This work was only possible thanks to developers of opencv at willowgarage.com and elsewhere and the developer of cvblob whose code is made freely available, with Python wrappers, as part of the Robotics Operating System project. Interpolated OLR and NCEP2 data was obtained from NOAA/OAR/ESRL PSD, Boulder, Colorado, USA through http://www.cdc.noaa.gov.

Appendix

The software platform underlying this work is:

- Operating System: Linux
- Software Libraries: OpenCV (http://opencv.willowgarage.com/), cvblob (http://code.google.com/p/cvblob/)
- Software platform: Python
- Python Modules: NumPy, ScientificPython (Hinsen, 2007), Matplotlib, Basemap, PyClimate
- PIL, python wrappers to cvblob and OpenCV

Part III

Characterising the season in terms of TTTs

What is the signature of the mean annual cycle of TTTs in synoptic climatology and rainfall?

Specific Questions:

- What is the seasonal cycle of cloud band frequency in the region?
- What is the importance of TTTs for regional rainfall, specifically with regards to: daily rainfall, monthly and seasonal total rainfall and the portion of variability attributable to TTT variability?
- How often are TTT systems responsible for extreme rainfall?
- Does the Madden-Julian oscillation modify TTT meteorology?

"To be interested in the changing seasons is a happier state of mind than to be hopelessly in love with spring" - George Santayana

Revisiting tropical temperate troughs and South African rainfall

Abstract

Tropical-extratropical cloud band systems over southern Africa, known as tropical temperate troughs (TTTs), are known to contribute substantially to South African summer rainfall. This study performs a reassessment of this contribution by using a novel object-based strategy that explicitly tracks these systems for their full life cycle. The methodology incorporates a simple assignment of station rainfall data to each event, thereby creating a database containing detailed rainfall characteristics for each TTT.

This is used to explore the importance of TTTs for rain days and climatological rainfall totals in October-March. Average contributions range from 30 to 60%, however substantial spatial heterogeneity is observed. TTTs appear more important to rainfall in the drier central South Africa and the Limpopo River Valley, a noted drought corridor. Contributions over the Highveld and eastern escarpment are lower, in contrast to earlier generalisations. A short analysis of TTT rainfall variability indicates TTTs provide substantial intraseasonal and interannual variability in station rainfall totals.

Results indicate that TTTs correspond to more heavy rainfall days than to lighter rainfall days. Further work discovered that of 52 extreme rainfall events in the 1979-1999 period, 30 are associated with these tropical-extratropical interactions. Cut-off lows were included in the evolution of 6 of these TTTs. It is noted that individual events can contribute over 20% of the total season rainfall at many locations.

The study concludes with an analysis of the question: does the Madden-Julian Oscillation (MJO) influence the intensity of cloud band rainfall over South Africa? The distributions of a proxy for the sustained intensity and the maximum intensity of TTT systems are plotted after stratifying all events by MJO phase. Results suggest a significant suppression (enhancement) of intensity during phase 1 (6). Composites of TTT circulation, by phase, hint that this could be due to more zonal (meridional) orientation of upper-level flow during phase 1 (6).

This study provides the most rigourous assessment of the importance of TTTs for regional rainfall to date. The findings support previous conclusions, however, contribution percentages indicate that other rainfall systems also produce considerable summer rainfall.

This part is under revision for publication in Climate Dynamics :
"Cloud bands over southern Africa: seasonality, contribution to rainfall variability and modulation by the MJO"
N.C.G. Hart, C.J.C. Reason and N. Fauchereau

1 Introduction

South Africa is a country characterised by sharp rainfall gradients (Fig. 1). Its subtropical location and complex topography produces substantial spatial heterogeneity in the seasonality and quantity of rainfall. Precipitation in the southwest is dominated by mid-latitude cyclones, primarily in winter, while the northeastern parts experience summer convective rainfall. The interior exhibits a strong east-west gradient with semi-arid conditions on the western boundary transitioning to annual totals in excess of 700mm in the eastern Highveld (Fig. 1, right). Fig. 1 (left) displays the sharp escarpment that separates the interior from wetter south and east coast regions; stations on the northeastern escarpment regularly experience annual totals above 1500mm.

The subtropical location of the country means tropical-extratropical weather systems are feasible. These involve interactions between synoptic scale mid-latitude waves and meso- to microscale convection common in the more tropical parts. Tropical temperate troughs (TTTs) represent such interactions and are a regular features of summer season weather in the region (Taljaard, 1996).

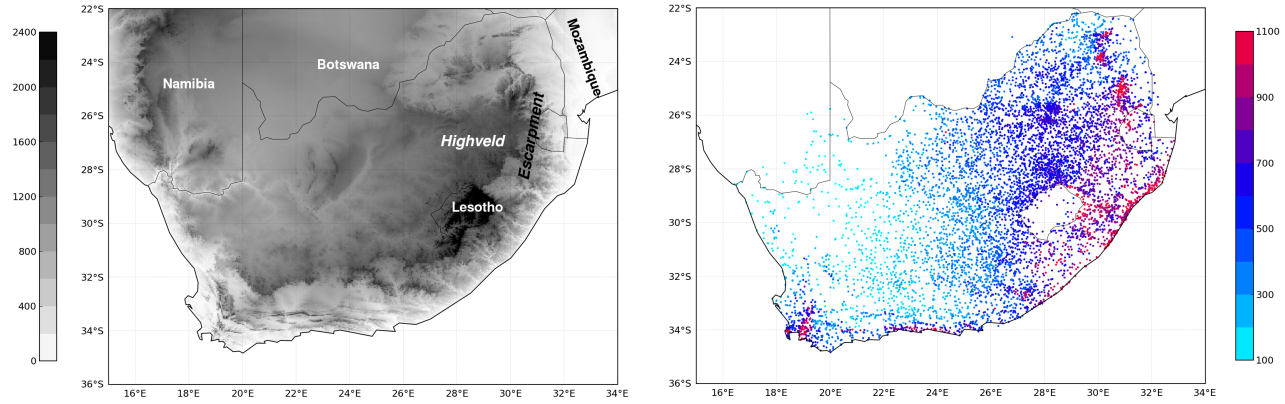

Figure 1: South African mean annual WRC data set precipitation (dots, mm) and topography (shaded, metres).

Harrison (1984) provided the first quantitative estimate of the contribution of TTTs to summer rainfall over the South African Highveld. The approach which used principal component (PC) analysis of monthly rainfall totals, together with available satellite imagery and synoptic maps, produced a comprehensive generalisation of the main synoptic drivers of rainfall for the region. His conclusion, that TTTs are a major contributor to summer rainfall and variability, has been supported by many subsequent studies. These have used PC analysis (Todd and Washington, 1998; Pohl et al., 2009), fuzzy clustering techniques (Fauchereau et al., 2009) and hierarchical cluster analysis (Crétat et al., 2010), applied to daily rainfall or outgoing longwave radiation fields.

PC analysis and cluster classification techniques provide a good estimation of the shape of rainfall seasons and typical circulation patterns. However, these techniques often assume Gaussian distributions which lead to difficulty when some individual events can substantially skew statistics. In addition, they treat each day as an independent observation. This results in partitioning of individual synoptic events across partitions, which are then represented graphically, as the average of each of these partitions. Various techniques work around this to develop an estimation of propagation between clusters (eg. Fauchereau et al., 2009, ; Table 1) however, they only provide an indication of this difficulty and not an explicit event scale solution. Potential interpretation issues arise: for example, it is not clear whether favouring of a particular cluster in El-Nino years indicates a modification of synoptic evolution of a particular weather system, or instead might suggest increased presence of a completely different system. Nevertheless, their

use is appropriate for objectively exploring statistics of the daily timescale; their use has substantially advanced insights into drivers of regional variability.

Mapping of the dominant daily weather states with these techniques has highlighted that TTT-like features make up a substantial portion of daily variability of rainfall and circulation during November through February, the core of the summer season (Washington and Todd, 1999; Pohl et al., 2009; Fauchereau et al., 2009; Manhique et al., 2009; Crétat et al., 2010). Thus, there is good foundation for a more detailed analysis of the role of TTTs in the region. It is appropriate to update the seminal work of Harrison (1986) using the abundance of meteorological data that has become available since the 1980's.

Elegant approaches to approximate synoptic evolution (1-3 days) from daily classifications, such as the ones discussed above, have been developed (eg. Polo et al., 2011). Despite this they remain statistical; however, the metbot methodology presented in Part II explicitly captures evolution of TTTs at the synoptic-scale. As such, it may be more appropriate for application to the question this study revisits: What is the contribution of TTTs to South Africa summer rainfall and variability?

While there are other important rain-bearing systems in the region, they are beyond the scope of this work. The exception is cut-off lows; satellite imagery shows cut-off low events can be associated with TE cloud bands (Harrison, 1984), especially as they decay (Singleton and Reason, 2007; Muller et al., 2008). Some of the most severe floods in South Africa have been attributed to these cut-off systems so this study makes use of tracks built by Favre et al. (2011) to associate cases of TTT events with cut-off lows.

This study investigates the seasonal timescale as part of a series of papers addressing interactions between the synoptic timescale TTTs and longer term climate variability modes. Thus, a cue is taken from Pohl et al. (2007) to investigate intraseasonal modulation of TTTs by the Madden-Julian Oscillation (MJO; Madden and Julian, 1994). Pohl et al. (2009) investigated regional scale interactions using PC-based partitions of daily OLR anomalies over southern Africa; they found no discernible MJO influence on the likelihood of TTT occurrence. The same study however, highlighted the result in Pohl et al. (2007) of the MJO modulation of moisture supply to subtropical southern Africa. So, while impacts of the MJO on non-TTT convection in the region have been demonstrated, this study will investigate the hypothesis that the MJO modulates continental TTT rainfall intensity. This hypothesis was beyond the scope of the Pohl et al. (2009) study; however, the work presented here is well suited to address the proposition.

Section 2 follows with an explanation of the techniques used to develop summary statistics appropriate to the questions in this study. The results in section 3 present four aspects of the synoptic climatology of TTTs: location and frequency of systems, their signature in climatological rainfall, the impact of extreme events, and intraseasonal modulation by the Madden-Julian Oscillation. A brief discussion and summary of these results follows in section 4. Section 5 contains some final remarks and conclusions.

2 Data and methodology

An estimation of southern African synoptic circulations are provided by satellite derived outgoing longwave radiation (OLR; Liebman and Smith, 1996) as a proxy for deep convection, and the National Centre for Environmental Prediction/Department of Energy Reanalysis II (NCEP2; Kanamitsu et al., 2002) as an estimate of the momentum and thermodynamic variables. Observed rainfall for 1979-1999 is obtained from the Water Research Commission

(WRC) daily station rainfall (Lynch, 2003), which Pohl et al. (2007) preprocessed to a data set of 7665 stations without missing values. The data set ends in 1999, which limits the full exploitation of NCEP2 and OLR data range. Use of this precipitation data allows direct comparison of our results with the recent contributions to regional variability literature (Pohl et al., 2007; Fauchereau et al., 2009; Crétat et al., 2010). Removal of the few stations in Zimbabwe confines this analysis to South Africa.

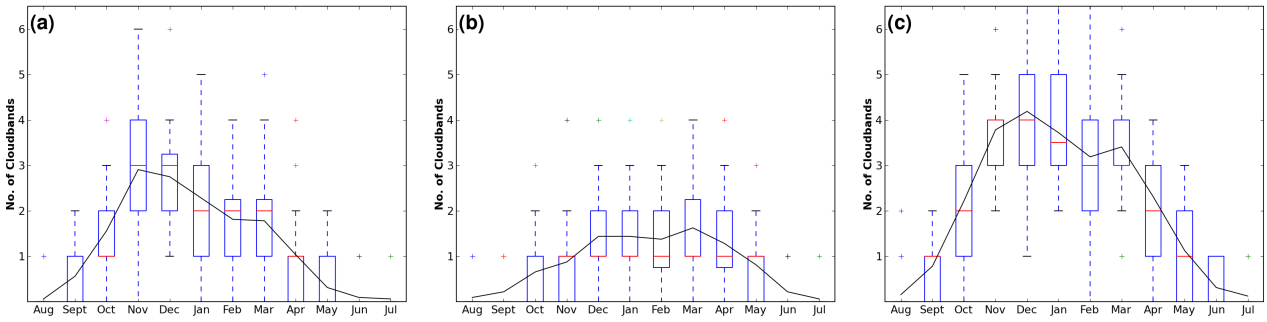

Figure 2: Seasonal cycle of cloud bands detected in OLR data for (a) continental, (b) Madagascan, and (c) all cloud bands (n = 32 seasons); boxes bound lower and upper quartile of values with red streak indicating median, solid curve depicts mean.

Identification of cloud band systems is performed by the metbot methodology detailed in Part II. To summarise, daily OLR data in the domain 0°- 60°S; 0°- 80°E, with a maxima threshold at 230 W.m^{-2}, is plotted and run through a blob detection algorithm. Tropical-extratropical cloud bands are flagged when blobs extend from the tropics (20°S) into the extratropics (40°S) with a positive tilt (poleward bearing from tropical root is in the interval [95°,180°]). OLR data is selected 48 hours either side of flagged days, and the process is repeated, with these criteria relaxed, to build base tracks of OLR blobs which meet cloud band criteria at some point on their track. The Laplacian operator $\nabla^2_{x,y}$ is applied to 250mb winds and 850mb moisture fluxes meteorological variables from NCEP2 to highlight jet zones ($\nabla^2 |\langle u, v \rangle_{lev}| < 0$). A similar thresholding and blob detection procedure is applied to these fields to produce tracks of meteorological features, which are then associated to the OLR basetrack. Rainfall data inside and outside the OLR blob contours are summarised for areal coverage and intensity. This produces a data object for each event, which describes detailed meteorology of each cloud band system. Selected fields from the metbot produced database used in this study are OLR blob tracks, associated WRC rainfall, low-level moisture jet features and upper-level jet zones.

The flexibility of the metbot methodology allows inclusion of other feature-based data sources. Association of cut-off low tracks presented in Favre et al. (2011) is performed under the same criteria, for blob track association: the feature track needs occur within 3000km of OLR basetrack for at least one time step. The relation is thus only for cut-off low events that are potentially related to TTTs. A full assessment of cut-off low impact on rainfall is beyond the scope of this work.

Caveats of the metbot methodology are highlighted in Part II. The most important caveat to this study is that we have assumed all cloud bands are TTTs, which may not be true. The present authors believe that the flagging criteria for cloud bands are appropriate for objectively identifying TTTs; subjective analysis of some of the flagged events may however, question their validity.

Methodologically, there is no need to constrain this investigation to the core summer season, typically November to February, as is common practice (eg. Fauchereau et al., 2009). Hence, the analysis is carried out for all months so as to allow the shape of the TTT season to emerge naturally.

Spatial representation of mean TTT locations is achieved by counting the number of times a grid point falls within a TTT-associated OLR blob. This count is performed by month for all events found during the period 1979-2010 and then divided by the number of years. The result is interpreted as the climatological number of cloud band days in a given month at a given grid-point. It is important to note that the values are computed for all OLR blobs in the OLR basetrack of each event. The results are qualitatively similar if this analysis is limited to flagged cloud band blobs only, however the grid-point per month counts are much lower. This difference is because the life cycle of an OLR blob may be a few days, but it might only meet cloud band criteria on one particular day.

The TTT contributions to wet days, monthly and seasonal total rainfall and extreme events are obtained by projecting metbot-described events into the station rainfall data, producing a TTT-rainfall-only station data set. This approach presents options. Firstly, does one choose to only keep rainfall within the footprint of the OLR blobs or include rain at all stations on an event day? The results presented in Part II, Fig. 5 suggest that the rainfall outside of the OLR footprint is associated, at least at the synoptic scale, with the same weather system. This study therefore chooses to include all rain stations on OLR days. Secondly, event days could be defined as flagged cloud band days only or, as all days associated with an OLR blob track which was flagged at some point in its evolution. By construction, OLR tracks do not extend more than 48hrs before or after a flagged cloud band day, therefore, since the focus is synoptic-scale rainfall, it is reasonable to assume rainfall for all days of an OLR blob track is likely associated with TTT synoptics.

Extreme synoptic rainfall days are defined here by totals exceeding the 95-th percentile for daily rainfall at at least 10% of stations. Event-scale statistics were maintained by collecting consecutive extreme days into events. These event dates were matched to TTTs, which were checked for cut-off low associations. The average percentage contribution of these events to their respective mean season rainfall accumulations was calculated by station. This process provided a representation of the power of individual extreme events to alter season total rainfall at each location.

An analysis of potential MJO influence was achieved by stratifying TTT events by phase of the multivariate real-time MJO index (Wheeler and Hendon, 2004). Histograms of summary rainfall statistics under the OLR footprints were plotted for all events in a given MJO phase. Full details of available statistics are provided in Part II (see Table 1). Since this study addresses a question of TTT intensity, it makes use of the "heavy" statistic chosen as the percentage of stations with daily totals over 20mm for each day of the event. For each event, the maximum heavy rainfall statistic and the mean heavy statistic for all days of the event were calculated to reduce dimensionality further. The purpose of this is elucidated in section 3.4.

3 Results

3.1 Seasonal cycle of cloud band occurrence and location

The seasonal cycle of regional cloud bands is dominated by a broad warm season peak of 3 to 4 cloud bands per month (Fig. 2c) during November to March. Since 24 of the 32 observations (32 years) lie within the boxes, the monthly differences in period 1979-2010 are rarely more than 1 event above or below the mean.

Fig. 2 (a) indicates that the greatest contribution of events to the regional total is provided by systems initiating near the continent. The continental systems peak at 2-4 events in November, however the whiskers of the plot

indicate years exist when this peak was up to 6 systems and years where none developed. One to two fewer systems occur in the following months and by April the core season has subsided. January also experiences a wide spread in system numbers, however with a lower mean than November. This November peak in system occurrence is suggested as being due to the stronger influence of upper-level westerly wave flow and the associated wave activity in the early summer (D'Abreton and Lindesay, 1993).

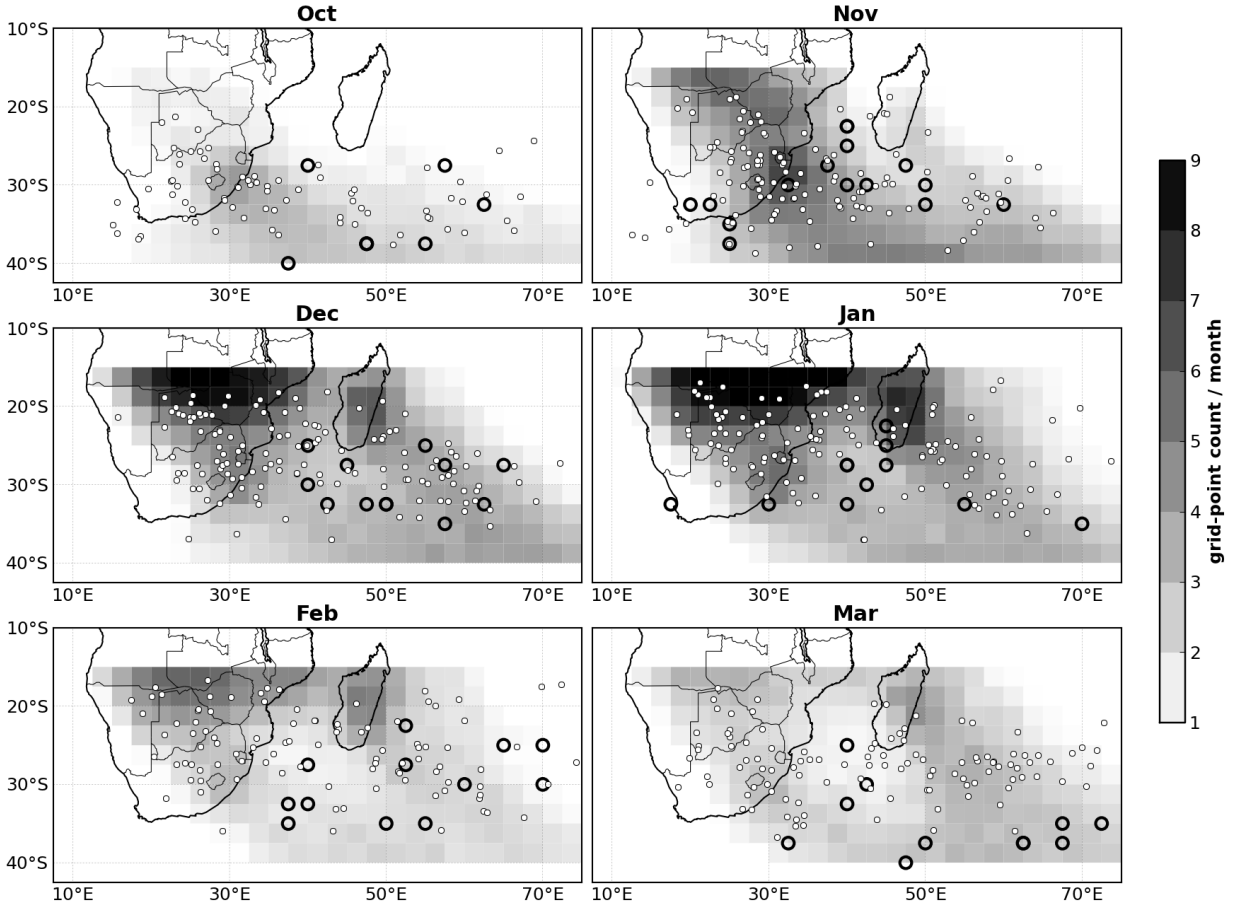

Figure 3: Seasonal cycle of cloud band grid-point counts (shaded), initiation centroids (dots) and cut-off lows (black circles).

The seasonal cycle for the more eastern systems over Madagascar has less amplitude than those over the mainland (Fig. 2b). The core season from December through April is one month longer than the mainland, with 1 to 2 systems forming per month. A minor peak in March is likely an effect of this month exhibiting a few years with up to 4 systems. Outlier years of 4 systems per month have however occurred for all these core season months.

Fig. 3 presents this seasonal march spatially. In October, one or two systems with a continental root may develop. The initiation positions indicate that systems in the east are rarer than the western systems during this month. By November, this has become a dominating feature with grid-points near the continent experiencing 3-6 cloud band days. A core of persistent deep convection over central southern Africa is starting to develop as the Intertropical Convergence Zone (ITCZ) migrates southwards. December and January exhibit very similar patterns, with persistent ITCZ convection dominating detected OLR blobs in the early and late stages of cloud band life cycles. The bimodal location preference of systems is well established, with initiation points common in both the western and

eastern locations. There is however a notable reduction in initiation points over western southern Africa, in contrast to October and November.

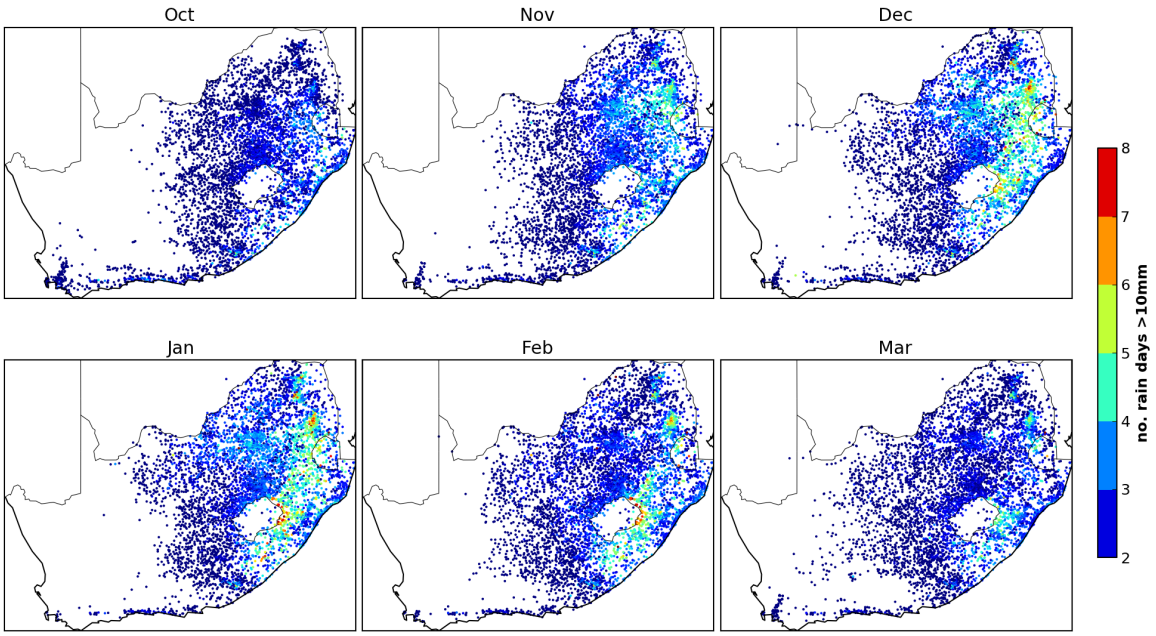

Figure 4: Climatology of rain days (>10mm) over South Africa during summer months.

February displays a reduction in grid-point loading throughout the domain associated with the decline in event numbers. This decrease may be related to a decrease in persistence of OLR blobs associated with flagged cloud bands. By March, there is a slight predominance of Madagascan systems. This distribution continues into April (not shown) with grid-point counts similar to October situated to the southeast of Madagascar.

Of the 821 systems captured by the metbot, 108 have some association with a cut-off low. Caution is needed as there may be fewer actual cut-off low systems, as suggested by (Fig. 3, circles), as during their life span they could be associated with more than one cloud band. A final note is that of the 302 continental rain-producing TTTs events identified in the 1979-1999 period, 28 have associations with cut-off lows, however as seen in Fig. 3, very few occur close to the continent. TTTs and cut-off lows are discussed in more detail later, in relation to extreme rainfall events. Based on the results of Fig. 2 and 3, the remaining analyses only discuss TTT impacts during October to March.

3.2 Importance for rainfall climatology

It is now appropriate to examine how the TTTs contribute to the wet season over South Africa. The first question to address is: how often are wet days associated with TTT events? The climatology of wet days (>1mm) is not presented here since the spatial loadings are similar to Fig4. In summary, TTTs are responsible for 30 to 60% of these wet days increasing from east to west. As will be shown, these systems are more important for substantial synoptic rainfall totals. Therefore, the discussion starts with results for days that experience more than 10mm of rainfall, which will be referred to as rain days .

Fig. 4 presents the mean summer season progression of rain days for 1979-1999. The eastern escarpment (Fig. 1) is the most frequently wet, increasing from 3 rain days in October to 6 days in December and January. By March, the frequency has returned to 3-4 days. The Highveld region north of Lesotho experiences 4-5 rain days during the core summer months, however west of this there is a sharp decline to less than 2 rain days in the semi-arid western interior. As summer progresses, this gradient weakens somewhat, particularly for wet days (not shown). The south coast typically experiences 2 to 3 rain days through the period shown. As expected, these features mirror the mean annual total rainfall for South Africa (Fig. 1).

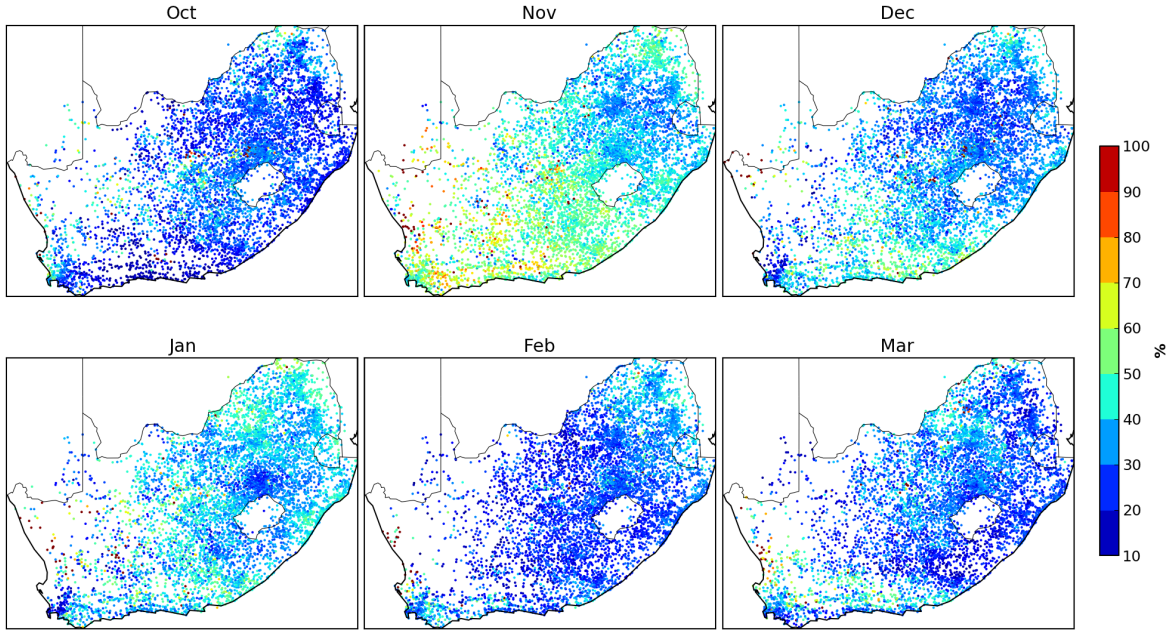

Figure 5: Climatological percentage of rain days (>10mm) contributed by TTT systems.

During October, 40 to 60% of wet days in regions peripheral to the core rain day area (Fig.4) are due to TTTs. Fig. 5 shows that this is especially true in the far north of the country and in the interior west of Lesotho. This pattern is due to the large-scale synoptic character of TTTs since it is expected that they produce the majority of the few rain days in the marginal rainfall zones. For November, this is particularly true in the western interior, which climatologically experiences peak rainfall in March. During November and January, TTTs produce as much as 60% of rain days over the Highveld. Surprisingly however, the contribution decreases to about 30% during December. During February, TTT frequency during rain days is lower everywhere except in the far north. March displays a marginal increase to values over 40% for much of the central interior and into the semi-arid southwest.

Daily precipitation totals greater than 20mm (not shown) follow a similar spatial distribution to Fig. 4 however at most only 3 such days occur on average during December to February. These events are confined to localised regions along the eastern escarpment. Again, TTTs are responsible for much of this rainfall, with values on average 10% higher than Fig. 5. This trend of increasing TTT importance during heavy rainfall days is confirmed by Fig. 6. Days of rainfall above 50mm are rare in the climatology with mean values below 0.5 days per month at most stations. This result is partly an artifact of the density of the station network, the nature of convective rainfall and the relatively short data record used; it is unlikely that a single station will experience a high hit rate of such days. Nevertheless such days do occur throughout the region, with small pockets in the eastern escarpment recording such days at least once a month for December through February. Fig. 6 therefore provides an indication that rare but

heavy rainfall events are frequently associated with TTTs, during all summer months. This association is strongest during October over the Highveld, during November and January it is widespread and during March its notable both in the central north and over the south coast.

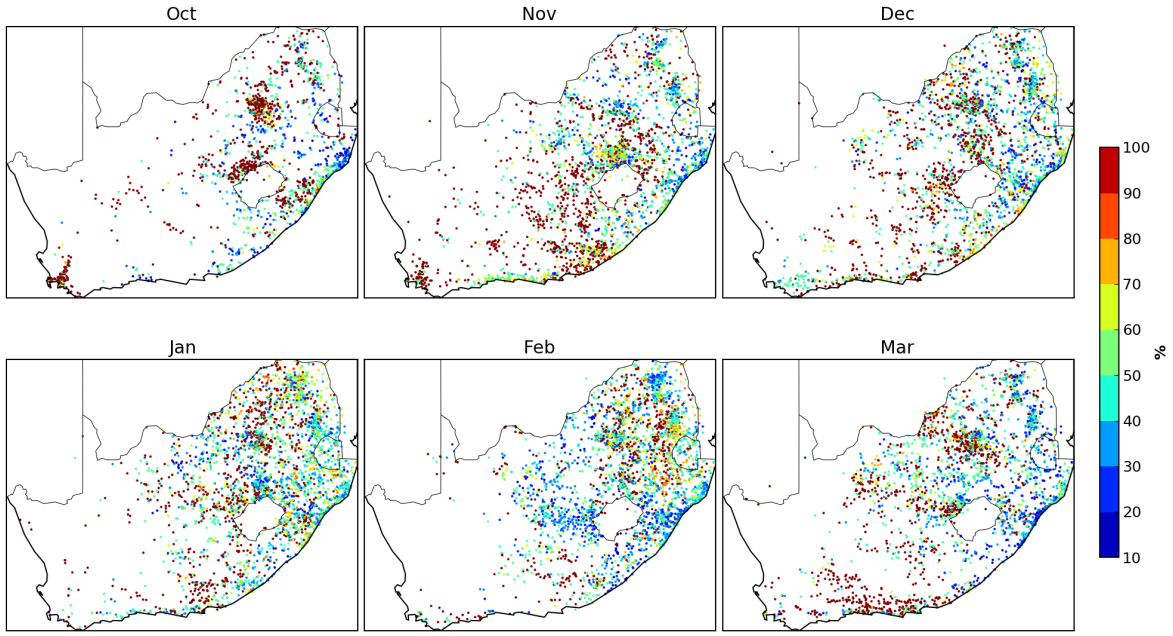

Figure 6: Climatological percentage of heavy rain days (>50mm) contributed by TTT systems.

It is clear that TTTs are associated with days experiencing substantial precipitation over South Africa but how does this behaviour contribute to monthly rainfall totals? First, however there is a need to discuss the seasonal cycle of monthly rainfall. Fig. 7 presents the mean monthly totals for the South African summer. In October, monthly totals above 90mm are only found along the eastern coastline and escarpment of South Africa. Widespread totals between 10 and 50mm are however common across much of the country. As summer progresses, monthly totals increase above 100mm at most stations in the eastern half of the country, peaking in January. Totals above 200mm are common at locations along the escarpment from south of Lesotho north toward Mozambique. February sees a slight reduction in values, however more stations on the western margin of the rainfall zone experience totals near 100mm. Monthly totals have eased marginally by March, however stations across the Highveld and eastern escarpment still receive substantial rainfall. Stations in the arid west experience progressively drier conditions through December to February, however by March the region is back to similar numbers of stations receiving more than 10mm per month.

Fig. 8 suggests that the one or two TTTs events that occur in October (Fig. 2) contribute over 30% of the total monthly rainfall at many of the stations across the region. This widespread contribution increases to above 40% for November and January. However, there is a decline during December, especially over the Highveld. Contributions from TTTs are reduced in February, however they are higher again in March (Fig. 8).

A key feature that emerges from this figure is that TTT contributions are highest in the marginal rainfall areas during all months. This result is most clearly visible during the peak TTT month, November, when contributions in the far north of South Africa and west of Lesotho exceed 60%. Contributions to monthly rainfall over the Highveld

and along the eastern escarpment are more variable with up to 60% of November and January rainfall associated with TTTs but less than 30% in December.

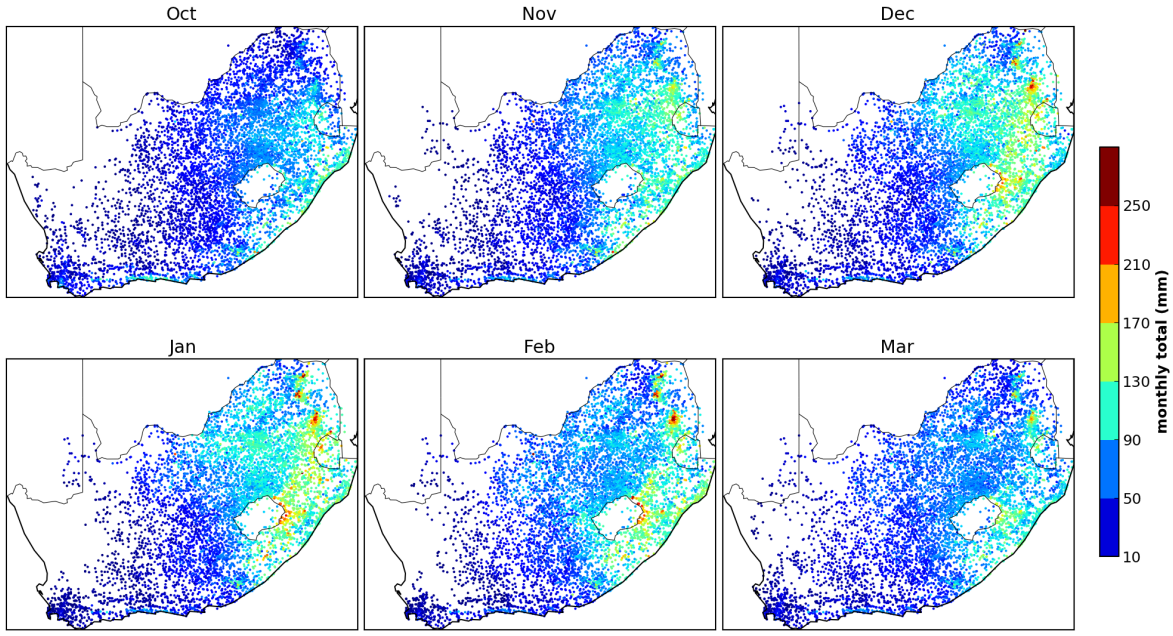

Figure 7: Mean monthly rainfall totals (mm); only stations with totals > 10mm/p.m are plotted.

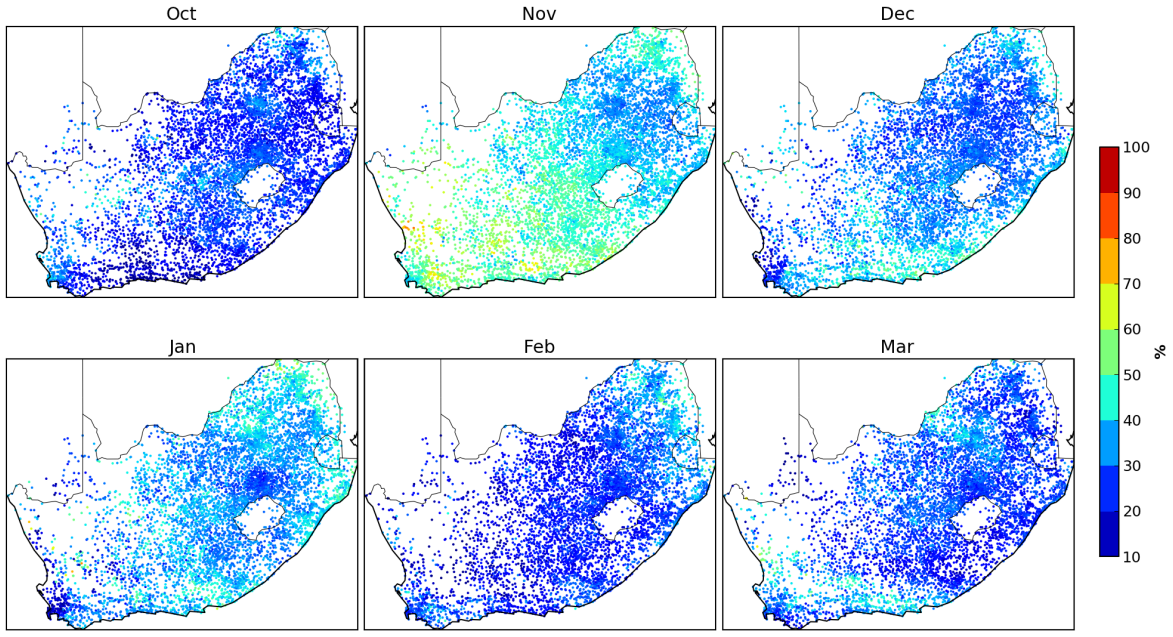

Figure 8: TTT contribution to monthly rainfall totals (%).

Fig. 9 summarises the above results at the seasonal timescale with some implications for rainfall variability. Contributions to ONDJFM total rainfall display a similar character to the monthly features since more arid regions

have higher dependence on TTT rainfall than the wetter regions (Fig. 9a). Along the escarpment, only 30% of rainfall is attributed to TTTs. Similar values are found through much of the Highveld. In the drier regions of the Limpopo River Valley, immediately west of Lesotho, and along the southern coast, the TTTs contribute between 35-45% of the summer total. Producing the same figure for the shorter season of NDJF only produces minor changes, with contributions rising in general by 5%. A final note on Fig. 9 (a) is that it appears that the southwestern interior gets a substantial amount of season rainfall from cloud band systems. There is also a notable contribution from these systems at southwestern coastal stations.

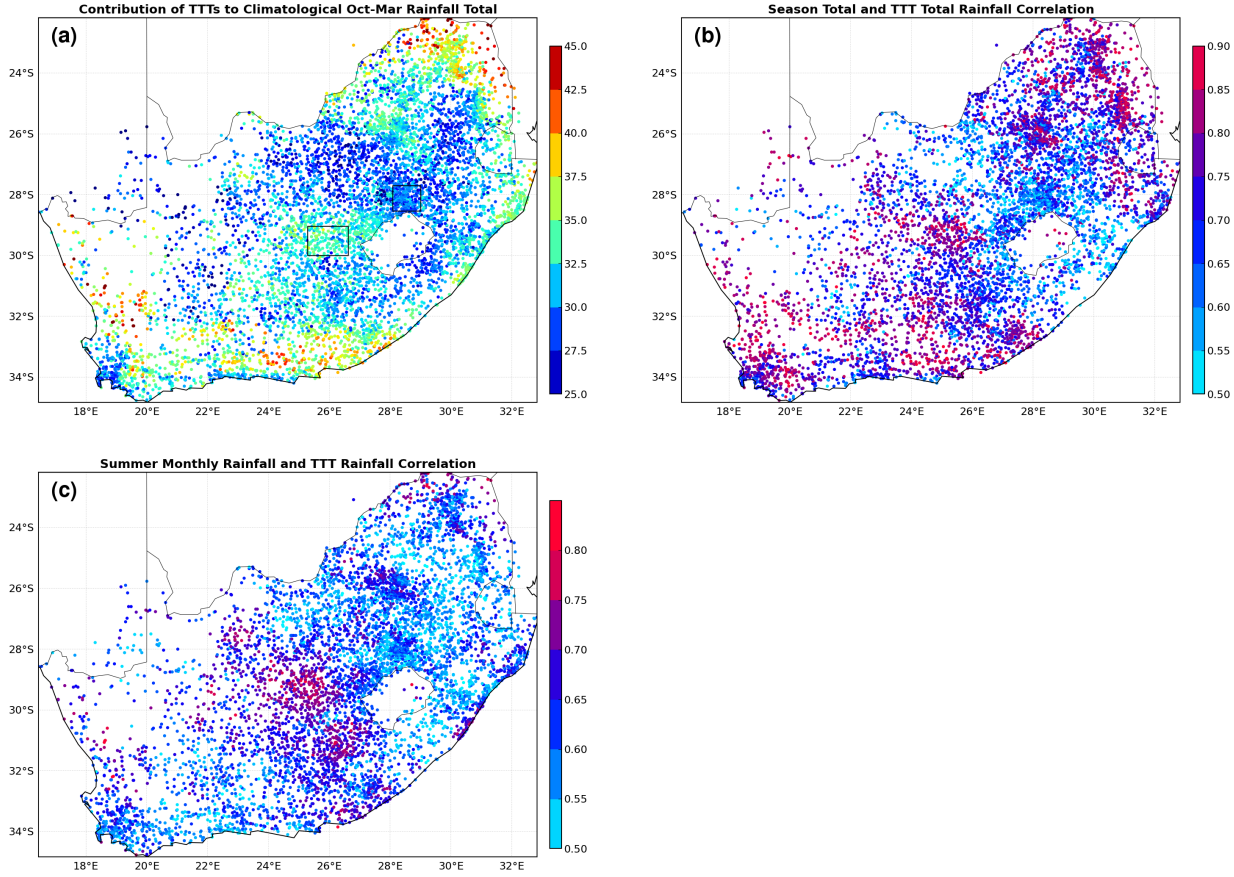

Figure 9: (a) TTT contribution to total ONDJFM rainfall totals (%), (b) correlation between normalised season total rainfall and season TTT rainfall (r-value), and (c) correlation between normalised monthly total rainfall and monthly TTT rainfall.

Correlation of ONDJFM accumulated rainfall with the total rainfall produced by TTTs alone is presented in Fig. 9 (b). The degrees of freedom in the correlation are low (n=19 seasons) so caution is needed; however, r-values above 0.5 occur at stations across the country, and increase above 0.8 in certain regions. This result is a clear indication that TTT variability is a major component of the interannual variability in the region. Fig. 9 (c) presents a similar analysis, correlation of monthly total rainfall with monthly TTT rainfall. R-values above 0.8 are particularly common between the longitude of 22°E and 28°E, suggesting that these synoptic systems control a large part of intraseasonal rainfall variability in this more marginal rainfall area. This region contains the western box used in Harrison (1984), which in comparison to the more eastward box (Fig. 9a), has r-values that are 0.2 higher. This result highlights again that TTTs are a more dominant influence in the lower rainfall regions than they are in the wetter regions of South Africa. The maps in of Fig. 9 b and c provide a qualitative confirmation of

TTT relevance to rainfall variability, however, due to the obvious auto-correlation that exists, these analyses have little quantitative value.

In summary, the metbot methodology applied to the 1979-1999 period has found that 14 (±3 s.d) continental TTTs occur on average during October to March producing rainfall for, on average, 3 to 4 days per event. This accounts for a mean contribution of 48 (±13 s.d) rain days to the 182 day summer long season. These figures also emphasise the spatial heterogeneity of South African rainfall and variability at monthly to interannual timescales. Comparison with Fig. 1 reveals much of the sub-regional differences are closely linked to topography.

3.3 Extremes and the season

It is plausible that rare extreme events can account for a substantial portion of variability in seasonal total rainfalls. The likelihood of this should increase westward across South Africa, concomitant with the increase in aridity to the west (Fig. 1). The relation of TTTs to such events is considered now. A total of 75 extreme rainfall days were found and collected into 52 events of, which 30 were associated with TTTs. Cut-off lows featured in the evolution of 6 of these TTTs. It is worth noting that the metbot identified the 1981 Laingsburg Flood cut-off low event, once it had dissipated into a cloud band (not shown).

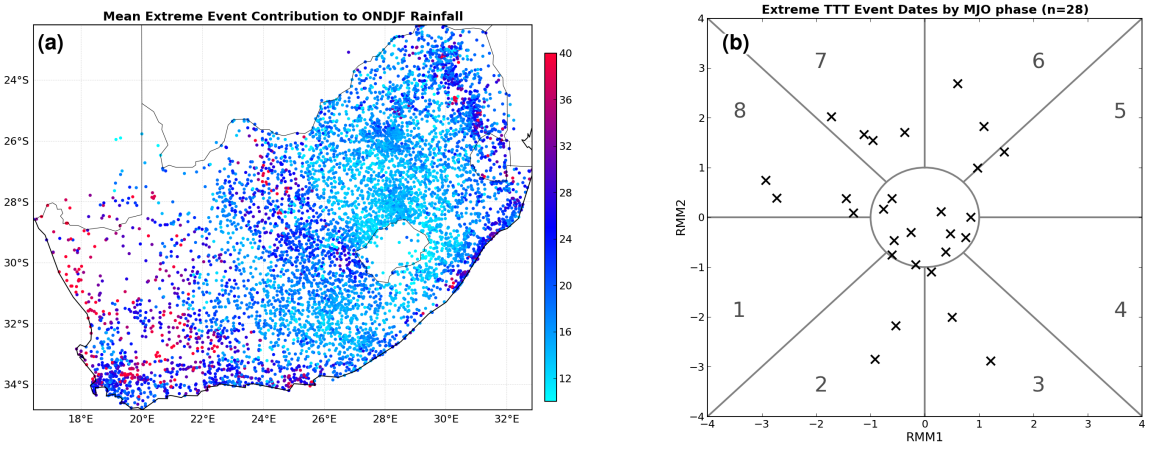

Figure 10: (a) Mean extreme event contribution to climatological ONDJFM Rainfall and (b) extreme TTT events plotted by RMM1 and RMM2 coordinates.

How much influence do these individual events have on seasonal totals? Fig. 10 (a) presents a summary of 28 extreme TTT events that occurred during ONDJFM in the form of their mean contribution to the climatological season total at each station. Stations are only included in the average when, for a given event, their total exceeds 10% or the climatological season total. Thus, the image gives a summary of the most heavily impacted stations for each event. The key point is that, at the least, these events can contribute 10% of the season total rainfall in 2-3 days. Single event contributions over 20% are common and at a few stations, contributions by extreme events to the six month summer rainfall of over 40% have been occurred.

Fig. 10 (b) presents the extreme TTT events plotted by their real-time multivariate MJO series 1 (RMM1) and 2 (RMM2) coordinates (Wheeler and Hendon, 2004). These observations present higher numbers of extreme TTTs during phases 6 to 8 of the MJO life-cycle. The number of extreme events occurring during phase 2 and 3 increases when inclusion of non-TTT days is made (not shown). The analysis was repeated using 90th percentile extreme

rainfall which introduced more equiprobable distributions by MJO phase, however, the scarcity of events occurring during phases 4 and 5 remained present. The following section investigates these results further.

3.4 MJO modulation of TTT intensity

Since the impact of the MJO on summer season rainfall has been established (Pohl et al., 2007), are the contributions of TTTs to monthly and seasonal rainfall modulated by its phase? Are the likelihood of extreme TTT events impacted too?

For reference, during phase 1 of the MJO, weak convection exists over tropical Africa and the Indian Ocean. During phases 2-4 this convection strengthens over the Indian Ocean and moves eastward reaching peak intensity during phases 4 and 5 over the Maritime Continent. As the the core MJO convective cluster moves into the Pacific Ocean, convection is suppressed across the Indian Ocean and over tropical Africa during phases 5 and 6, propagating towards the Maritime continent where strong suppression occurs in phase 7 and 8. During these later phases of the MJO, the suppressed Indian Ocean convection seems to enhance low-level flow towards tropical Africa (Fig. 8; Wheeler and Hendon, 2004).

Section 2 detailed the calculation of the two summary rainfall statistics used here: mean heavy rainfall percentage and maximum heavy rainfall percentage. In essence, these provide a measure of a) the overall areal coverage and persistence of heavy rainfall conditions, and b) the maximum areal coverage of heavy rainfall produced by a TTT at any point in its evolution. These two values serve as proxies to a) the sustained intensity of a system, and b) the maximum intensity reached during a TTT event.

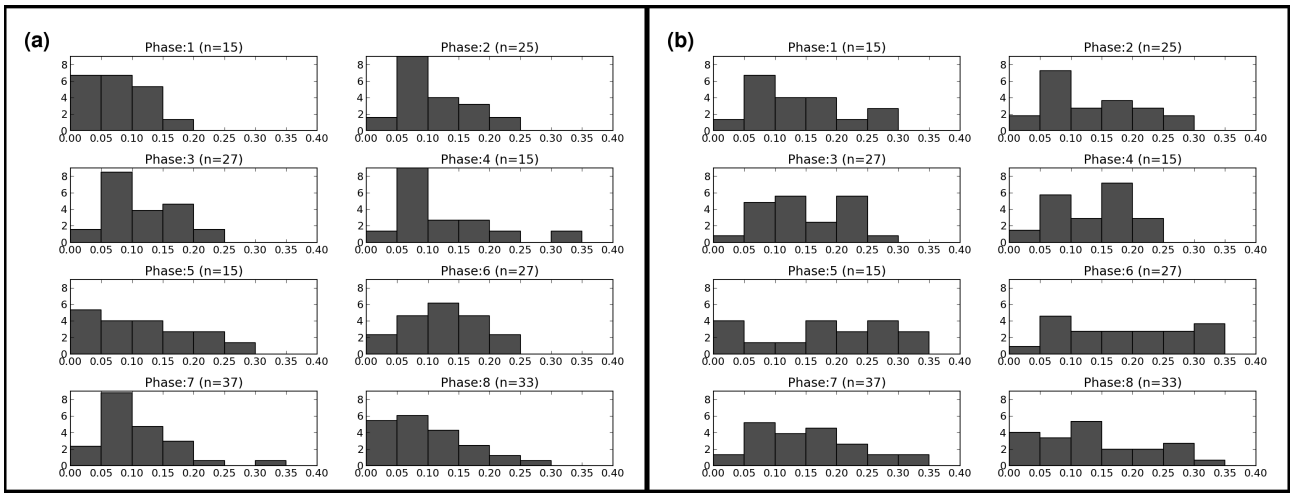

Figure 11: Histograms of a) mean heaviness and b) maximum heaviness during TTT events stratified by MJO phase; x-axis values denote the fraction of stations with daily rainfall in excess of 20mm; y-axis values are the normalised counts of number of events representing a given fraction (x-axis).

Fig. 11 (a) and (b) show histograms of these respective values, stratified by MJO phase. The only striking feature of Fig. 11 (a) is the confinement of values below 0.2 during phase 1, implying that a TTT during this phase does not sustain heavy rainfall at more than 20% of stations. During phases 2-4 and 7 there is a strong peak between 5 and 10%. These histograms closely resemble the probability distribution function (pdf) of the full population of values before phase stratification (not shown). In phase 6, Fig. 11 (a), however, suggests a pdf shifted towards

higher sustained event intensities, while for phase 3, theres is also a substantial number of systems with sustained intensities (15-20%).

With the assumption of student-t distributions for these pdfs, significance of distribution shifts was tested with the null hypothesis that the mean of the phase subset of values is no different to that of the full pdf of all values. The phase 6 shift to greater intensities was only significant at the 80th-percentile, however this was the most significant of all the other phases, except phase 1 which was significant at the 98th-percentile. Thus, sustained rainfall intensity during TTT events appears to be reduced during phase 1 of the MJO, but weakly promoted during phase 6.

A slightly different synoptic characteristic is that of maximum intensity of rainfall during a TTT life-cycle. Fig. 11 (b) shows that values of the maximum areal coverage of heavy precipitation have much broader distributions than the sustained intensity metric used in Fig. 11 (a). As such, the assumption of student-t distribution is questionable, nevertheless p-values of 0.05 for phase 1 and 6 confirm what is apparent visually, that maximal event intensities seem lower in phase 1 and have the potential to be higher during phase 6. Visually, it appears that intensities are slightly suppressed during phases 3 and 4, when compared to the wide spread of values in phases 5-8.

Due to the low number of events per phase and the uneven apportioning of these events between phases, these results need to be treated with caution. Building composite TTTs by phase may however reveal synoptic differences that could add some weight to the tentative conclusions. Fig. 12 presents composites based on low-level moisture jets, upper-level jets, and the low OLR values identified by the metbot procedure. The mean composite for events initiating during a given MJO phase are calculated from all time steps in the 24 hours leading up to, and including, mature TTTs.

By construction, all phase composites resemble a classic TTT (Fig. 12), however inter-phase differences are apparent. Based on OLR, phase 1 TTTs are dominated by deep convection in the tropics as suggested by the low values. Weak coherence in the northwest-southeast orientated band of low OLR values is present and persists through phases 2-4. The later phases exhibit strong cloud band features, especially for phase 6, where lower OLR values suggest more intense deep convection than 5, 7 or 8.

Moisture fluxes over tropical southern Africa are more zonal during phases 2-3, returning to more northeasterly orientations during other phases. Surprisingly, the extent and direction of the fluxes are very similar during phase 1 and phase 6, despite opposite tendencies of the rainfall intensity metrics in these phases. The answer to these differences may lie in the upper-level flow field since, during phase 1 TTTs, upper-level jets occur directly over the continent with slightly more zonal orientation that during phase 6. Phase 6 upper-level jets lie further west, with more poleward orientation of the flow encouraging stronger and more extensive cloud band systems.

These differences would lead to stronger upper-tropospheric divergence during phase 6 than phase 1, favouring more intense rainfall production. A more eastward location of upper-level flow during phase 1 could imply shorter residence time of the convection-favouring leading edge of an upper-level trough, before the westerly wave propagates into the southwest Indian Ocean. While these explanations are plausible, marked differences in upper-level flow during the other phases do not correspond to significant rainfall intensity changes.

With the exception of phases 1 and 2, strong tropical-extratropical moisture fluxes feed into the poleward end of these cloud bands, south of Madagascar, and are likely associated with the South Indian High. This finding suggests that the primary export of tropical moisture and heat into the extratropics may well not be located in the core of the continental cloud bands.

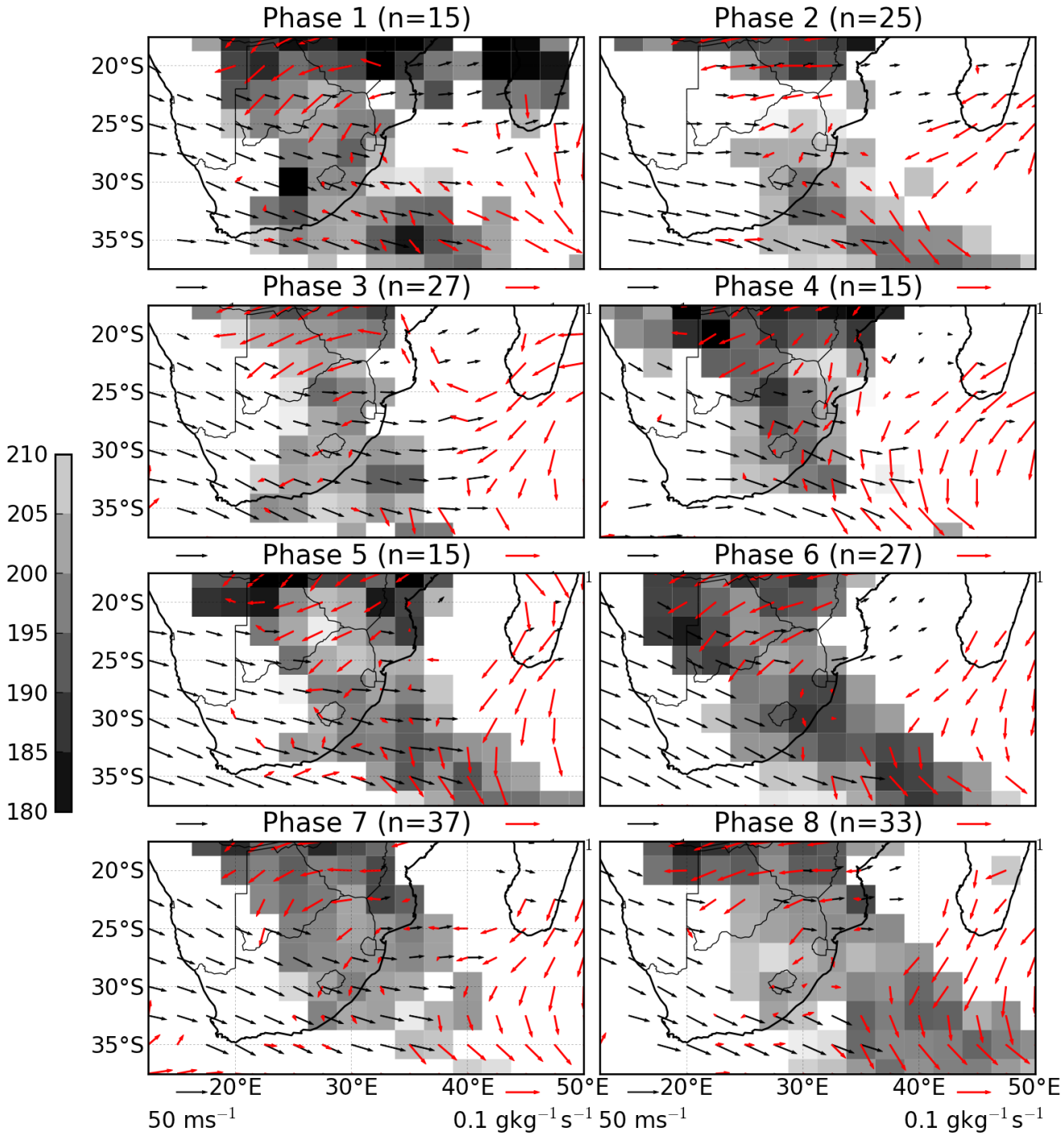

Figure 12: Composite TTT synoptics stratified by MJO phase for OLR (shaded, W.m^{-2}), 250mb jet regions (black vectors, m.s^{-1}) and 850mb moisture jets (red vectors, g.kg^{-1})

4 Discussion

The TTT identification methodology has allowed the first full description of the cloud band seasonal cycle over southern Africa. The peak occurrence of TTTs during November supports earlier conclusions that the influence of westerly waves on South African rainfall is stronger in earlier summer (D'Abreton and Lindesay, 1993); however that study regarded October as early summer. The spatial distribution of cloud band frequency (Fig. 3) provides a more detailed description of the march in TTT location than was possible in earlier studies (Harrison, 1984; Harangozo and Harrison, 1983). This result supports their finding of two preferred locations of development. An implication is that there are two axes of subtropical diabatic heating in the southwest Indian Ocean region, which corresponds very well to Fig. 7 in D'Abreton and Tyson (1995). However, the potential feed backs of these features and the associated heating onto the mean circulation field within the South Indian Convergence Zone are beyond the scope of this study.

Section 3.2 demonstrated that the signature of TTTs throughout the South African summer rainfall season is varied and spatially heterogeneous. The lower impact of TTTs on stations which receive higher rainfall totals supports the accepted understanding of seasonal cycle over the Highveld and escarpment. This understanding is that once enough moisture is brought onto the continent from the adjacent ocean, a diurnal cycle of rainfall can develop. Thus, even in the absence of the large-scale forcing provided by a synoptic-scale system such as TTTs, convective rainfall may occur via scattered thunderstorm activity associated with the diurnal cycle of surface heating.

The contribution of TTTs to climatological monthly total rainfall (Fig. 5) is closely linked to the number of rain days they produce, a point made by Harrison (1984). These contributions display a marked seasonal cycle with peak contributions over 40% during November and January. The December decline in contributions in northern South Africa is puzzling. A semi-annual cycle in the strength and position of the South Atlantic and South Indian high pressure systems is known to exists (Tyson and Preston-Whyte, 2000) so there may be an associated change in the upper-level westerly flow, mid-season, which has an impact on TTT rainfall contributions.

Higher TTT contributions to both rain days and monthly rainfall totals in lower rainfall areas suggest that the synoptic-scale forcing provided by TTT systems is necessary for rainfall in the more arid regions of South Africa. Generally, this rainfall is convective in nature, hence the synoptic forcing helps trigger convection in a conditionally unstable atmosphere, as discussed in Part I. This suggests that these regions are more sensitive to interannual variability in TTT frequency. Fig. 9 lends weight to such a conclusion.

TTTs account for over 30% of the total accumulated climatological rainfall for ONDJFM. This contribution reaches over 45% along the southern coast and adjacent interior and in northernmost South Africa. Correlations of monthly and seasonal total rainfall with the corresponding TTT-contributed rainfall (Fig. 9 c and b) further emphasise the role of TTTs in regional rainfall variability from subseasonal to interannual timescales. The higher correlations in the west and far north of South Africa correspond well to areas experiencing high dry spell frequency during the summer rainy season (Fig. 5 in Usman and Reason, 2004). The results presented here support conclusions that TTTs are a dominant driver of wet and dry spell frequencies (Cook et al., 2004; Usman and Reason, 2004).

The importance of TTT rainfall in the Kwazulu-Natal region, on the east coast of South Africa, compares well with Diab et al. (1991). Contributions to station rainfall over 40% are common during November to February, with climatological ONDJFM contributions near 35%. An open question remains in how the rainfall climatology is apportioned between TTTs and smaller scale systems such as mesoscale convective complexes (Blamey and Reason, 2012).

The analysis of the potential impact of extreme TTT events on season totals has highlighted an important feature for regional rainfall variability: single extreme events have the potential to drastically alter seasonal rainfall totals. This contribution can add substantial variability, without the need for persistent circulation anomalies. Analysis of heavy rainfall days by month has shown that TTTs are the dominant synoptic type responsible for intense precipitation events in much of the region. The exception to this is over the eastern escarpment.

The MJO may modulate the likelihood of such events. Examining Indo-Pacific composites of MJO circulation reveal that moisture flux anomalies are directed away from Africa during phases 2 to 4, and towards Africa during phases 6 to 8. At first order, this would suggest increased (decreased) moisture supply into subtropical Africa during late (early) MJO phases (Fig. 8 in Wheeler and Hendon, 2004). Poleward movement of this moisture is suggested by Pohl et al. (2007), Fig. 13. However, the results here reveal little change in synoptic-scale low-level moisture supply to TTTs. A tentative conclusion is that the upper-level wave formation is a more notable influence than the MJO on TTT behaviour. In answer to the question posed in the introduction, it is unlikely that the MJO has a strong modulating effect on TTT intensity. However, any suggestions of less (more) intense TTTs during phase 1 (phase 6) will need to be explored with a longer data record and perhaps, other rainfall metrics.

5 Conclusions

This study revisited the question: what is the contribution of TTTs to South African summer rainfall? The results strongly supported the findings put forward in Harrison (1984) that TTTs contribute a substantial portion of summer season rainfall (30-50%) during all months. This is, however, somewhat lower than the 60% often quoted in literature. The use of a high-resolution daily station rainfall data set has demonstrated that there are marked month to month changes in these contributions through the season. All regions however, are not equal. Lower rainfall regions along the sharp rainfall gradient in central South Africa are more sensitive to TTT occurrence than the Highveld and eastern escarpment.

The seasonal cycle of TTTs has been described in substantially more detail than previously. Its shape highlights the importance of November for TTT impacts which supports use of a NDJF season in summer rainfall variability studies. The presentation of the progression in location of TTTs through the season, opens up a slightly different angle in southern Africa variability studies: How do large-scale climate modes amplify or suppress the seasonal cycle of TTT frequency and location?

This study has used a novel methodology to identify TTTs over southern Africa with the strong ability to capture details of event scale rainfall. This methodology has facilitated the first clear description of the TTT seasonal cycle and its influence on regional rainfall, without the need to artificial define the season of interest. The use of multiple rainfall metrics is demonstrated in assessment of the influence of the MJO on system intensity.

Acknowledgements

Benjamin Pohl is thanked for his preprocessing of the WRC station rainfall data. Interpolated OLR and NCEP2 data was obtained from NOAA/OAR/ESRL PSD, Boulder, Colorado, USA through http://www.cdc.noaa.gov.

Part IV

The influence of large-scale climate modes on tropical temperate troughs

How does ENSO project onto this annual cycle (Part III) and into weather timescales?

Specific Questions:

- Does ENSO influence TTT frequency and/or intensity?
- Do local modes of sea surface temperature variability influence TTT characteristics?
- Is the El-Niño teleconnection to southern Africa affected by longitudinal position of maximum Pacific warming?
- What are the general characteristics of regional circulation during years with high or low numbers of cloud band events?

"It's the little details that are vital. Little things make big things happen" - John Wooden

On the projection of ENSO into cloud bands over southern Africa

Abstract

The impact of the El-Niño Southern Oscillation (ENSO) on tropical-extratropical cloud bands over southern Africa is investigated. A novel object-based methodology is used to explicitly identify these systems known regionally as tropical temperate troughs (TTT). This allows for the first detailed description of year to year variability in cloud band location and frequency. The TTT climatology produced indicates two preferential regions for system development, a Madagascan location and a more favoured continental location. El-Niño NDJF seasons, especially those associated with severe regional droughts, are characterised by a strong reduction in the total number of systems in both locations, which challenges current understanding that systems move offshore during these seasons. A ratio of offshore systems to continental systems does however, suggest a more equal apportioning of systems during warm ENSO events with favouring of the continental systems during cool events. While El-Niño years correspond to almost all of the very low cloud band years, La-Niña does not correspond to peak years but maintains climatology.

The methodology allows for detailed rainfall characteristics to be assigned to each event. La-Niña years display increased likelihood of more intense and persistent systems. El-Niño years show a weaker synoptic-scale response however, increased likelihood of less persistent systems is suggested.

Investigation of circulation associated with low and high frequency seasons of continental TTT systems is presented, including a discussion of the weak response in cloud band frequency during 1997-1999 El-Niño/La-Niña. The analysis included an investigation of the possible association between regions of negative stretching deformation of 250mb zonal flow and cloud band frequency. The relationship was not stable between seasons, which indicates that increased negative zonal stretching deformation, alone, is insufficient in enhancing cloud band activity in the South Indian Convergence Zone. Further analysis of the unusual 2009-2010 season reveals that circulation patterns were as expected for El-Niño with substantially fewer systems. However, two unusually persistent TTT episodes in January and then February may have contributed to a near normal cloud band count and mitigated the drought that was expected.

A first order investigation into the sensitivity of southern African climate to El-Niño flavours was performed with an atmosphere-only general circulation model and idealised SST forcing. The response to Eastern Pacific warming was weak, however the central Pacific warming produced increased cloud band activity in the central Indian Ocean. The response over subtropical southern Africa was weak. Limitations to the experiment are discussed.

A manuscript based on this part is in preparation for Journal of Climate:
"On the projection of ENSO into cloud bands over southern Africa"
N.C.G. Hart, C.J.C. Reason, N. Fauchereau and M. Tadross

1 Introduction

The consequences of anomalous warming or cooling in the equatorial Pacific for southern African climate are well known (Van Heerden et al., 1988; Nicholson and Kim, 1997). Composites of El-Niño (La-Niña) years for subtropical southern Africa reveal drier (wetter) conditions for the summer rainy season. Correlations between total November-February regional rainfall and ENSO-related indices are often above 0.5 for periods after the 1960s (eg. Richard et al., 2000) with higher values displayed for rainfall sub-regions (Hart et al., 2009). Despite this strong first-order relationship, predictive skill during ENSO events remains fickle. Weak El-Niño events, such the 1991/1992 2002/2003 event, have produced severe regional droughts while the strong event of 1997/1998 had little effect.

This lack of a linear response to ENSO events has contributed to difficulty in understanding the mechanism of the teleconnection between southern Africa and ENSO, despite the in-phase peak of ENSO warming or cooling and the southern African summer rainfall season. The prevailing understanding is analogous to the shifting of the South Pacific Convergence Zone (SPCZ) towards the El-Niño sea surface temperate (SST) warming anomaly, as noted by Trenberth (1976). Regionally, Lindesay (1988) suggested that during El-Niño years, the displacement of the rising branch of the Walker circulation from tropical Africa into the central Indian Ocean is associated with a northeastward shift of the South Indian Convergence Zone (SICZ) and the associated cloud band systems, known as tropical temperature troughs (TTTs).

This equatorward and eastward displacement of one of the main synoptic rain-producing systems during El-Niño events (Harrison, 1984) would be associated with an equatorward shift in the subtropical jet and lower than normal rainfall over southern Africa. Subsequent studies have, for the most part, accepted this understanding, citing the offshore location of TTTs as a plausible explanation for reduced continental rainfall (eg. Cook, 2000; Mulenga et al., 2003). In general, the understanding of the La-Niña influence is that convection over tropical Africa is enhanced as the strength of the rising branch of the Walker cell is enhanced. Similarly, the continental location of cloud bands is strongly favoured, enhancing the SICZ at the seasonal timescale and increasing rainfall totals over subtropical southern Africa (Harrison, 1986).

The puzzling lack of drought during the 1997-1998 El-Niño events spurred further studies that investigated the importance of regional SST (eg. Reason and Mulenga, 1999; Hansingo and Reason, 2009) and differences between ENSO events (Reason et al., 2005; Lyon and Mason, 2007). Furthermore, the changing influence of Indian Ocean SST likely has enhanced non-linearities in the regional teleconnection (Landman and Mason, 1999). Reason and Jagadheesha (2005) showed the importance of the Angolan Low in modulating the regional response to El-Niño events using modelled and reanalysed 3-month average circulations. The importance of this cyclonic feature for subtropical southern African rainfall at subseasonal timescales was demonstrated by Cook et al. (2004) who suggested a fundamental role of the low in TTT development. This has been supported at the synoptic-scale by case studies (eg. Hart et al., 2010).

Recently, the multi-scale nature of the regional climate has been studied by discriminating daily weather regimes using cluster analysis (Fauchereau et al., 2009; Crétat et al., 2010) and principal component (PC) scores (Pohl et al., 2009). These methods have provided further insight into the regional ENSO response. Fauchereau et al. (2009) showed that two different convection regimes were favoured during El-Niño years, however, only one was associated with substantial anomalies over southern Africa. During the 1997/1998 summer, this regime, however was suppressed and the regime with little continental impact was favoured. Further detail was unpacked by Pohl et al. (2009) where they suggested a separation of predominantly Madden-Jullian Oscillation related convection from TTT-related convection. The indications were that El-Niño years suppressed the tropical convection PC modes

but had little effect on the TTT modes which were responsible for high-frequency synoptic-scale wet spells. They postulated that this could interfere with the general drying that is expected during El-Niño.

In addition to modification of the Walker circulations, many studies have emphasised the role of mid-latitude wave activity in regional cloud band development (Harangozo and Harrison, 1983; Todd and Washington, 1999) and suggested an extratropical pathway for communication of Pacific anomalies to southern Africa (eg. Hart et al., 2010). Thus to summarise the current understanding, anomalous Pacific warming can be communicated to southern Africa via modifications in Walker circulation and extratropical westerly wave flow. This signal is further modified by regional SSTs and the state of quasi-stationary Angola Low and influenced by Madden-Julian Oscillation (Pohl et al., 2007). Within the subtropics, tropical-extratropical interactions produce regular cloud bands which add up at the seasonal timescale to a subtropical convergence zone known as the SICZ (Cook, 2000).

Since this study focuses strongly on these tropical-extratropical interactions, the multi-scale conceptual framework elucidated by Widlanksy et al. (2011) is tested for its potential usefulness in framing the variability of regional cloud bands. Their study addressed the northwest-southeast tilt of the subtropical convergence zones of the Southern Hemisphere. The hypothesis they tested is that the east-west SST gradient maintains a region of negative zonal stretching deformation of the zonal mean flow ($\frac{\partial \bar{U}}{\partial x} < 0$). Theory dictates that mid-latitude Rossby waves propagating into the $\frac{\partial \bar{U}}{\partial x} < 0$ region, slow down, and amplify meridionally (Webster and Chang, 1997). This helps trigger convection and rainfall and accounts for the tilted orientation of the convergence zones. The focus of Widlanksy et al. (2011) was the SPCZ, however, some results for the weaker SICZ warrant further use of this framework for the southern Africa region. Understanding regional tropical-extratropical interactions in this way provides a link between the influence of ENSO through both tropical and extratropical pathways.

Despite being repeatedly invoked in explanations of the regional influence of ENSO, TTTs have not been explicitly identified in climate studies until now. Part II presented a novel methodology that achieves this by exploiting the northwest-southeast cloud bands that define these systems. A regional climatology of cloud bands using this automated identification procedure was developed in Part III. Thus, the first aim of this study is to use this methodology to investigate the regional cloud band response to ENSO and the impact this has on South African rainfall variability.

Much has been made of the non-linearity of the regional response to remote Pacific SST anomalies, however, it is plausible that some of this may be due to linear responses to different expressions of ENSO events, the so called "flavours" which have shown to be important to regional El-Niño teleconnections (eg. Trenberth and Stepaniak, 2001; Wang and Hendon, 2007). In this study, a set of idealised model experiments is used to perform a first order investigation of this hypothesis, in relation to cloud band frequency.

The final aspect of this study is an attempt to clarify the regional processes associated with interannual cloud band variability in terms of changes in $\frac{\partial \bar{U}}{\partial x}$, regional SST anomalies and moisture transports. This approach is first used to interpret the idealised experiment results and then applied to observations.

The next section outlines the data and methodologies used in the sections that follow. The average cloud band response to El-Niño and La-Niña years is discussed next, followed by implications for South African rainfall. Results from the El-Niño flavours experiment are then presented and finally, seasonal mean circulation is discussed in section 6. The paper ends with a results summary and some conclusions.

2 Data and Methods

To achieve the aims of this work it was necessary to automatically identify cloud bands in multiple data sets, a task for which the metbot methodology of Part II is well suited. To summarise, daily OLR data in the domain 0º- 60ºS; 0º- 80ºE, is thresholded at 230 W.m^{-2}, plotted and run through a blob detection algorithm. Tropical-extratropical cloud bands are flagged when blobs extend from the tropics (<20ºS) into the extratropics (>40ºS) with a positive tilt. OLR data is selected 48 hours either side of flagged days, and the process is repeated, with these criteria relaxed, to build base tracks of OLR blobs which meet cloud band criteria at some point on their track.

For the observational part of this study, the methodology was to applied daily outgoing longwave radiation (OLR) data provided by NOAA (Liebman and Smith, 1996). Seasonal circulation means for November to February (NDJF) were constructed from 6-hourly NCEP-DOE Reanalysis II (NCEP2) described in Kanamitsu et al. (2002). Both products were used for the period 1979-2011 on a 2.5ºx 2.5ºlat-lon grid, with the metbot identifying 821 events in the period each lasting about 3-4 days. Cloud band frequency and location is displayed using a grid-point count. This was calculated by counting the number of times a grid-point falls within the perimeter of all OLR blobs for a specified time period. One could constrain this to only blobs that are flagged as cloud bands, however, since the interest is the synoptic-scale, these authors chose to include all OLR blobs on each base track. The results show little qualitative difference in location however grid-point counts are 3-4 times lower than those presented here. For climatology, the total grid-point count was divided by the number of months or seasons used in the calculation. Since the time resolution of OLR data is daily, these grid-point counts can be interpreted as a count of cloud band associated days.

The rainfall associated with cloud band events is obtained using the Water Research Commission daily station rainfall data comprising of 7445 stations and is used for 1979-1999 period (Lynch, 2003). Unfortunately, this data set does not extend beyond 1999. To measure TTT rainfall characteristics, rain statistics were computed by event, for all stations that fell within the cloud band perimeter. Seasonal rainfall indices were calculated by normalising accumulated NDJF rainfall at each station. These times series were averaged together for stations within each summer rain region defined by Tennant and Hewitson (2002).

For simplicity, the NDJF seasons are referred to by the year that they start. Using the multivariate ENSO index (Wolter and Timlin, 1998), the chosen El-Niño event starting years are: 1982,1987,1991,1994,1997,2002, 2004, 2009. The chosen La-Niña years are: 1984,1988,1995,1998,1999,2000,2007,2010. The equal number (n=8) of warm and cool events will ensure comparability of composites and event-based statistics.

3 Cloud band response to El-Niño and La-Niña events

Before addressing TTT rainfall over South Africa, the direct TTT response to ENSO is explored now in the observational data. Results are constructed from the 184 (177) events occurring during El-Niño (La-Niña) years. This first result therefore, indicates little effect of ENSO on South Indian Ocean cloud band totals. The climatology motivates for a split of events into continental and Madagascan events at about 45ºE (eg. January in Fig. 1a; see Part III for more details). The climatological ratio in the number of events $\frac{NContinental}{NMadagascan}$ is 1.5. Calculating this for all events during El-Niño years gives 1.16, while La-Niña year events have a ratio of 1.9. To some degree, this supports the general understanding of enhancement of offshore events during El-Niño, since the ratio nears 1:1, and favouring of continental events during La-Niña, with nearly two times as many systems in the west. An

important caveat is that this split does not account for systems that move across both regions. While rare, it is worth noting that systems may form west of 45°E but slightly offshore from southern Africa and therefore produce little continental rainfall (i.e. in the Mozambique Channel) (Manhique et al., 2009)).

The ENSO cloud band grid-point count anomalies are presented in Fig. 1 with monthly climatology values contoured for ease of reference. A more detailed discussion on the monthly climatology of regional cloud band activity is available in Part III. In summary, the climatology exhibits two preferential locations of cloud band formation: one rooted in southern Africa, the other, over Madagascar. During early summer months, continental systems dominate, by midsummer systems are common at both locations, and as summer wanes, systems become confined to the Madagascan region in the Southwest Indian Ocean.

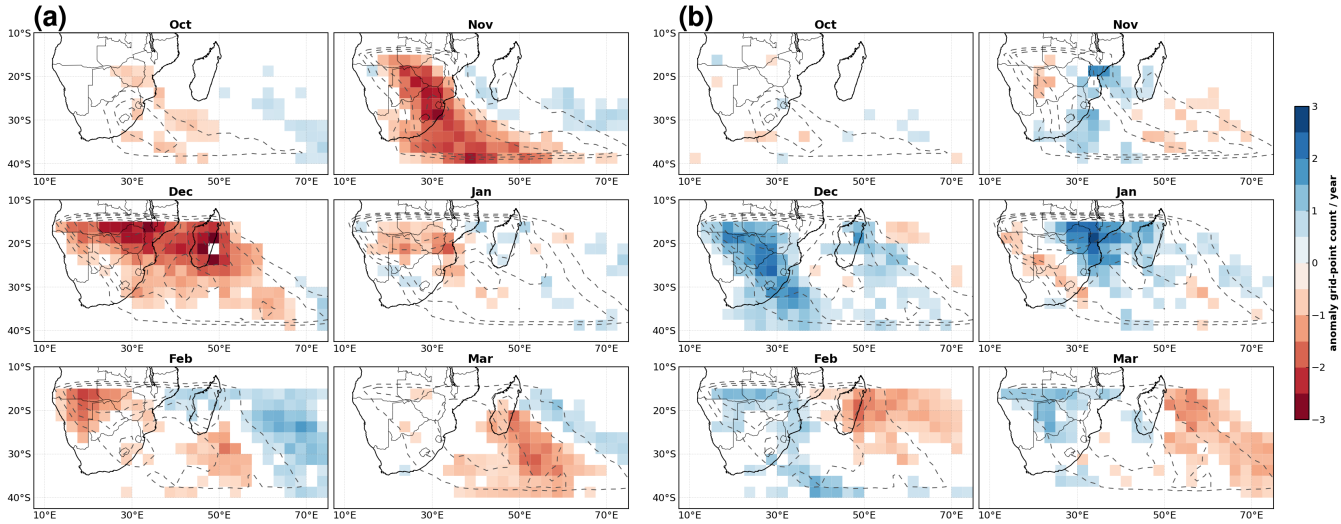

Figure 1: Cloud band grid-point count mean anomaly for (a) El-Niño seasons and (b) La-Niña seasons; climatology grid-point count is contoured (dashed line) starting at 2.

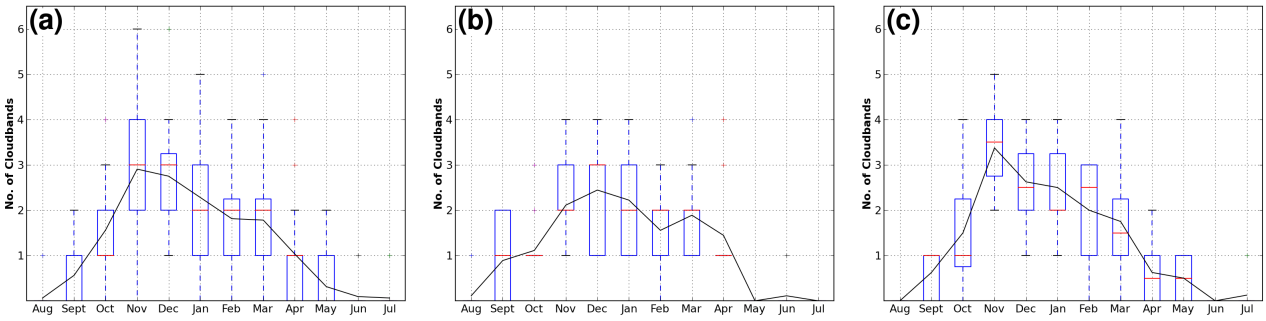

Figure 2: Seasonal cycle of continental cloud band occurrence during all 32 (a), 8 El-Niño (b), and 8 La-Niña (c) seasons ; boxes bound lower and upper quartile of values with red streak indicating median, solid curve depicts mean.

During El-Niño, the response in cloud band occurrence shows a strong reduction in November, which continues into December (Fig. 1a), with up to 3 fewer cloud band days. The effect is in the core formation regions during these months. The reductions are weaker during January and February, however February suggests an increase in systems east of the Madagascan formation zone. This increase persists weakly into March, while reduction in Madagascan cloud bands remain substantial.

The mean La-Niña response, however, indicates a mild increase of systems during November (Fig. 1b). The strongest effect occurs in December, with 2-3 extra cloud band days experienced over southern Africa and 1-2 in the Madagascan location. The January panel suggests a shift in system locations towards Mozambique, causing a small reduction in occurrence across central South Africa. Minor increases in grid-point count remain over much of southern Africa during February and March, however 1-2 fewer cloud band days are experienced east of Madagascar.

The event-to-event variations in response, however, are substantial. Fig. 2 displays the spread of the number of the number of cloud bands systems over southern Africa, by month. The average response of a suppressed (enhanced) seasonal cycle during El-Niño (La-Niña) events is highlighted by the black curve. This, however, betrays the key point of Fig. 2, the event-to-event variability is high, as illustrated by the box and whisker features. Examination of individual seasonal cycles during ENSO seasons revealed substantial differences, in both the shape and magnitude of the seasonal cycles (not shown). The remainder of this study focuses on NDJF totals and averages in order to avoid this subseasonal noise in ENSO reponses. To this end, Fig. 3 presents a time series of the total number of NDJF continental TTT events with SST mode events included for comparison. A non-linearity between the regional cloud band response to cool and warm ENSO events is observed: most low TTT count years correspond to El-Niño events, however, the opposite is not true during La-Niña events. As for regional SST modes, there is little obvious correspondence between TTTs and the South Indian Ocean Dipole (SIOD), Tropical Indian Dipole (IOD) and Benguela Niño events. A full description of response variations between individual El-Niño and La-Niña events is beyond the present scope. The next question is: What is the relation between this TTT variability and summer rainfall?

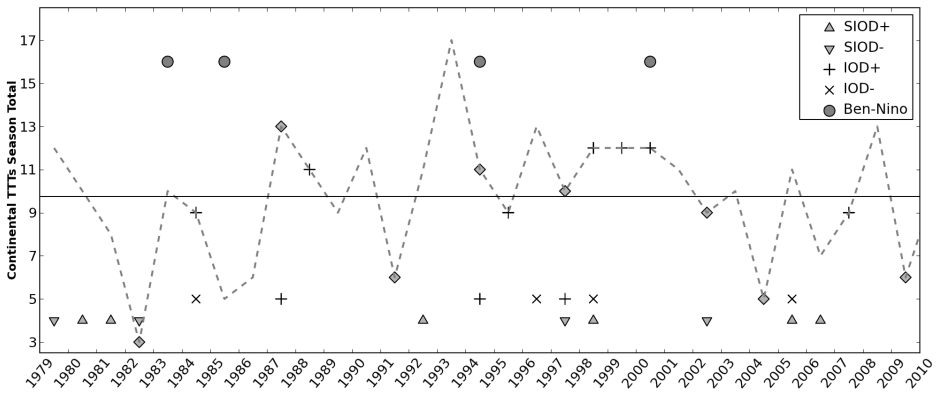

Figure 3: Continental TTT NDJF totals for 1979-2009 with inclusion of El-Niño (La-Niña) events on the timeseries curve as diamonds ("+"); off-curve symbols depict regional SST mode events (see legend).

4 Impact on regional rainfall

At the synoptic-scale, the rainfall impact of TTT systems is broadly due to two factors: persistence and intensity. Fig. 4 presents an answer to the question, do El-Niño and La-Niña events modify these aspects of TTT-produced rainfall over South Africa? The proxy for system intensity, HMX, is defined as the maximum daily percentage of stations that recorded heavy rainfall (>20mm), during the lifespan of a TTT. Persistence is obtained by the number of wet days produced by a TTT over South Africa. Normalised histograms of these values were produced for all events (Fig. 4 a and b, top panels), and then for the subset of events occurring during El-Niño (Fig. 4 a and b, middle panels) and La-Niña (Fig. 4 a and b, bottom panels). Note that results are produced from 302 continental

rain-producing TTTs events that were identified in the 1979-1999 period, of which, 60 occurred during El-Niño years and 62 during La-Niña years.

On average, there is a wide spread of HMX values with between 5% and 35% of stations recording heavy precipitation during an event, with a peak at 5-10% (Fig. 4a). This distribution seems to shift little during El-Niño. During La-Niña however, the peak shifts to 10-15% and there is a weighting of the distribution tail to values above 25%, indicating a higher probability of intense TTTs during these seasons. As for the length of rain spells, there seems to be a tightening of their likely duration in El-Niño seasons (Fig. 4b) to 3-4 days. During La-Niña there is great spread in the persistence, however systems regularly produce rain for more than 4 days and sometimes up to a week. These results highlight an important complexity in that rainfall due to TTTs is unlikely to be related to the seasonal frequency of TTTs alone. A case in point may be 1995, which had record rains with a near average TTT count (Fig. 5). Of course other rainfall synoptic systems such as cut-off low events or tropical depressions may have been more important in that summer.

Despite the near equal number of total events during ENSO warm or cool events, 62 to 60, Fig. 4 (c) indicates that the likelihood of few continental cloud bands is substantially higher during warm events. In contrast, La-Niña years are characterised by average to higher numbers of TTT events. This result, however, belies the strong event to event differences in ENSO event response as demonstrated in Fig. 3.

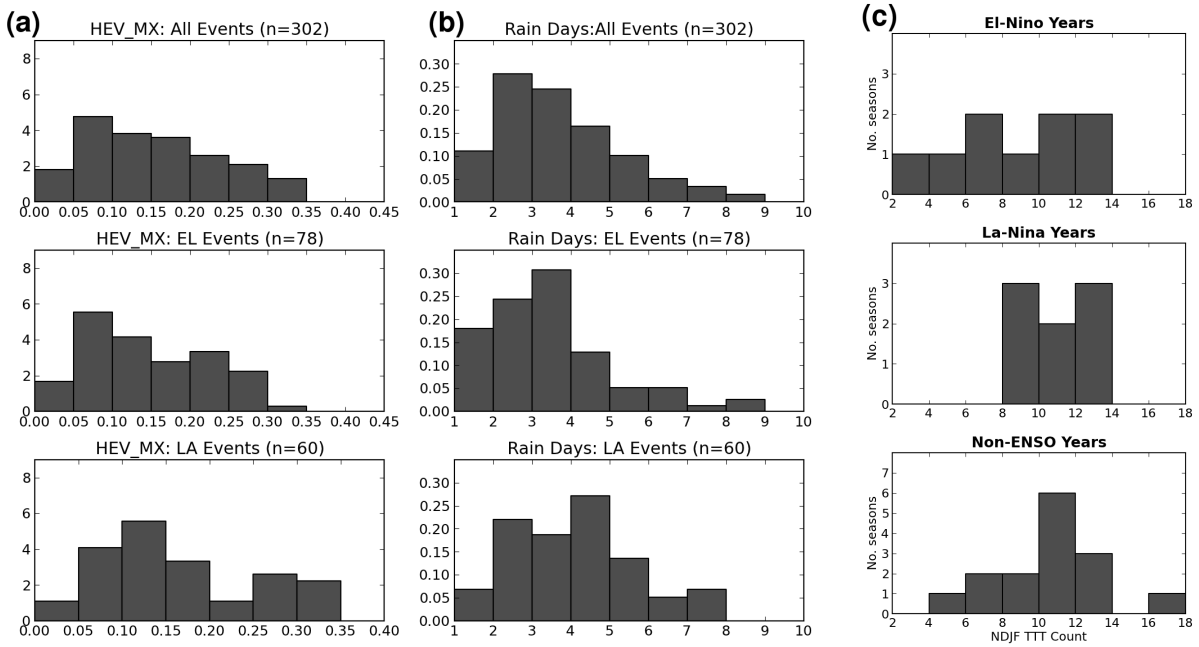

Figure 4: Intensity (a), persistence (b) and NDJF TTT count (c) histograms for El-Niño and La-Niña events.

TTT rainfall contributions have substantial subregion heterogeneity (see Part III), hence the independent representation of four summer rainfall regions in Fig. 5 (b) (after Tennant and Hewitson, 2002). The time series of the number of continental cloud bands during NDJF is overlaid with El-Niño and La-Niña provided near the x-axis as diamonds and cross-hairs, respectively (Fig. 5b). Note that the zero-line for rainfall anomalies is aligned with the mean number of cloud bands of 9.75. Little correspondence is exhibited between cloud band maxima and the ENSO events in this short time period. However, years of few TTTs correspond to El-Niño events in 1982, 1991, 2004 and 2009 (the latter two are not shown). Region-wide droughts corresponded to the 1982 and 1991 El-Niño

seasons (Rouault and Richard, 2003). Few TTTs occurred in the season of 1985/1986, and were associated with a mild drought as represented by the normalised rainfall anomalies.

The usefulness of using rainfall sub-regions is demonstrated by the highlighting of the drought-prone region 1 (black bar) which exhibits dry anomalies more frequently than in the other regions. Attention has been drawn to this drought corridor in the Limpopo River valley by Usman and Reason (2004) and their work on dry spell frequencies. Reason et al. (2005) showed that summer dry spell frequency in the Limpopo region was well correlated with ENSO. For example, during the 1988 season, La-Niña conditions were accompanied by higher rainfall totals in region 3 and 4 but low rainfall in region 1.

The most striking feature in Fig. 5 occurs in 1993: nearly double the average cloud band count is accompanied by only a marginally wetter region 3 and 4. The drought the following season is then followed by the wettest year in this record during the 1995/1996 La-Niña year, despite a near average number of TTTs. Despite the generally accepted view that TTTs are the dominant summer rainfall producing system, this result highlights that cloud band frequency alone is an insufficient predictor of summer rainfall. Therefore, interpreting the remaining cloud band results as direct indications of rainfall variability would be unwise.

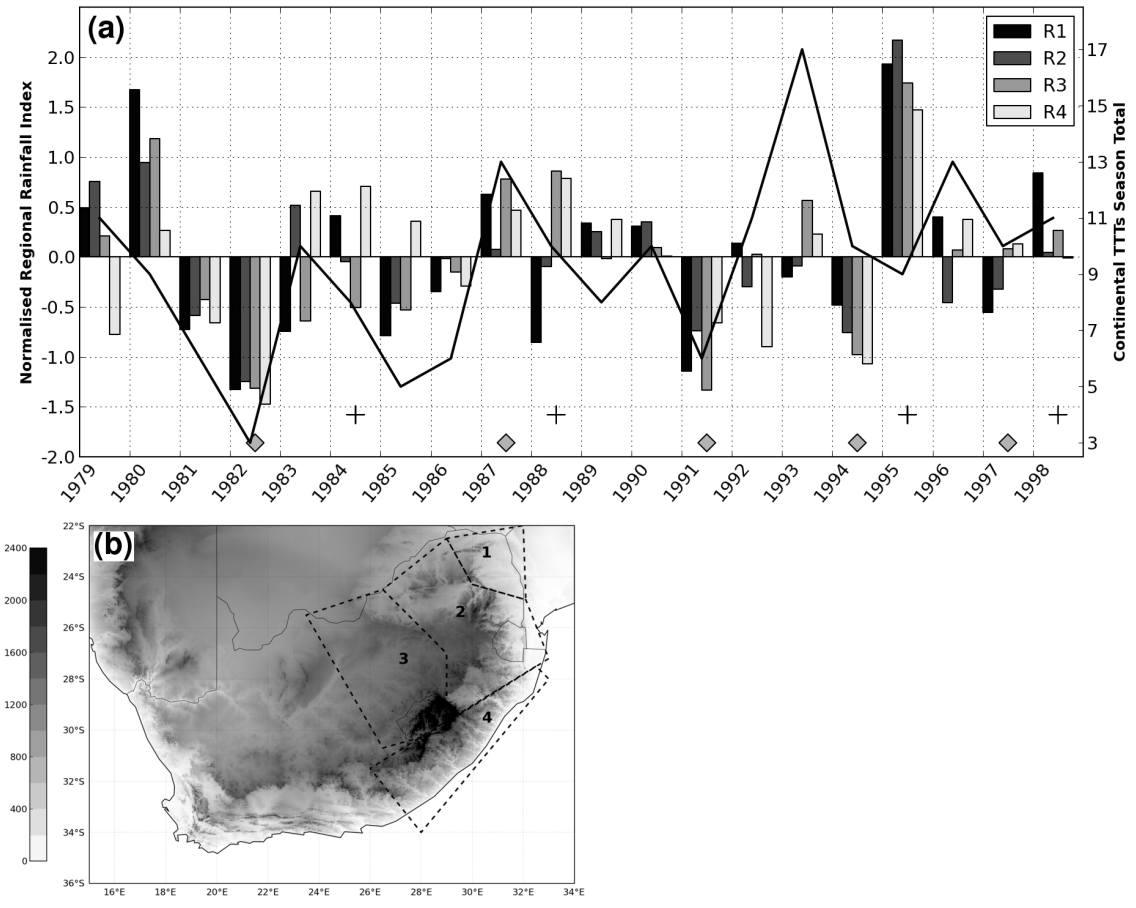

Figure 5: (a) Time series of four main summer rainfall regions (bars) and NDJF cloud band count (solid line) with El-Niño (diamonds) and La-Niña (cross-hairs) plotted for reference; (b) topography (shaded) and subregion polygons.

5 Idealised El-Niño flavour experiments

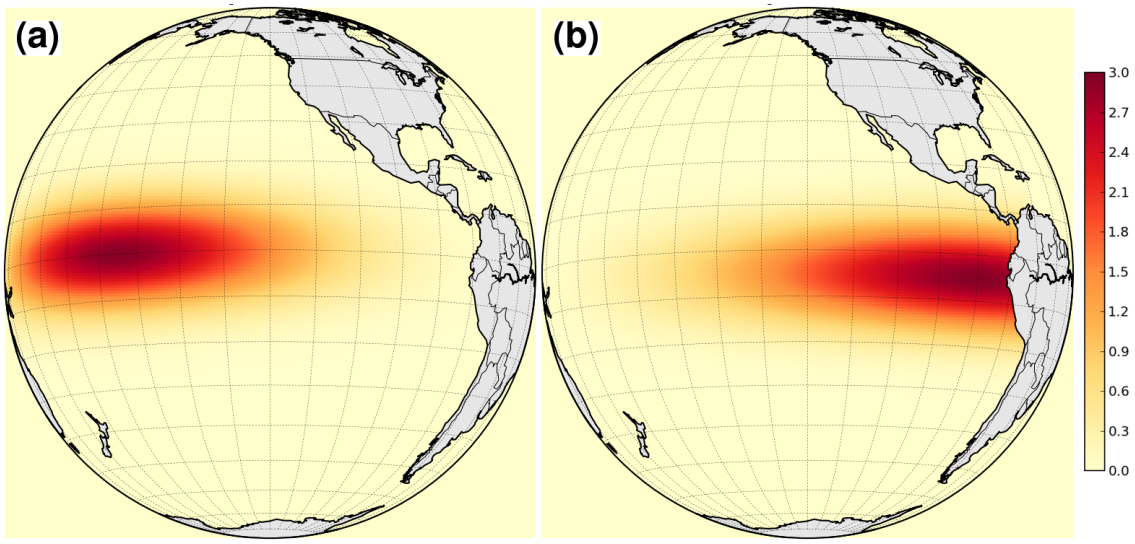

Figure 6: Anomaly forcing fields for Central Pacific (a) and Eastern Pacific (b) warming experiments (shading represents °C added to climatology)

Can the non-linearity of the regional El-Niño response be simply explained by the different "flavours" of ENSO warming? Two idealised SST forcing fields were designed to test the hypothesis: Is subtropical southern Africa sensitive to the longitude of maximal El-Niño warming? The scope of the experiments are, by construction, very narrow since without regional SST responses the results only indicate a direct atmospheric response, similar to Cook (2001).

HadAM3P, a 1.85°x 1.25° lat-lon resolution, mixed-phase precipitation configuration of the Unified Model v. 4.5, was the atmosphere-only general circulation (AGCM) model chosen for the experiments (Pope et al., 2000). This AGCM produces seasonal forecasts at the University of Cape Town; thus, prescribing SST forcing fields was relatively simple. The ability of this model to represent regional climate is poorly studied and so this choice had the additional benefit of providing some assessment of the skill of this model in simulating cloud band climatology. NOAA optimally interpolated monthly SST was used to build the forcing fields (Reynolds et al., 2002). Warm anomalies were added to climatological SST in the central Pacific and eastern Pacific (Fig. 6) , with specifics summarised in Table 2. In the all cases, anomalous warming was Gaussian in time for July to July reaching maximum expression in December/January (the height of the summer rainy season) at 3°C with the breadth of the peak controlled by σ= 2 months. A 2-D Gaussian function smoothed the lat-lon expression of the warming. Summaries of the σ-values for the spatial smoothing can be found in Table 2. Twenty runs were completed for each experiment by starting each ensemble member with different initial atmospheric states. Since the focus was the summer season, each member ran from July to July with the the first July discarded as the spin-up.

Exp. Name	Warming Position	σ values
CLIM	n/a	n/a
EP	5°S 90°W	xσ, yσ = 20°, 4°
CP	0°S 165°W	xσ, yσ = 20°, 4°

Table 2: Summary table of idealised SST constructions

The metbot was applied to the modelled daily mean of OLR at the top of the atmosphere to identify cloud bands in the model. Parameters were the same as those used to identify systems in the satellite-observed OLR field with the only change being the threshold value: 245 W.m^{-2} since the modelled radiation values were about 15 W.m^{-2} higher than observed daily mean values. This change has also been found necessary in preliminary work done applying this method to the new Coupled Forecast System Reanalysis (Saha and Coauthors, 2010). Grid-point counts for simulated cloud bands were calculated on the same lat-lon grid used for the observed cloud bands. This method allows comparison, as counts using the model grid are lower, since it has finer resolution.

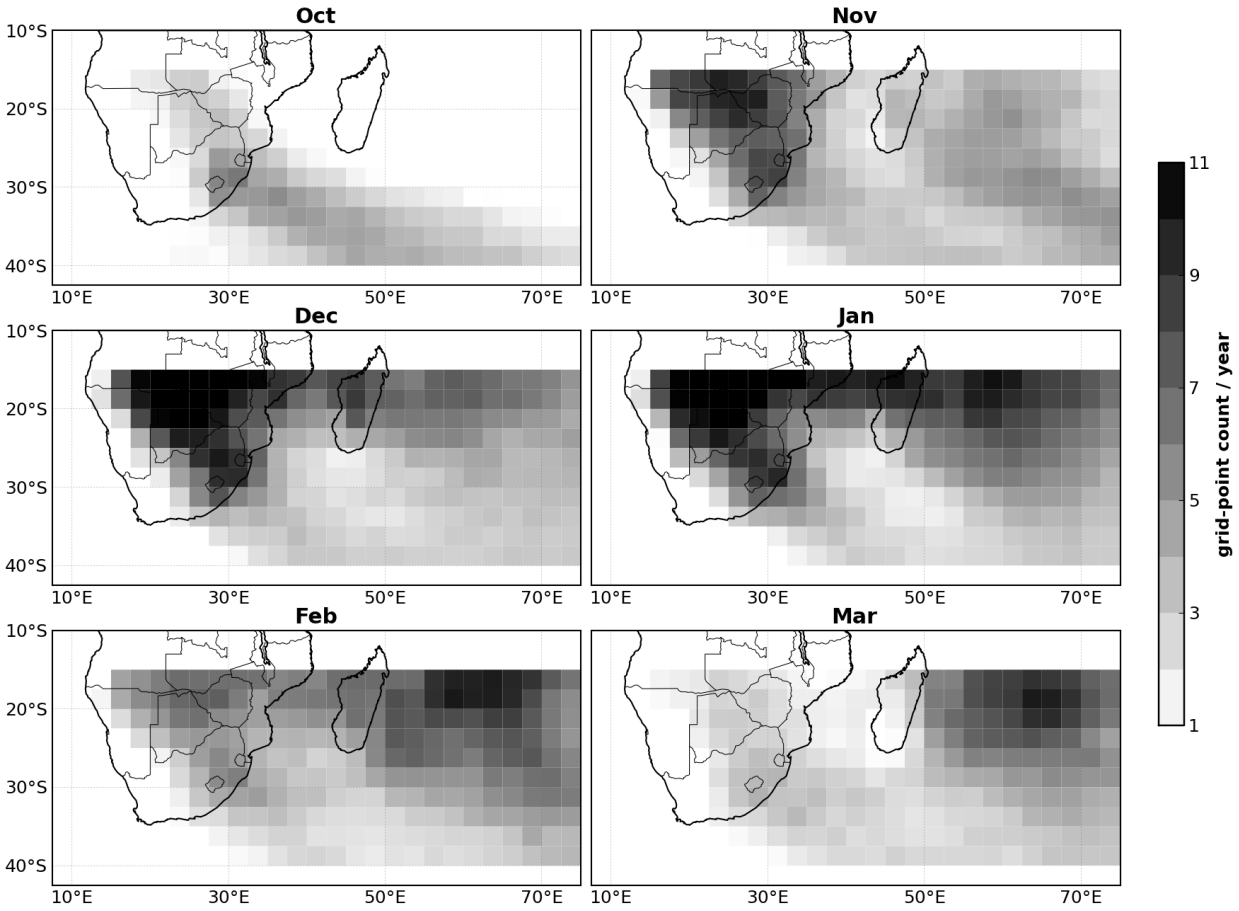

Figure 7: CLIM ensemble mean seasonal cycle of cloud band grid-point counts

The CLIM ensemble mean produces an adequate monthly climatology of cloud band grid-point counts (Fig. 7). Systems start forming over the continent in October, increase in number through November and December and then gradually decline into March. Since OLR tracks associated with cloud bands last on average 3 days, the peak count in December of 10 cloud band days, implies an average of 3 cloud bands per month, close to what is expected in the observational climatology. The model also reproduces the dual location of regional tropical-extratropical interaction. The Madagascan events, however, are simulated too far east, and the grid-point count has a weak northwest-southeast orientation in comparison to observations (eg. January and March in Fig. 1b). This error is not as severe during November, when it is likely that there is more westerly wave influence. This result indicates that the problem may be overactive model tropical convection in the central Indian Ocean later in summer, which may bias cloud bands in the east.

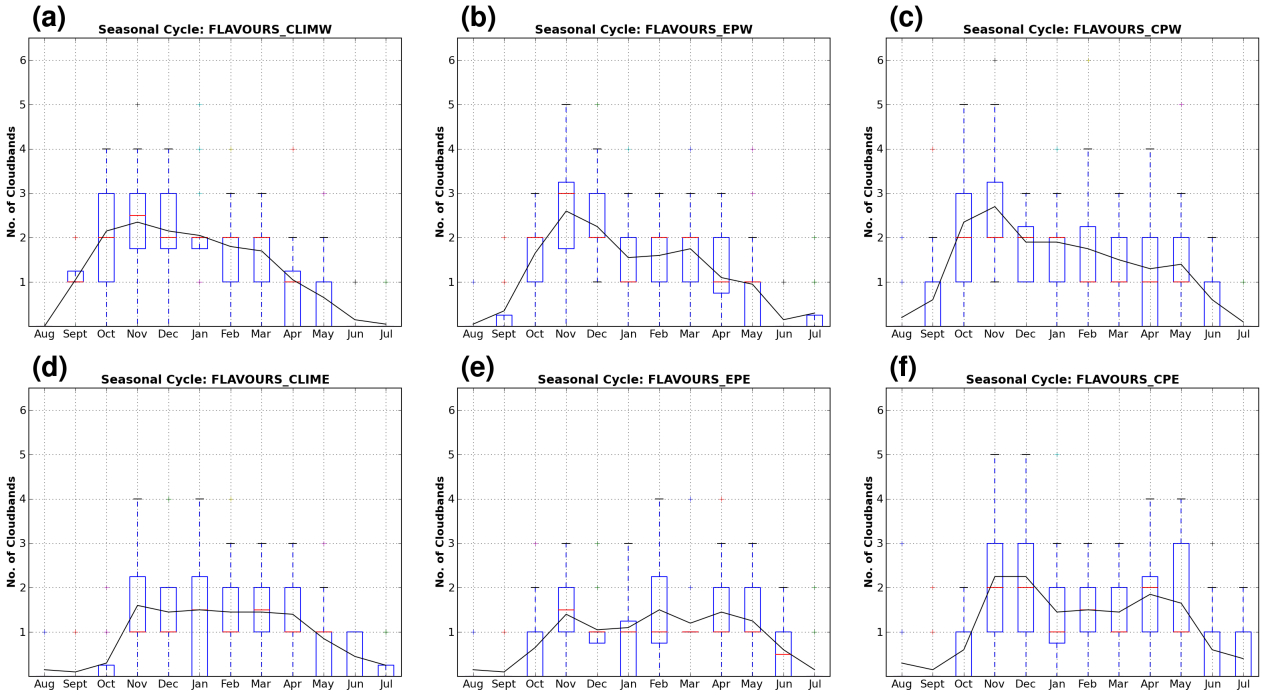

Figure 8: Seasonal cycle of simulated cloud bands over southern Africa for the CLIM (a), EP (b) and CP (d) experiments with the Madagascan systems represented in d-f; spread of ensemble members is represented by box and whiskers as in Fig. 3

The seasonal cycle of modelled continental TTT events matches reality well, simulating the November/December peak in event numbers and the subsequent decline to April (Fig. 8a). However, too many events are produced in October, but this result was not stable across ensemble members, as indicated by the wide range of values. The response to EP warming suggests a slight shift to more November systems and significant decrease in January systems (Fig. 8b). The CP experiment produced a similar result, however there appeared to be continued influence later in the year with increased likelihood of systems developing into May compared to the CLIM or EP experiments (Fig. 8c). Despite the eastward displacement discussed above and too many November systems, the number of Madagascan systems were well-simulated in the climatology experiment compared to observations (Fig. 8d). In the EP experiment a more bimodal distribution occurred with peaks in November and April (Fig. 8e). This was enhanced further in the CP experiment (Fig. 8f). To investigate these changes further, NDJF circulation anomalies are presented in Fig. 9.

The simulated NDJF climatology circulation displays a westward extension of the South Indian High south of Madagascar into southern Africa (Fig. 9a), comparing well with observations (eg. Fig. 10-12). This extension supports easterly moisture fluxes onto the continent, which are then directed southwestward by the model Angola Low. Absent from this picture however, are the northeasterly moisture fluxes across eastern tropical Africa that emanate from the tropical western Indian Ocean and are the most important moisture source for subtropical southern Africa summer rainfall (Reason et al., 2006). The eastward bias of Madagascan cloud bands noted earlier may be partly due to the strong cyclonic feature northeast of the island in the model. This feature is uncommon in NCEP2 seasonal means; however, it occurs in observations in a location further northeast in regional drought years (eg. Fig.10a; left). The fact that it existed in an older configuration of this model (eg. Reason and Jagadheesha, 2005, ; Fig. 2b) supports the idea that it is caused by model overestimation of ITCZ convection over the tropical Indian Ocean. Fig. 9 (a; right) shows the CLIM mean NDJF cloud band count which captures the higher prevalence

of continental systems versus Madagascan systems. This pattern is supported by a region of of negative zonal stretching deformation that extends from southern Africa into the Southwest Indian Ocean.

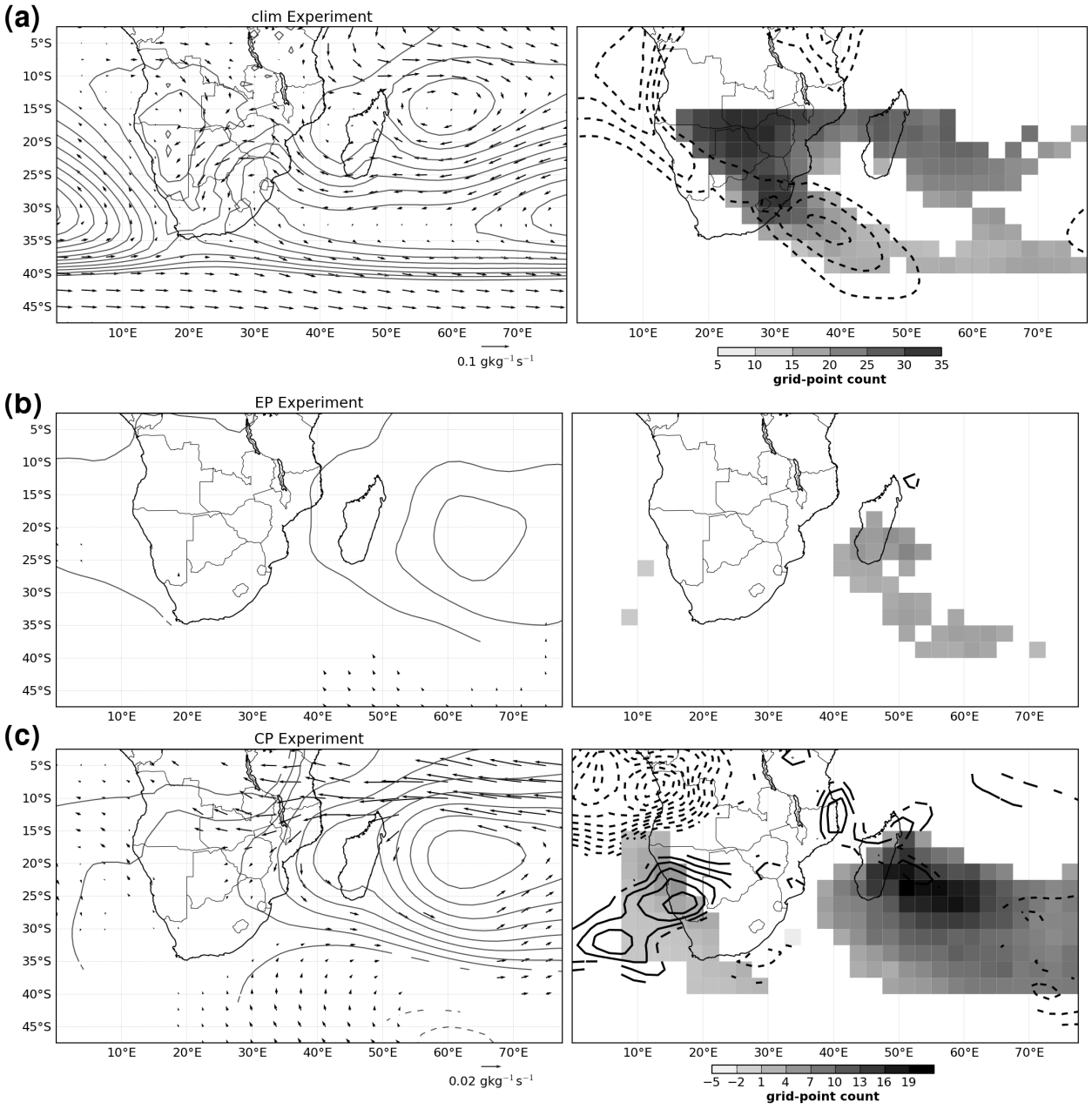

Figure 9: CLIM ensemble mean NDJF circulation depicted (a) by 850mb moisture fluxes (vectors) and gph (contours start at 1485, increments at 5gpm) on left and cloud band occurrence (shaded; NDJF grid-point count) and 250mb $\frac{\partial \bar{U}}{\partial x} < 0$ (contoured every -5 x10^{-7}s^{-1}) on the right; (b) and (c) display NDJF anomalies relative to CLIM of 850mb moisture flux (vectors) and gph (contours; every 2gpm) on left panels and cloud band count (shaded) and 250mb $\frac{\partial \bar{U}}{\partial x}$anomalies (contoured every 2 x10^{-7}s^{-1}), for the EP and CP experiments respectivley. Significance (95%) is determined using t-test (Hotelling test for vectors) between CLIM and EP/CP ensemble populations, with only significant anomalies plotted.

Fig. 9 (b) confirms suggestions in Fig. 8(b) and (e) that the response to idealised EP warming is very weak. The anomalies that are significant suggest an increase in 850mb geopotential height east of Madagascar and an increase in cloud bands rooted on the island. For CP warming however, this increase is more substantial, indicating 3-4 more cloud band events in the east (Fig. 9 c). This increase is accompanied by an anticyclonic increase of up to 14 geopotential meters east of Madagascar and hence in easterly moisture fluxes towards tropical southern Africa of up to 0.5 g.kg^{-1}s^{-1}. This indicates that the cyclonic feature simulated in the climatology experiment is shut down by adjustment of the Walker circulation to the imposed Pacific warming. This explanation is plausible if the remote warming favours an ascending branch of the Indian Ocean Walker circulation which is located further east and closer to the equator since this would reduce model solutions that set up strong ascending motions immediately east of Madagascar. Increases in $\frac{\partial \bar{U}}{\partial x}$ over the west coast of of southern Africa suggest more zonally orientated upper-level flow over the continent, however the presence of cloud bands over this region is unexpected. Beyond these features however, there is little significant increase or decrease in continental cloud bands to the these imposed warming anomalies. The implication of the model results is that a direct atmospheric response to El-Niño warming is weak over subtropical southern Africa, despite enhancement of cloud band activity in the Indian Ocean east of Madagascar. The sensitivity to the flavour of El-Niño is therefore likely due to the greater proximity of the warming to southern Africa in the CP case.

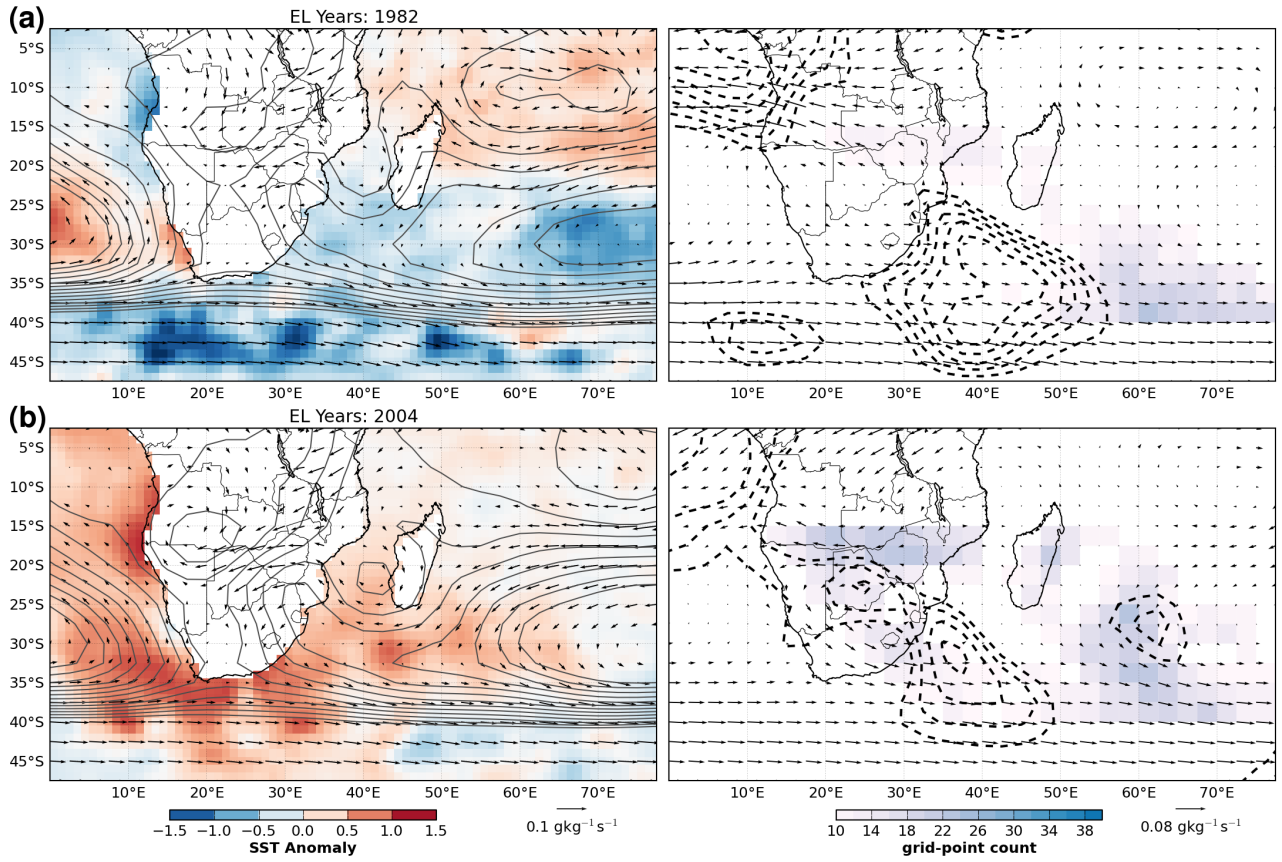

Figure 10: Low count TTT NJDF seasons starting in 1982 (a) and 2004 (b): Left panels show SSTA (shaded) and 850mb moisture flux vectors and gph (contours as in Fig. 9 a) while right panels display cloud band grid-point count (shaded) , 250mb $\frac{\partial \bar{U}}{\partial x} < 0$ (contours as in Fig. 9a) and 700mb moisture fluxes.

6 Seasonal Circulation Dynamics

What is the mean circulation that characterises years with high or low numbers of cloud bands, and does this relate to El-Niño and La-Niña seasons? Earlier work (eg. Lindesay, 1988; Reason et al., 2000) focussed on pressure changes and implied shifts in the Walker circulation; here for the first time in the region the $\frac{\partial \bar{U}}{\partial x}$ field is considered. In this section, interannual differences in cloud band counts are explored through NDJF mean circulation. To achieve this, SST anomalies, raw 850mb moisture flux and geopotential height are plotted alongside cloud band grid-point counts. In an attempt to frame these fields in the conceptual model outlined in the introduction, regions of $\frac{\partial \bar{U}}{\partial x} < 0$ are overlaid on the cloud band data with the inclusion of 700mb moisture fluxes. Showing representative years better serves the purposes of this study without the loss of detail or potential bias by strong events that can occur in compositing.

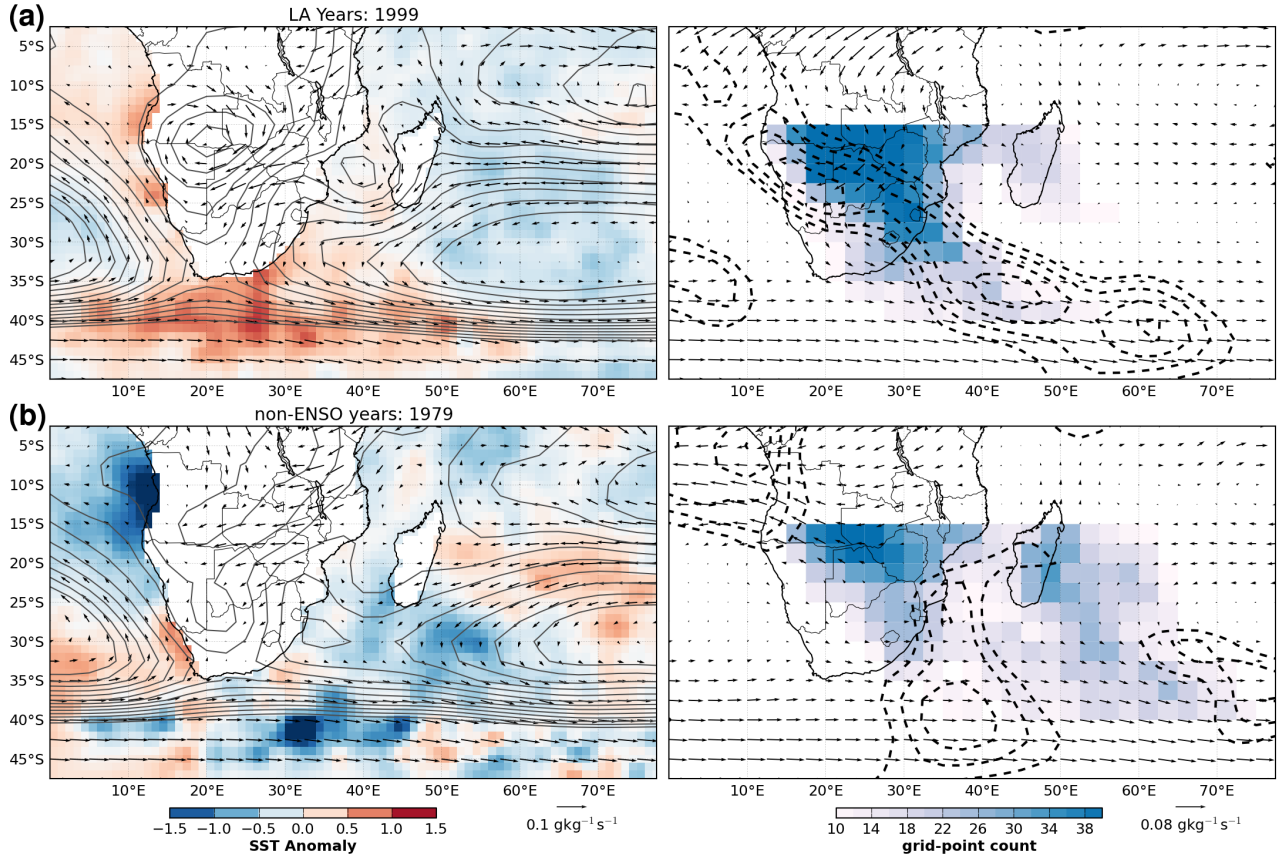

Figure 11: High count TTT NDJF seasons starting in 1999 (a) and 1979 (b) with shading and contours as in Fig. 10

Fig. 10 (a; right) presents the 1982/3 season cloud band grid-point count and negative zonal stretching deformation region. This configuration of TTT system occurrence and $\frac{\partial \bar{U}}{\partial x} < 0$ closely resembles that of El-Niño events starting in 1991, 2002 and non-ENSO events in 1985, 1986 and 2006. As indicated in Fig. 5, this El-Niño season was characterised by a strong reduction in continental cloud bands, and indeed Madagascan systems too. The sub-tropical and mid-latitude Indian Ocean was characterised by cooler SSTs and a weak South Indian High, which together, suggested a reduced ability to supply the necessary moisture to support tropical-extratropical cloud systems (Fig. 10a; left). Low seasonal moisture fluxes support this hypothesis. A depression and cyclonic feature in the central Indian Ocean overlaid on warm SST anomalies of 0.5°C, suggested enhanced ITCZ convection displaced

eastward from Africa, as expected during El-Niño. Over southern Africa, a weak Angola Low with cool adjacent SST anomalies, meant low-level circulation was weak and zonal near 20°S. This, combined with low moisture flux from the adjacent ocean, paints a compelling scenario for the dry conditions that South Africa experienced during 1983 (Fig. 5a). The circulation characteristics of the 1982 season closely resemble the seasons mentioned above. The main difference is with the 2002 season which had a more well-defined Angola Low, South Indian High and stronger cyclonic circulation in the Mozambican Channel.

Strong deformation of the zonal flow existed in a broad region southeast of the continent indicating a strong subtropical jet situated across the far south of the continent in 1982, a feature which appears robustly for most El-Niño events.

An exception to this pattern was the low count cloud count cloud band season of 2004/2005, also coincident with an El-Niño event. Fig. 10 (b) displays this season, with $\frac{\partial \bar{U}}{\partial x} < 0$ values extending across much of southern Africa. Based on the climatology of the SPCZ in Widlanksy et al. (2011), there could be an expectation that the region of $\frac{\partial \bar{U}}{\partial x} < 0$ would be co-located with cloud band location. This result however, suggests that $\frac{\partial \bar{U}}{\partial x} < 0$ alone is insufficient for encouraging cloud band activity in the region. Clearly more detail is needed to understand the 2004 season, as other factors regarded as favourable for rainfall were in place too. The Angola Low dominated continental circulation and warm SST anomalies had developed in both adjacent oceans. This suggested that perhaps strong cyclonic circulation in the Mozambican channel diverted moisture too far north to support cloud band formation.

As noted earlier, La-Niña years are associated with near average numbers of TTTs, and only the 1998-2000 La-Niña summers are associated with above average frequencies (Fig. 3). The seasonal circulation and cloud band count for 1999, representative of high-frequency years (1990, 1993, 1996) and some mean count years (2001, 2003 and 2005) is presented in Fig. 11. This summer was dominated by continental cloud bands with very few Madagascan systems. Low $\frac{\partial \bar{U}}{\partial x}$ values that extended across the continent would, theoretically, favour slowing and amplification of upper-level waves as they propagated over southern Africa, allowing substantial interaction with low-level tropical moisture that was supplied by the well-formed Angola Low. The strong South Indian High present during this season also supported easterly moisture supply to southern Africa from below Madagascar. The negative zonal stretching deformation field in this figure is very similar for the seasons starting in 1987 and 2008, however their circulation fields lack a well-defined Angola Low. Nevertheless, a strong east-west pressure gradient exists due to a meridional trough that extends the full length of southern Africa, somewhat similar to 2009/2010 (Fig. 12c; left), which helped support poleward moisture fluxes over the subcontinent.

In contrast to the general circulation pattern for high TTT count years, Fig. 11 presents the season of 1979, which also experienced a high number of TTT systems. Compared to 1999, this high number is surprising since it had a weaker Angola Low, a less pronounced South Indian High and the $\frac{\partial \bar{U}}{\partial x}$ field that resembles that of low count years described in Fig. 10. Even the 700mb tropical moisture jet, situated over central Africa (Fig. 10a; right), a prominent feature of the low-count years in 1982 and 1991 (not shown), is present in this season. On possible reason for the higher than average number of TTTs could that a higher frequency of upper-level westerly wave disturbances were propagating through the region.

So how does this information relate to the weak southern African response to the strongest El-Niño/La-Niña event of the century (1997/1998)? Fig. 12 (a) shows that the region of negative $\frac{\partial \bar{U}}{\partial x}$ was generally similar to the 1983 and 1991 events, however the cloud band grid-point was substantially higher throughout the SICZ domain. The eastward shift of the SICZ, common to the SPCZ El-Niño response, had also occurred, with many more Madagascan TTTs and continental systems. However, the grid-point count indicates that some systems did still form near southern Africa. This behaviour was perhaps aided by the unusually strong Angola Low and moisture fluxes off the anomalous

warm tropical Indian and Atlantic Oceans, features already noted by other authors (Reason and Jagadheesha, 2005; Lyon and Mason, 2007). During the La-Niña that followed in the 1998/1999 season, the Angola Low developed to a similar mean strength despite the cooler adjacent oceans (Fig. 12b) . The South Indian High was substantially stronger and further west than during the previous El-Niño season, and this likely supported enhanced cloud band formation over Mozambique and the Southwest Indian Ocean near 35°E. This pattern represents enhanced system activity between the two climatological action centres. Despite substantial TTT activity, negative zonal stretching was confined to a small region southeast of southern Africa, implying that large-scale deformation of the zonal flow was somewhat subdued. These results show that this period of strong El-Niño/La-Niña expression did produce a strong regional cloud band response. The centres of action, however, were remote to the subcontinent, and the systems that occurred on the eastern periphery of these action centres were sufficient to maintain expected seasonal frequencies. Two such events are described in Part I, Cases I and II.

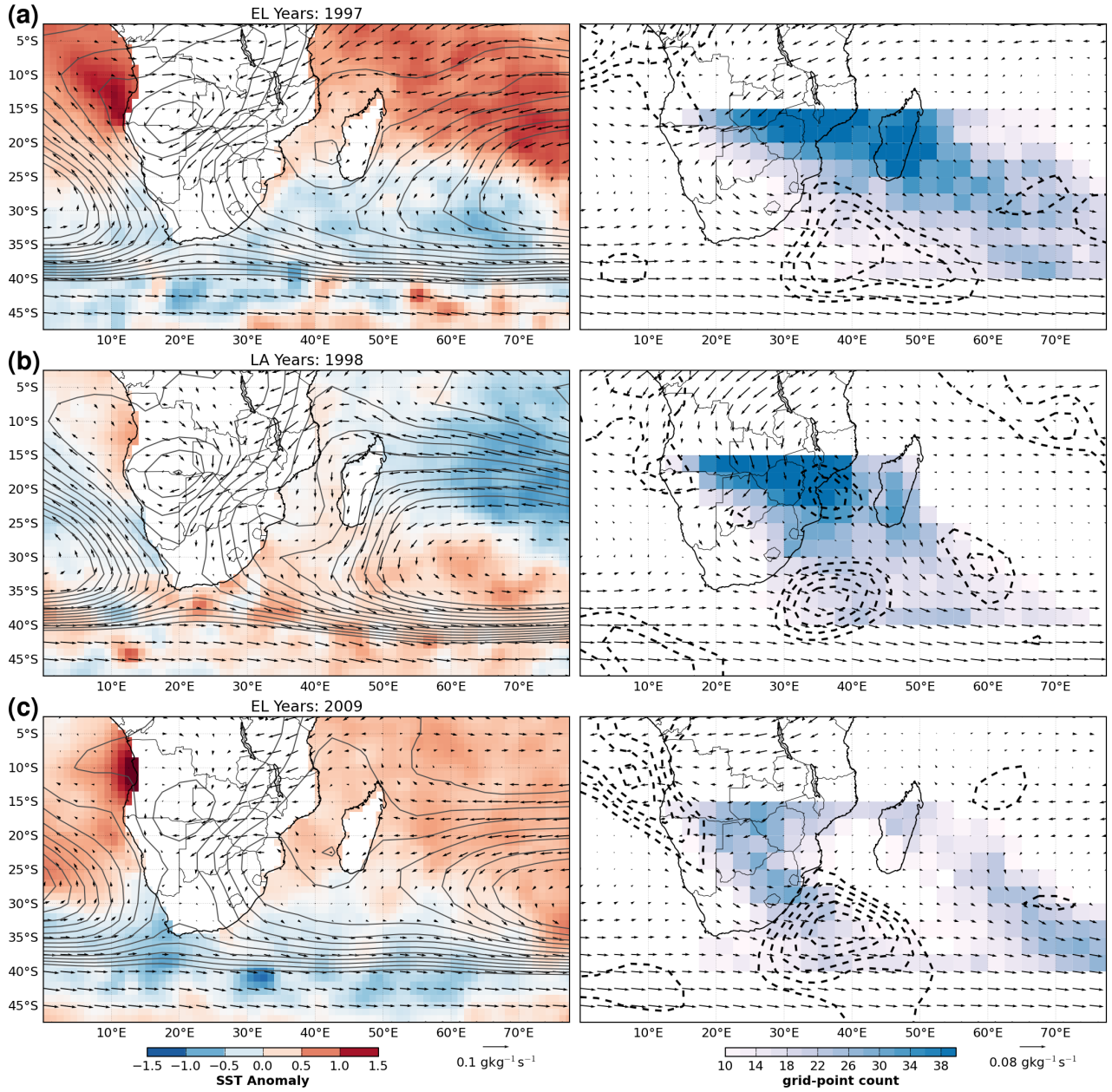

Figure 12: El-Niño 1997/1998 and La-Niña 1998/1999, El-Niño 2009/2010 with shading and contours as in Fig. 10

And what of the El-Niño event of 2009-2010, an event which failed to produce the forecasted drought in subtropical southern Africa? Key features of the El-Niño related low TTT count and drought years were present. A region of strong negative zonal stretching deformation was present southeast of Africa, the tropical easterly moisture flow was moving 700mb level moisture off the tropical continent and a weakened Angola Low existed, despite a strong warming in the South Atlantic coastal ocean (Fig.12c). Analysis of the 6 continental events tracked by the metbot (Fig. 3) reveal that two of those systems produced persistent deep convection for 12 days in January and then another 9 days in February. Despite the weaker Angola Low in the seasonal mean, the January system was accompanied by a spin-up of the synoptic-scale Angola Low into a vortex-like structure, revealed by satellite imagery. The first day of this event is shown in Part II, Fig. 1. These two prolonged events account for the higher grid-point count than would be expected from only 6 systems (Fig.12c; right). Similarly, these events may be a reason for the near-normal season total rainfall that was recorded.

7 Summary and Conclusions

This analysis has provided strong support to conclusions reached in previous work (eg. Fauchereau et al., 2009) that the regional ENSO response is not equal and opposite for El-Niño and La-Niña events. In general, El-Niño years suppress continental cloud band activity, with three of the lowest TTT count years occurring during an El-Niño event. La-Niña events however, rarely correspond to peak TTT years and instead seem to maintain the seasonal mean. In contrast to the early work in the region, the El-Niño response is rarely characterised by an offshore shift in TTT formation. It is more common to see a decrease in systems throughout the western Indian Ocean.

This analysis method allowed further insight into the El-Niño/La-Niña period of 1997/8 and 1998/9. During the El-Niño season, TTT formation was higher throughout the western Indian Ocean, but centered on Madagascar as expected. Enough systems formed in the periphery of the main formation region, to maintain season norms. This behaviour may have been aided by the strong Angola Low. During the La-Niña event, a strong South Indian High and Angola Low continued to provide the necessary moisture supply to support a high number of systems forming in the Mozambican Channel. The slightly offshore location for development, meant that there was neither the high TTT count nor wet rainfall anomalies as would have been expected from current understanding.

A first-order test of the sensitivity of cloud bands to the flavour of El-Niño was conducted with an idealised forcing of an atmospheric general circulation model, HadAM3p. The climatology run produced a realistic seasonal cycle of continental cloud bands, however the Madagascan systems were simulated too far east. Based on comparison with reanalysis circulation fields from 1982, it appears that the model produces an El-Niño-like bias, possibly due to overactive ITCZ convection east of Madagascar. A weak modelled Angola Low may also be a problematic factor in the ability of HadAM3p to accurately depict regional processes. Nevertheless, the response to an eastern Pacific warming was small, but the response the to central Pacific warming was significant in the central Indian Ocean. Cloud band grid-point counts were substantially enhanced, supporting the idea of enhanced cloud band activity in the Indian Ocean during El-Niño events when the Walker circulation is displaced eastward from Africa. No significant cloud band anomalies occurring over the summer rainfall regions of southern Africa suggests that a direct atmospheric response to tropical Pacific warming is unlikely. However, Lyon (2009) noted that even coupled models struggled to produce a robust ENSO teleconnection to the region. Since the present study did not fully consider upper-level flow, nor rainfall, these conclusions are narrowly focused on TTTs. A final note is that TTTs have been suggested to be associated with late rainy season onset for the Maize growing regions (Tadross et al., 2005). Indications are, in both the CLIM and CP experiments, that TTT predictablity is low in October, since there is a wide spread in TTT count in the ensembles.

TTT variability seems to have unstable correspondence with South African rainfall variability, however the very dry years are accompanied by reduced TTT frequency. A novel approach to assign rainfall characteristics to each event helped reveal that the likelihood of more intense and/or persistent TTTs is increased during La-Nina years. This work also demonstrated that splitting rainfall into homogeneous sub-regions for variability studies is a useful and apt approach. The rainfall data available had a high spatial resolution allowing for detailed, robust rainfall statistics and metrics, but the fact that the data ends in 1999 meant that only two-thirds of the identified cloud band systems in the OLR data have been used in the present study. Further analysis performed on an update station data set of this quality would add much value to this paper.

Investigations into the seasonal circulation that supports low or high frequency TTT NDJF seasons revealed some general characteristics. Many low-TTT seasons lack a well defined Angola Low and display cyclonic flow in the Mozambican Channel. A weakened South Indian High implies reduce moisture supply towards southern Africa from the tropical and subtropical Indian Ocean. In a novel analysis for the region, negative zonal stretching deformation was included. During low count El-Niño seasons, strong deformation of the mean flow is present southeast of Africa, suggesting the presence of a strong upper-level jet lying over eastern southern Africa.

Years with high TTT frequency seasons are sometimes characterised by a strong Angola Low and a $\frac{\partial \bar{U}}{\partial x} < 0$ region extending across the subcontinent. Exceptions, however, do occur, especially with regards to the $\frac{\partial \bar{U}}{\partial x} < 0$ zone. Thus, a conclusion is that $\frac{\partial \bar{U}}{\partial x} < 0$ is apparently neither sufficient nor necessary for TTT development. A quantification of extratropical wave activity, variability and association with regional tropical-extratropical interactions is beyond the scope of this study, however it is needed for further discussion of the role of $\frac{\partial \bar{U}}{\partial x} < 0$. Indeed further work on this is needed to better understanding how much of the ENSO signal can reach southern Africa through the extratropics. Cloud band frequency is strongly linked to upper-level extratropical wave activity (Vigaud et al., 2012) so these results will be useful to continued work in that direction.

Future studies of rainfall system contributions to season total rainfall would do well to discriminate frequency, intensity and persistence. The results presented here indicate variability in all three may be independent and therefore confound attempts to understand the importance of a particular weather phenomenon of interest, in regional rainfall variability. The importance of this was illustrated with the El-Niño event of 2009/2010. Circulation features matched those of previous events and few cloud bands occurred. However, the cloud band grid-point count suggested a near-normal season. Event scale analysis revealed that two TTT events showed remarkable persistence and strongly modified the pattern for that season.

In conclusion, this study has provided the first detailed investigation of the interannual variability of explicitly-identified cloud band systems over southern Africa. Investigations into the role of ENSO-related variability have revealed further nuances and complexities in the regional response to El-Niño and La-Niña events. This work represents an important contribution to the research efforts of understanding regional variability processes.

Acknowledgements

M. Rouault, B. Pohl and N. Viguad are thanked for helpful discussions. Interpolated OLR and NCEP2 data was obtained from NOAA/OAR/ESRL PSD, Boulder, Colorado, USA through http://www.cdc.noaa.gov.

Final Conclusions

This dissertation has presented the most thorough description of TTTs over southern Africa to date. The successful development of an automated cloud band identification tool allowed for detailed event descriptions of TTTs in the region of the SICZ. This work enabled assessment of the climatological importance of cloud bands for South African rainfall in a high density rain-gauge data set, revealing important spatial heterogeneities across the country. The modulation of the frequency, intensity and persistence of TTT rainfall by the MJO at the intraseasonal and by ENSO at the interannual time scale was investigated with a level of precision unavailable to previous methodologies. The key findings are as follows:

The investigation of the meteorological dynamics supported the view that the Angola Low is a key synoptic feature in the import of moisture to subtropical southern Africa. Upper-level westerly troughs passing across the subcontinent provided the necessary uplift to trigger convection and heavy rainfall. An association with larger-scale planetary wave structures was demonstrated through the use of potential vorticity maps, providing fresh insight into potential sensitivity of TTTs to upstream dynamics and the possible influence on Rossby wave breaking downstream in the South Indian Ocean. A case was made that these systems fall within a theoretical framework for tropical plumes developed in review paper by (Knippertz, 2007).

A cue was taken from a methodology discussed in Hodges (1994) to develop an appropriate, computer vision-based approach to automatically identify tropical-extratropical cloud bands in the region. Extension of the system to identify meteorological features of interest was included. It was demonstrated that the system effectively identifies, tracks and describes detailed meteorology of each TTT event. A composite life cycle of these weather systems was presented, providing robust support to the generalisation suggested in the case studies paper (Part I). The ability of this metbot to provide a synthesis of individual events and include detailed rainfall metrics suggests it may have potential use in addressing a detail gap that currently exists between meteorological case studies and object-based climatologies and variability studies. This potential has been partly realised in this dissertation, however, further work could use the approach to provide some quantification of moisture supply, upper-level wind strengths and other meteorological features of individual events and how these may vary interannually.

The first quantified seasonal cycle of tropical-extratropical cloud bands over southern Africa was built from the database of TTT events that the metbot created. An assessment of the contribution of TTTs to South African summer rainfall was performed using a rainfall station data set and the TTT event database. In general, the results agreed with those presented by Harrison (1984), however, the percentage contributions (30-50%) found here were about 10% lower than that earlier work. An implication is that future work should attempt to understand what produces the remaining 50-70% of seasonal rainfall. Spatial heterogeneities in these contributions were highlighted, providing a level of detail previously unattained. Important to studies of variability, it was shown that individual extreme events can alter seasonal totals, often in excess of 20%, suggesting the role that individual events and not persistent circulation anomalies, can have in producing substantial rainfall variations.

The question was asked whether the MJO can modulate TTT intensity? Weak but significant results suggests that indeed, the MJO may suppress intensity during its earlier phase 1 and favour heavy rainfall in phase 6. The small event sample sizes highlight the need for the study to be repeated with a rainfall data set that extends beyond 1999.

The final part of the dissertation presented a detailed exploration of the variability in cloud band frequency in the region. The average results indicate the presence of two preferred locations for cloud band development in the region, one on the southern African landmass and the other rooted on Madagascar. As with other studies,

a nonlinearity in response to El-Niño versus La-Niña events was found. Fewer systems occur during November-February of El-Niño events but near normal numbers of systems form during La-Niña events. In contrast to the accepted understanding, there is generally a domain-wide decrease in systems during El-Niño, rather than the offshore shift posited by early researchers. An analysis of the rainfall characteristics of the cloud band events indicated an increased likelihood of more intense and/or persistent events during La-Niña, corroborating results from other studies looking at intraseasonal characteristics (eg. Cook et al., 2004). Little response in these characteristics seem apparent during El-Niño summers. An important note for further studies in the region is that the association between cloud band count over southern Africa and rainfall is weak, however El-Niño years are often coincident with the years of low cloud band counts and on occasion, strong drought.

A set of idealised sensitivity experiments has suggested that there is difficulty, at least in models, in communicating an El-Niño signal to subtropical southern Africa. This has been suggested previously (Mason and Jury, 1997; Lyon and Mason, 2009). However, there does seem to be a stronger regional response to warming in the central tropical Pacific Ocean than warming in the eastern parts. There is a statistically significant increase in cloud band days over the central South Indian Ocean, and an eastward shift in the South Indian High. Climatological runs, using the same model, HadAM3P, indicate that it reproduces the seasonal cycle in regional cloud bands well, however may produce too many early season systems. A wide response in system numbers during October, in all the experiments, suggests that the crucial onset date (Usman et al., 2005) of the rainy season may have low predictability especially if it is linked to TTT systems.

Analysis of representative mean seasonal circulation during high count and low count cloud band years, revealed that substantial season to season differences exists and compositing of years may well remove important nuances. A well-defined Angola Low was often associated with high count years, however, it was sometimes present in low count years too. Associations with regional SST anomalies was unclear, however analysis of rainfall statistics associated with these anomalies was not performed, so that is a possibility that cannot be ruled out. In general, however, the eastward shift and weakening of the South Indian High is a common feature of low count TTT years, which often coincide with El-Niño events.

A framework for understanding the mean state of the subtropical convergence zones which relies on negative zonal stretching deformation $\frac{\partial \bar{U}}{\partial x} < 0$ (Widlanksy et al., 2011) was tested for usefulness in understanding cloud band variability in the SICZ. Although regions of $\frac{\partial \bar{U}}{\partial x} < 0$ did extend across southern Africa during some years of frequent TTT formation, this was not always the case and, in general, the association between the preferred location of systems in a given season and the zone of negative stretching deformation was weak. Further work is needed to understand the interaction between moisture supply, low-level circulation and wave propagation in this subtropical convergence region. This work will be needed to more fully understand the role of extratropical variability in driving TTT variability.

In conclusion, this work has attempted to address the knowledge gap exposed in the introduction through a series of scientific questions, which have built upon one another. After investigating the dynamics associated with tropical-extratropical cloud bands, a novel approach was developed to quantify the synoptic-scale nature of these systems with a minimal loss of detail. This enabled a thorough investigation of the importance of these systems for regional rainfall variability and also provided a useful way to quantify the influence of large-scale variability modes on synoptic-scale weather over southern Africa. The results presented here represent an important contribution to understanding of regional climate variability and highlight a number of interesting topics for future research.

References

Benestad, R. E. and Chen, D. (2006). The use of a calculus-based cyclone identification method for generating storm statistics. *Tellus*, 58A(4):473–486.

Blamey, R. C. and Reason, C. J. C. (2009). Numerical simulation of a mesoscale convective system over the east coast of South Africa. *Tellus*, 61A:17–34.

Blamey, R. C. and Reason, C. J. C. (2012). Mesoscale convective complexes over southern Africa. *J. Climate*, 25:753–766.

Bradski, G. (2000). The OpenCV Library. *Dr. Dobb's Journal of Software Tools*.

Cammas, J.-P., Keyser, D., Lackmann, G. M., and Molinari, J. (1987). Diabatic redistribution of potential vorticity accompanying the development of an outflow jet within a strong extratropical cyclone. *Preprints: Int. Symp.on the Life Cycles of Extratropical Cyclones*, 2:403–409.

Carvalho, L. M. V. and Jones, C. (2001). A satellite method to identify structural properties of mesoscale convection systems based on the maximum spatial correlation technique (MASCOTTE). *J. Appl. Meteorol.*, 40:1683–1701.

Chang, F., Chen, C.-J., and Lu, C.-J. (2004). A linear-time component-labeling algorithm using contour tracing technique. *Computer Vision and Image Understanding*, 93(2):206–220.

Cobbing, J. E. (2008). Institutional linkages and acid mine drainage: the case of the Western Basin in South Africa. *Int. J. Water Res. Devel.*, 24(3):451–462.

Colberg, F., Reason, C. J. C., and Rodgers, K. (2004). South Atlantic response to El Nino-Southern Oscillation induced climate variability in an ocean general circulation model. *J. Geophys. Res.*, 109:C12015, doi:10.1029/2004JC002301.

Cook, C., Reason, C. J. C., and Hewitson, B. C. (2004). Wet and dry spells within particularly wet and dry summers in the South African summer rainfall region. *Climate Res.*, 26:17–31.

Cook, K. H. (2000). The South Indian Convergence Zone and interannual rainfall variability over southern Africa. *J. Climate*, 13:3789–3804.

Cook, K. H. (2001). A Southern Hemisphere wave response to ENSO with implications for southern Africa precipitation. *J. Atmos. Sci.*, 58:2146–2162.

Crétat, J., Richard, Y., Pohl, B., Rouault, M., Reason, C. J. C., and Fauchereau, N. (2010). Recurrent daily rainfall patterns over South Africa and associated dynamics during the core of the austral summer. *Int. J. Climatol.* DOI: 10.1002/joc.2266.

D'Abreton, P. and Lindesay, J. (1993). Water vapour transport over southern Africa during wet and dry early and late summer months. *Int. J. Climatol.*, 13:151–170.

D'Abreton, P. C. (1993). *The dynamics and energetics of tropical-temperate troughs over southern Africa*. PhD thesis, University of the Witwatersrand.

D'Abreton, P. C. and Tyson, P. D. (1995). Divergent and non-divergent water vapour transport over southern Africa during wet and dry conditions. *Meteor. Atmos. Phys.*, 55:47–59.

D'Abreton, P. C. and Tyson, P. D. (1996). Three-dimensional kinematic trajectory modelling of water vapour transport over Southern Africa. *Water SA*, 22(4):297–306.

De Coning, E., Forbes, G. S., and Poolman (1998). Heavy precipitation and flooding on 12-14 February 1996 over the summer rainfall regions of South Africa: synoptic and isentropic analyses. *Natl. Wea. Dig.*, 22(3):25–36.

Demuzere, M., Kassomenos, P., and Philipp, A. (2011). The COST733 circulation type classification software: an example for surface ozone concentrations in Central Europe. *Theor. Appl. Climatol.*, 105:143–166.

Diab, R. D., Preston-Whyte, R. A., and Washington, R. (1991). Distribution of rainfall by synoptic type over Natal, South Africa. *Int. J. Climatol.*, 11:877–888.

Dommenget, D. and Latif, M. (2002). A cautionary note of the interpretation of EOFs. *J. Climate*, 15:216–225.

Emanuel, K. A., Fantini, M., and Thorpe, A. J. (1987). Baroclinic instability in an environment of small stability to slantwise moist convection. part i: two dimensional models. *J. Atmos. Sci.*, 44:1559–1573.

Fauchereau, N., Pohl, B., Reason, C., Rouault, M., and Richard, Y. (2009). Recurrent daily OLR patterns in the Southern Africa / Southwest Indian Ocean region, implications for South African rainfall and teleconnections. *Climate Dyn.*, 32:575–591.

Fauchereau, N., Trzaska, S., Richard, Y., Roucou, P., and Camberlin, P. (2003). Sea surface temperature co-variability in the Southern Atlantic and Indian Oceans and its connections with the atmospheric circulation in the Southern Hemisphere. *Int. J. Climatol.*, 23:663–677.

Favre, A., Hewitson, B., Tadross, M., Lennard, C., and Cerezo-Mota, R. (2011). Relationships between cut-off lows and the semi-annual and southern oscillations. *Clim. Dyn.*, 10.1007/s00382-011-1030-4.

Hachigonta, S., Reason, C. J. C., and Tadross, M. (2008). An analysis of onset date and rainy season duration over Zambia. *Theor. App. Climatol.*, 91:229–243.

Hansen, J. W., Mason, S. J., Sun, L., and Tall, A. (2011). Review of seasonal climate forecasting for agriculture in sub-Saharan Africa. *Expl Agric.*, 47(2):205–240.

Hansingo, K. and Reason, C. J. C. (2006). Sensitivity of the atmospheric response to sea-surface temperature focing in the South West Indian Ocean: a regional. *S. Afr. J. Sci.*, 102:137–143.

Hansingo, K. and Reason, C. J. C. (2009). Modelling the atmospheric resoponse over southern Africa to SST forcing in the southeast tropical Atlantic and southwest subtropical Indian Oceans. *Int. J. Climatol.*, 29:1001–1012.

Harangozo, S. A. and Harrison, M. S. J. (1983). On the use of synoptic data in indicating the presence of cloud bands over southern Africa. *S. Afr. J. Sci.*, 79(10):413–414.

Harrison, M. S. J. (1984). A generalized classification of South African rain-bearing synoptic systems. *J. Climatol.*, 4:547–560.

Harrison, M. S. J. (1986). *A synoptic climatology of South African rainfall variations.* PhD thesis, University of Witwatersrand, Johannesburg.

Hart, N., Fauchereau, N., and Reason, C. J. C. (2009). El-nino's flavours: Implications for South African rainfall. In *Proceedings of the South Africa Society for Atmospheric Sciences 25th Annual Conference*, pages 19–20, Tulbagh, South Africa.

Hart, N., Reason, C. J. C., and Fauchereau, N. (2010). Tropical-extratropical interactions over southern Africa: three cases of heavy summer season rainfall. *Mon. Wea. Rev.*, 138:2608–2623.

Hermes, J. C. and Reason, C. J. C. (2009). Variability in sea-surface temperature and winds in the tropical south-east Atlantic Ocean and regional rainfall relationships. *Int. J. Climatol.*, 29:11–21.

Hewson, T. and Titley, H. A. (2010). Objective identification, typing and tracking of the complete life-cycles of cyclonic features at high spatial resolution. *Meteorol. Appl.*, 17:355–381.

Hinsen, K. (2007). Scientific python. http://dirac.cnrs-orleans.fr/ScientificPython/.

Hodges, K. I. (1994). A general method for tracking analysis and its application to meteorological data. *Mon. Wea. Rev.*, 122:2573–2586.

Hodges, K. I. (1999). Adaptive constraints for feature tracking. *Mon. Wea. Rev.*, 127:1362–1373.

Hodges, K. I., Lee, R. W., and Bengtsson, L. (2011). A comparison of extratropical cyclones in recent reanalyses ERA-Interim, NASA MERRA, NCEP CFSR, AND JRA-25. *J. Climate*, 24:4888–4906.

Hodges, K. I. and Thorncroft, C. D. (1998). Distribution and statistics of African mesoscale convective weather systems based on ISCCP meteosat imagery. *Mon. Wea. Rev.*, 125:2821–2837.

Holton, J. R. (2004). *An introduction to dynamic meteorology*. Int. Geophys. Series. Elsevier, 4th edition. pg. 260.

Hunter, J. D. (2007). Matplotlib: A 2D graphics environment. *Comp. in Sci. & Eng.*, 9(3):90–95.

Iskenderian, H. (1995). A 10-year climatology of northern hemisphere tropical cloud plumes and their composite flow patterns. *J. Climate*, 8:1630–1637.

Jiang, T. and Deng, Y. (2011). Downstream modulation of North Pacifc atmospheric river activity by East Asian cold surges. *Geophys. Res. Lett.*, 38:L20807.

Kanamitsu, M., Ebisuzaki, W., Woollen, J., Yang, S. K., J. Hnilo, Fiorino, M., and Potter, G. L. (2002). NCEP-DOE AMIP II reanalysis (R-2). *Bull. Amer. Meteor. Soc.*, 83(11):1631–1643.

Knippertz, P. (2003). Tropical-extratropical interactions causing precipitation in northwest Africa: Statistical Analysis and Seasonal Variations. *Mon. Wea. Rev.*, 131:3069–3076.

Knippertz, P. (2005). Tropical-extratropical interactions associated with an Atlantic tropical plume and subtropical jet streak. *Mon. Wea. Rev.*, 133:2759–2776.

Knippertz, P. (2007). Tropical-extratropical interactions related to upper-level troughs at low latitudes. *Dyn. Atmos. Oceans*, 43:36–62.

Knippertz, P., Fink, A., Reiner, A., and Speth, P. (2003). Three late summer/early autumn cases of tropical-extratropical interactions causing precipitation in northwest Africa. *Mon. Wea. Rev.*, 131:116–135.

Knippertz, P. and Martin, J. E. (2005). Tropical plumes and extreme precipitation in subtropical and tropical West Africa. *Quart. J. Roy. Meteor. Soc.*, 131:2337–2365.

Knippertz, P. and Martin, J. E. (2007). The role of dynamic and diabatic processes in the generation of cut-off lows over northwest Africa. *Meteor. Atmos. Phys.*, 96:3–19.

Kuhnel, I. (1989). Tropical-extratropical cloudband climatology based on satellite data. *Int. J. Climatol.*, 9:441–463.

Landman, W. A. and Beraki, A. (2012). Multi-model forecast skill for mid-summer rainfall over southern Africa. *Int. J. Climatol.*, 23:303–314.

Landman, W. A. and Mason, S. J. (1999). Change in the association between Indian Ocean sea-surface temperatures and summer rainfall over South African and Namibia. *Int. J. Climatol.*, 19:1447–1492.

Liñán, C. C. (2008). cvBlob. http://cvblob.googlecode.com.

Liebman, B. and Smith, C. A. (1996). Description of complete (interpolated) outgoing longwave radiation dataset. *Bull. Amer. Meteor. Soc.*, 77:1275–1277.

Liebmann, B., Kiladis, G. N., Marengo, J. A., Ambrizzi, T., and Glick, J. D. (1999). Submonthly convective variability over South America and the South Atlantic convergence zone. *J. Climate*, 12:1977–1991.

Lindesay, J. A. (1988). South African rainfall, the Southern Oscillation and a Southern Hemisphere semi-annual cycle. *Int. J. Climatol.*, 8:17–30.

Lindesay, J. A. and Jury, M. R. (1991). Atmospheric circulation controls and characteristics of a flood event in central South Africa. *Int. J. Climatol.*, 11(6):609–627.

Lynch, S. (2003). Development of a RASTER database of annual, monthly and daily rainfall for Southern Africa. Report 1156/1/03, WRC.

Lyon, B. (2009). Southern Africa summer drought and heat waves: Observations and coupled model behaviour. *J. Climate*, 22:6033–6046.

Lyon, B. and Mason, S. (2007). The 1997-1998 summer rainfall season in southern Africa. part 1: Observations. *J. Climate*, 20:5134–5148.

Lyon, B. and Mason, S. (2009). The 1997-1998 summer rainfall season in southern Africa. part 2: Model simulations and coupled model forecasts. *J. Climate*, 22:3802–3818.

Lyons, S. W. (1991). Origins of convective variability over equatorial Southern Africa during austral summer. *J. Climate*, 4:23–39.

Madden, R. A. and Julian, P. R. (1994). Observations of the 40-50 tropical oscillation - A review. *Mon. Wea. Rev.*, 122:814–837.

Manhique, A., Reason, C. J. C., Rydberg, L., and Fauchereau, N. (2009). El Nino Southern Oscillation and Indian Ocean sea surface temperature and their relation with tropical temperate troughs over southern Africa. *Int. J. Climatol.* DOI:10.1002/joc.2050.

Mason, S. J. and Joubert, A. M. (1995). A note on the inter-annual rainfall variability and water demand in the Johannesburg region. *WaterSA*, 21:269–270.

Mason, S. J. and Jury, M. R. (1997). Climatic variability and change over southern Africa: a reflection on the underlying processes. *Prog. Phy. Geog.*, 21(1):23–50.

Matthews, A. J. (2012). A multiscale framework for the origin and variability of the South Pacfic Convergence Zone. *Quart. J. Roy. Meteor. Soc.* DOI: 10.1002/qj.1870.

McGuirk, J. P., Thompson, A. H., and Smith, N. R. (1987). Moisture bursts over the tropical Pacific Ocean. *Mon. Wea. Rev.*, 115:787–798.

McGuirk, J. P. and Ulsh, D. J. (1990). Evolution of tropical plumes in VAS water vapor imagery. *Mon. Wea. Rev.*, 118:1758–1766.

Mecikalski, J. R. and Tripoli, G. J. (1998). Inertial available kinetic energy and the dynamics of tropical plume formation. *Mon. Wea. Rev.*, 126:2200–2216.

Meehl, G. A., Lukas, R., Kiladis, G. N., Weickmann, K. M., Matthews, A. J., and Wheeler, M. (2001). A conceptual framework for time and space scale interactions in the climate system. *Clim. Dyn.*, 17:753–775.

Mo, K. C. and Nogues-Paegle, J. (2001). The pacific-south american modes and their downstream effects. *Int. J. Climatol.*, 21:1211–1229.

Monahan, A. H., Fyfe, J. C., Ambaum, M. H. P., Stephenson, D., and North, G. R. (2009). Empirical orthogonal functions: The medium is the message. *J. Climate*, 22:6501–6514.

Mulenga, H. M., Rouault, M., and Reason, C. J. C. (2003). Dry summers over northeastern South Africa and associated circulation anomalies. *Clim. Res.*, 25:29–41.

Muller, A., Reason, C. J. C., and Fauchereau, N. (2008). Extreme rainfall in the Namib Desert during late summer 2006 and influences of the regional ocean variability. *Int. J. Climatol.*, 28:1061–1070.

Murray, R. J. and Simmonds, I. (1991a). A numerical scheme for tracking cyclone centres from digital data Part 1: application to January and July general circulation simulations. *Aust. Met. Mag.*, 39:167–180.

Murray, R. J. and Simmonds, I. (1991b). A numerical scheme for tracking cyclone centres from digital data Part 1: development and operation of the scheme. *Aust. Met. Mag.*, 39:155–166.

Nicholson, S. E. and Kim, J. (1997). The relationship of the El-Niño-Southern Oscillation to African rainfall. *Int. J. Climatol.*, 17:117–135.

Oliphant, T. E. (2006). *Guide to NumPy*. Provo, Utah.

Pohl, B. and Fauchereau, N. (2012). The southern annular mode seen through weather regimes. *J. Climate*.

Pohl, B., Fauchereau, N., Reason, C., and Rouault, M. (2010). Relationships between the Antartic Oscillation, the Madden-Julian Oscillation, and ENSO and consequences for rainfall analysis. *J. Climate*, 23:238–254.

Pohl, B., Fauchereau, N., Richard, Y., Rouault, M., and Reason, C. J. C. (2009). Interactions between synoptic, intraseasonal and interannual convective variability over Southern Africa. *Climate Dyn.*, 33:1033–1050.

Pohl, B., Richard, Y., and Fauchereau, N. (2007). The influence of the Madden Julian Oscillation on southern African summer rainfall. *J. Climate*, 11:2659–2674.

Polo, I., Ullmann, A., Roucou, P., and Fontaine, B. (2011). Weather regimes in the Euro-Atlantic and Mediterranean sector, and relationship with West African rainfall over the 1989-2008 period from a self-organizing maps approach. *J. Climate*, 24:3423–3432.

Pope, V. D., Gallani, M. L., Rowntree, P. R., and Stratton, R. A. (2000). The impact of the new physical parameterizations in the hadley centre climate model: Hadam3p. *Clim. Dyn.*, 16:123–146.

Posselt, D. J. and Martin, J. E. (2004). The effect of latent heat releaseon the evolution of a warm occluded thermal structure. *Mon. Wea. Rev.*, 132:578–599.

Postel, G. A. and Hitchman, M. H. (1999). Climatology of Rossby wave breaking along the subtropical tropopause. *J. Atmos. Sci.*, 56:359–373.

Racz, Z. and Smith, R. K. (1999). The dynamics of heat lows. *Quart. J. Roy. Meteor. Soc.*, 125:225–252.

Ralph, F. M., Neiman, P. J., Kiladis, G. N., and Weickmann, K. (2011). A multiscale observational case study of a Pacfic atmospheric river exhibiting tropical-extratropical connectsion and a mesoscale frontal wave. *Mon. Wea. Rev.*, 139:1169–1189.

Reason, C., Hachigonta, S., and Phaladi, R. (2005). Interannual variability in rainy season characteristics over the Limpopo region of southern Africa. *Int. J. Climatol.*, 25(14):1835–1853.

Reason, C. J. C., Allan, R. J., Lindesay, J. A., and Ansell, T. J. (2000). ENSO and climatic signals across the Indian Ocean Basin in the global context: part i, interannual composite patterns. *Int. J. Climatol.*, 20(11):1285–1327.

Reason, C. J. C. and Jagadheesha, D. (2005). A model investigation of recent ENSO impacts over southern Africa. *Meteor. Atmos. Phys.*, 89:181–205.

Reason, C. J. C. and Keibel, A. (2004). Tropical cyclone Eline and its unusual penetration and impacts over southern Africa. *Wea. Forecasting*, 19:789–805.

Reason, C. J. C., Landman, W., and Tennant, W. (2006). Seasonal to decadal prediction of southern African climate and its links with variability of the Atlantic Ocean. *Bull. Amer. Meteor. Soc.*, pages 941–955.

Reason, C. J. C. and Mulenga, H. (1999). Relationships between South African rainfall and SST anomalies in the southwest Indian Ocean. *Int. J. Climatol.*, 19:1651.

Reynolds, R. W., Rayner, N. A., Stokes, T. M. S. D., and Wang, W. (2002). An improved in situ and satellite sst analysis for climate. *J. Climate*, 15:1609–1625.

Richard, Y., Fauchereau, N., Poccard, I., Rouault, M., and Trzaska, S. (2001). 20th century droughts in southern Africa: spatial and temporal variability, teleconnections with oceanic and atmospheric conditions. *Int. J. Climatol.*, 21:873–885.

Richard, Y., Trzaska, S., Roucou, P., and Rouault, M. (2000). Modification of the southern African rainfall variability/enso relationship since the late 1960s. *Clim. Dyn.*, 16:883–895.

Richardson, L. F. (1922). *Weather Prediction by Numerical Process*, page 66. Cambridge University Press.

Rouault, M., Florenchie, P., Fauchereau, N., and Reason, C. J. C. (2003). South East Atlantic warm events and southern African rainfall. *Geophys. Res. Lett.*, 30:GL014840.

Rouault, M. and Richard, Y. (2003). Intensity and spatial extent of drought in South Africa at different timescales. *Water SA*, 29(4):489–500.

Sáenz, J., Zubillaga, J., and Fernández, J. (2002). Geophysical data analysis using python. *Comp. & Geosci.*, 28(4):457 – 465.

Saha, S. and Coauthors (2010). The NCEP climate forecast system reanalysis. *Bull. Amer. Meteor. Soc.*, 91:1015–1057.

Scharenbroich, L., Magnusdottir, G., Smyth, P., Stern, H., and chi Wang, C. (2010). A bayesian framework for storm tracking using a hidden-state representation. *Mon. Wea. Rev.*, 138(6):2132–2148.

Shen, R., Bresch, J. F., and Reiter, E. R. (1986). Vertical Interpolation of Meteorological Variables. *Mon. Wea. Rev.*, 114:123–134.

Singleton, A. T. and Reason, C. J. C. (2007). A numerical model study of an intense cutoff low pressure system over South Africa. *Mon. Wea. Rev.*, 135:1128–1150.

Skok, G., Tribbia, J., Rakovec, J., and Brown, B. (2009). Object-based analysis of satellite-derived precipitation systems over the low- and midlatitude pacific ocean. *Mon. Wea. Rev.*, 137:3196–3128.

Streten, N. (1973). Some characteristics of satellite-observed bands of persistent cloudiness over the southern hemisphere. *Mon. Wea. Rev.*, 101(6):486–495.

Tadross, M. A., Hewitson, B. C., and Usman, M. T. (2005). The interannual variability of the onset of the maize growing seaon over South Africa and Zimbabwe. *J. Climate*, 18:3356–3372.

Taljaard, J. J. (1996). Atmospheric circulation systems, synoptic climatology and weather phenomena of South Africa. Technical Paper 32, South African Weather Bureau, Pretoria.

Tennant, W. J. and Hewitson, B. C. (2002). Intra-seasonal rainfall characteristics and their importance to the seasonal prediction problem. *Int. J. Climatol.*, 22:1033–1048.

Thompson, D. W. J. and Wallace, J. M. (2000). Annular modes in the extratropical circulation. part I: Month-to-month variability. *J. Climate*, 13:1000–1016.

Todd, M. and Washington, R. (1999). Circulation anomalies associated with tropical-temperate troughs in Southern Africa and the south west Indian Ocean. *Climate Dyn.*, 15:937–951.

Todd, M. C. and Washington, R. (1998). Extreme daily rainfall in southern African and southwest Indian Ocean tropical-temperate links. *S. Afr. J. Sci.*, 94:64–70.

Todd, M. C., Washington, R., and . Palmer, P. I. (2004). Water vapour transport associated with tropical-temperate trough systems over southern Africa and the southwest Indian Ocean. *Int. J. Climatol.*, 24:555–568.

Trenberth, K. E. (1976). Spatial and temporal variations of the Southern Oscillation. *Quart. J. Roy. Meteor. Soc.*, 102:639–653.

Trenberth, K. E. and Stepaniak, D. P. (2001). Indices of El-Nino evolution. *J. Climate*, 14:1697–1701.

Tyson, P. D. and Preston-Whyte, R. A. (2000). *The weather and climate of southern Africa.* Oxford University Press, 2nd edition.

Usman, M. T., adn P. Johnston, E. A., and Tadross, M. (2005). A conceptual framework for enhancing the utility of rainfall hazard forecasts for agriculture in marginal environments. *Nat. Hazards*, 34:111–129.

Usman, M. T. and Reason, C. J. C. (2004). Dry spell frequencies and their variability over southern Africa. *Clim. Res.*, 26:199–211.

Van Heerden, J., Terblanche, D. E., and Schulze, G. C. (1988). The southern oscillation and South African summer rainfall. *J. Climatol.*, 8:557–597.

Vigaud, N., Pohl, B., and Crétat, J. (2012). Tropical-temperate interactions over southern Africa simulated by a regional model. *Climate Dyn.*, DOI 10.1007/s00382-012-1314-3.

Vigaud, N., Richard, Y., Rouault, M., and Fauchereau, N. (2009). Moisture transport between the South Atlantic Ocean and southern Africa: relationships with summer rainfall and associated dynamics. *Climate Dyn.*, 32:113–123.

Walker, N. D. and Lindesay, J. A. (1989). Preliminary observations of oceanic influences on the February-March 1988 floods in central South Africa. *S. Afr. J. Sci.*, 85:164–169.

Walker, T. N. (1990). Links between South African summer rainfall and temperature variability of the Agulhas and Bengueal current systems. *J. Geophys. Res.*, 95(C3):3297–3319.

Wang, G. and Hendon, H. H. (2007). Sensitivity of Australian rainfall to inter-El-Nino variations. *J. Climate*, 20:4212–4226.

Washington, R. and Todd, M. (1999). Tropical-temperate links in Southern Africa and Southwest Indian Ocean satellite-derived daily rainfall. *Int. J. Climatol.*, 19:1601–1616.

Webster, P. J. and Chang, H. R. (1997). Atmospheric wave propagation in heteorogenous flow: basic flow controls on tropical-extratropical interaction and equatorial wave modification. *Dyn. Atmos. Oceans*, 27:91–134.

Wheeler, M. C. and Hendon, H. H. (2004). an all-season real-time multivariate MJO index: Development of an index for monitoring and prediction. *Mon. Wea. Rev.*, 132:1917–1932.

Whitaker, J. S. (2007). Basemap. http://matplotlib.github.com/basemap.

Widlanksy, M. J., Webster, P. J., and Hoyos, C. D. (2011). On the location and orientation of the South Pacific Convergence Zone. *Clim. Dyn.*, 36:561–578.

Wolter, K. and Timlin, M. S. (1998). Measuring the strength of ENSO events: how does 1997/98 rank? *Weather*, 53:315–324.

Ziv, B. (2001). A subtropical rainstorm associated with a tropical plume over Africa and the Middle-East. *Theor. Appl. Climatol.*, 69:91–102.

Ziv, B. and Alpert, P. (1994). Isobaric to isentropic interpolation errors and implication to potential vorticity analysis. *J. Appl. Meteorol.*, 33:694–703.